Decarbonizing Long-haul Trucking

by

Robert Jones

B.S. Chemical Engineering, The University of California Santa Barbara (2019)
M.S. Chemical Engineering Practice, Massachusetts Institute of Technology (2022)

Submitted to the Department of Chemical Engineering
in partial fulfillment of the requirements for the degree of

Doctor of Philosophy in Chemical Engineering Practice

at the

MASSACHUSETTS INSTITUTE OF TECHNOLOGY

May 2024

Author .....
Department of Chemical Engineering
August 29, 2022

Certified by .....
William H. Green
Hoyt C. Hottel Professor in Chemical Engineering
Thesis Supervisor

Accepted by .....
Hadley D. Sikes
Willard Henry Dow Professor of Chemical Engineering
Graduate Officer

Decarbonizing Long-haul Trucking

by

Robert Jones

Submitted to the Department of Chemical Engineering
on August 29, 2022, in partial fulfillment of the
requirements for the degree of
Doctor of Philosophy in Chemical Engineering Practice

Abstract

As climate change poses an ever-increasing challenge for the world, the transportation sector has experienced significant troubles in mitigating its carbon dioxide emissions. Particularly responsible for this development is the heavy-duty trucking sector. Heavy-duty freight trucks are responsible for approximately 30 % of the highway transportation emissions even though they only represent about 5.5 % of vehicles on the road. Heavy-duty trucks are also the backbone of US freight, as they account for 71 % of freight delivered to the American people. The corresponding road freight energy consumption has been consistently increasing over the last decades and is expected to grow even further in the future. Emissions must be drastically reduced in order to adhere to the proposed targets of the 2015 Paris Agreement and to limit global warming. This contrast raises a crucial question: how can road freight emissions be substantially reduced while at the same time facing a growing transportation demand? Especially for long-haul class 8 trucks, this question is difficult to answer. This study seeks to elucidate potential competitive powertrain and fuel combinations and eliminate other poor alternative options.

Thesis Supervisor: William H. Green
Title: Hoyt C. Hottel Professor in Chemical Engineering

Acknowledgments

First, let me say this thesis was one hell of a ride with more highs and lows than a Tinderella relationship.

Contents

List of Figures

List of Tables

List of Acronyms

ANL Argonne National Lab

ATRI American Transportation Research Institute

BD20 biodiesel

BET battery electric truck

BMEP break mean effective pressure

BOP balance of plant

BSET battery swap electric truck

BTE break thermal efficiency

BTS Bureau of Transportation Statistics

CAISO California Independent System Operator

CARB California Air Resources Board

CCUS carbon capture, utilization, and storage

CET caternary electric truck

CNG compressed natural gas

CO carbon monoxide

CO_2 carbon dioxide

DF discount factor

DGE diesel gallon equivalent

D-ICET diesel internal combustion engine truck

DOE Department of Energy

DOT Department of Transportation

EAT exhaust aftertreatment system

EGR exhaust gas recirculation

EIA Energy Information Agency

EPA Environmental Protection Agency

FAF freight analysis framework

FCET fuel cell electric truck

FCEV fuel cell electric vehicle

Fleet DNA Commercial Fleet Vehicle Operating Data

GHG greenhouse gas

GREET The Greenhouse Gases Regulated Emissions and Energy Use in Technologies Model

GWP global warming potential

H_2 hydrogen

H2A hydrogen analysis

HDRSAM Heavy-duty Refueling Station Analysis Model

HDSAM Hydrogen Delivery Scenario Analysis Model

HDT heavy-duty truck

HDUDDS Heavy-duty Urban Dynamometer Driving Schedule

HDV Heavy-duty Vehicles

HET hybrid electric truck

H-FCET hydrogen fuel cell electric truck

H-FCETHEV hydrogen fuel cell electric truck (standard hybrid)

H-FCETPHEV hydrogen fuel cell electric truck (plug in hybrid)

HFTO Hydrogen and Fuel Cell Technology Office

HHDDT Heavy-duty Diesel Truck Cruise Mode drive cycle

H-ICE hydrogen combustion engine

H-ICET hydrogen combustion engine truck

HTDC Oak Ridge National Laboratory Heavy Duty Cycle Project

HWFET Highway Fuel Economy driving schedule

ICCT International Council on Clean Transportation

ICE internal combustion engine

ICET internal combustion engine truck

IEA International Energy Agency

ILUC Induced land use change

KS Kolmogorov-Smirnov

LCOE levelized cost of energy

LCOH levelized cost of hydrogen

LDV Light Duty Vehicles

LFP lithium iron phosphate batter

LNG liquid natural gas

M&M maintenance and repair

MeOH methanol

MPG miles per gallon

NACFE North American Council for Freight Efficiency

NAP National Academies Press

NESCCAF Northeastern States Center for a Clean Air Future driving schedule

NHTSA National Highway and Traffic Safety Administration

NMC nickel manganese cobalt battery

NO_x nitrogen oxides

NREL National Renewable Energy Laboratory

NRELATB NREL's Annual Technology Baseline

NSW nuclear, solar, and wind

PHEV plug-in hybrid electric vehicle

PM particulate matter

PTW pump-to-wheel

RD renewable diesel

ROL17 Run on Less 2017 Roadshow

ROLR Run on Less Regional Roadshow

RPM revolutions per minute

SCC social cost of carbon

SCR selective catalytic reduction aftertreament system

SMR steam methane reformation

SMRCCS steam methane reformation with carbon capture and sequestration

SO_x sulfur oxides

SR stoichiometric ratio

TCO total cost of ownership

TCS total cost to society

TCU transmission control unit

USLHC8 Unite States Long-haul Class 8 Drive Cycle

VIUS Vehicle Inventory and Use Survey

VMT vehicle miles traveled

WCAC water charge air cooler

WHR waste heat recovery

WTP well-to-pump

WTW well-to-wheel

Chapter 1

Introduction

1.1 Introduction

While climate change poses an ever-increasing challenge for the world, the transportation sector brings additional barriers to reducing carbon dioxide emissions, particularly for heavy-duty trucking [1]. Heavy-duty freight trucks are responsible for approximately 30% of the highway transportation emissions even though they only represent about 5.5 % of vehicles on the road [2]. Heavy-duty trucks are also the backbone of US freight, as they account for 71 % of freight deliveries [3]. The corresponding on-road freight energy consumption has been consistently increasing over the last decades and is expected to grow even further in the future [4, 5].

Different alternative powertrains are being explored to answer the crucial question: how can road freight emissions be cut to net-zero carbon by 2050 while at the same time facing a growing transportation demand? The complexity of this question presents a challenging dilemma for the transportation sector: neither the scientific community nor large auto manufacturers have reached a consensus on which powertrain will be the best solution for the future of the long-haul sector. This lack of consensus has impacted decision-making among stakeholders. For example, policymakers are hesitant on large-scale incentives because an excessive bias towards one technology option could hinder the market penetration of competing technologies. However, these competing technologies might turn out to be a significantly better solution in the long run. Moreover, investors typically avoid substantial uncertainty, which makes it even more difficult for manufacturers to carry the burden of research and development costs for a multitude of different possible future powertrain solutions. Lastly, truck operators are uncertain which powertrains to purchase for their fleet to comply with future regulations and customer sustainability demands.

Twenty powertrain and fuel combinations were assessed and compared to conventional diesel on the basis of cost and emissions. Powertrains studied include the internal combustion engine truck (ICET), fuel cell electric truck (FCET), battery electric truck (BET), hybrid electric truck (HET), battery swap electric truck (BSET), and caternary electric truck (CET). Fuels considered include

diesel, compressed natural gas (CNG), liquid natural gas (LNG), methanol (MeOH), biodiesel (BD20), renewable diesel (RD), hydrogen (H_2), and electricity (table 1.1). The energy densities and specific energies of the considered fuels is given in figure 1.1.

Table 1.1. The powertrain and fuel combinations considered in the elimination process. The columns refer to fuels and the rows refer to powertrains. ICET - internal combustion engine truck, FCET - fuel cell electric truck, BET - battery electric truck, HET - hybrid electric truck, BSET - battery electric truck, CET - caternary electric truck, CNG - compressed natural gas, LNG - liquid natural gas, MeOH - methanol, BD - biodiesel, RD - renewable diesel, H2 - hydrogen, Elec - electricity

	Diesel	**CNG**	**LNG**	**MeOH**	**BD**	**RD**	**H2**	**Elec**
ICET	✓	✓	✓	✓	✓	✓	✓	x
FCET	x	x	x	✓	x	x	✓	✓
BET	x	x	x	x	x	x	x	✓
HET	✓	✓	✓	x	✓	✓	✓	✓
BSET	x	x	x	x	x	x	x	✓
CET	x	x	x	x	x	x	x	✓

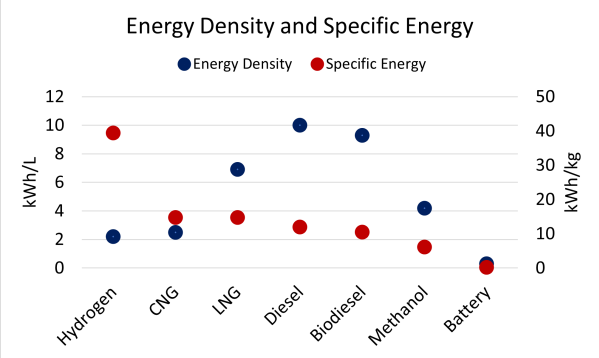

(a) Energy densities and specific energies of fuels considered.

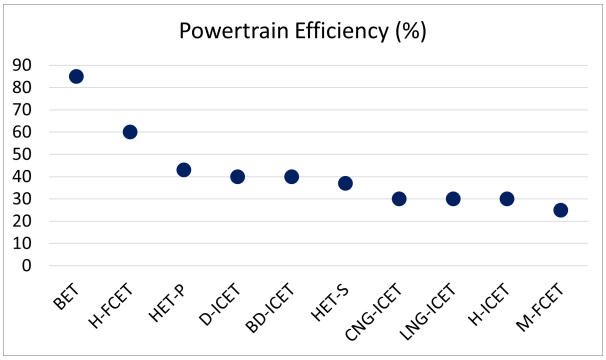

(b) Literature review efficiencies used in back of the envelop calculations.

Figure 1.1

For the large number of powertrain and fuel combinations, simple "back of the envelope" algebraic models were constructed for high throughput evaluation. Natural gas and methanol based powertrains were ultimately eliminated due to their inability to meet long term emission target goals. Natural gas based powertrains in particular show slight improvement in on road emissions, however due to methane leakage, many studies estimate natural gas to have more emissions than diesel. Compressed natural gas configurations significantly reduce the daily range of the truck, needing to be refilled often. The main benefit for using natural gas based powertrains would be energy security and lower costs relative to diesel.

Methanol powertrains considered include the direct methanol fuel cell and methanol combustion engine. A large benefit to methanol as a fuel is its liquid form. Methanol could be easily implemented into the existing diesel infrastructure. Carbon dioxide is a main product of methanol oxidation, pre-

venting methanol powertrains from being a low carbon option when considering tailpipe emissions. The direct methanol fuel cell is an underdeveloped technology that is hindered by slow kinetics at the catalyst and methanol crossover through the membrane (doi:10.1557/mre.2015.4). This leads to very low efficiencies and power densities. Ultimately, methanol powertrains were eliminated due to poor emission potential and powertrain performance.

Biofuels include a wide variety of fuels and powertrains. Explicitly covered biofuels include biodiesel, renewable diesel, renewable natural gas, renewable hydrogen, and renewable methanol. While biofuels have emission reduction potential due to the carbon fixation of plants, biofuels become an issue at large scale production. Large scale production requires more land than is available when considering first and second generation biofuels. Third generation biofuels, algal biomass, have much higher yields however, algae need large amounts of water, nitrogen, and phosphorous to grow. This means third generation biofuels are expensive and have large emissions due to the amount of fertilizer used to grow them. Biofuels were ultimately eliminated due to their inability to scale and meet energy demand.

The powertrain fuel combinations that were accepted for in depth analysis include the battery electric, hydrogen fuel cell, and hydrogen combustion engine. These powertrains have the potential for zero life cycle emissions when using clean production methods. A total cost to society analysis was conducted to compare powertrains. The total cost to society incorporates the emission costs into the total cost of ownership, allowing the use of only one metric to compare powertrains. When considering the long term scenario, utilizing large production volume, the social cost of carbon, these powertrains not only have emission benefits, but are cost competitive to conventional diesel.

A short review is provided to establish the pros and cons of each powertrain and fuel combination considered.

1.2 Current Status and Considerations for Alternative Powertrains and Fuels

.

Battery Electric

The battery electric model has seen major market penetration in light duty vehicles over the past decade. This optimism has spilled over into the heavy-duty sector. In January 2020, the national average cost of electricity was $4.81/DGE compared to $3.05 for diesel [6]. There are currently 25,000 charging stations in the US; however, they are not ideal for heavy duty trucks [7]. Battery electric powertrains have zero tail pipe emissions with the potential for zero well to wheel emissions when coupled with clean electricity production. They offer superior powertrain efficiencies at low

loads up to 90%. Furthermore, regenerative breaking allows for energy to be recovered when slowing down; however, it should be noted that for long haul trucking, regenerative breaking benefits are slight. The upcoming of battery electric light duty vehicles has led to decreasing battery prices and increasing battery energy density; however, prices still remain high and energy densities low when compared to other alternatives. Pure battery electric powertrains lead to a range dilemma. Very large battery are required to achieve the standard range of a long haul truck; however, the battery becomes so large that the carrying capacity is significantly reduced and the battery capital cost becomes prohibitively expensive.

The current status of charging is also a clash to the standard refueling procedure of long-haul heavy-duty trucking today. Even under fast charging conditions, a battery takes many hours to charge. Current commercial chargers are at most 250kW. Tesla and other electric companies have been in progressing with constructing a 1 MW charger. However, even when this state-of-the-art charger is commercialized, under a conservative simple calculation, this would require almost 2 hours to charge a standard long-haul truck. The battery swap idea is a possible solution to slow charging times; however, the idea of battery ownership would have to be reinvented. Another point to note is the temperature sensitivity of batteries. Lithium ion battery capacity can be reduced to 60% at -10deg which is a common winter temperature in cold US climates [8]. Hot climates significantly affect the battery's durability. Finally, large implementation of battery electric trucks would require grid infrastructure to be bolstered.

The large battery dilemma induces the idea of catenary battery electric powertrains. These powertrains do not require a large on board battery, but instead are connected to overhead power lines. The power lines would run along common long haul routes. When the truck neared it's destination, it would detached from the catenary lines and operate off a small onboard battery. For this option to be realistic, the power line infrastructure cost would have to be more appealing than the scenario with large on board batteries.

Hybrid Electric

Hybrid vehicles are a mix of multiple powertrains. This study considered the variations of a mix of internal combustion and battery electric powertrain components. Hybrid components vary by size and configuration of components. Micro systems provide power to auxiliary equipment and can prevent major losses due to idling. Mild systems provide the benefits of micro systems, with the added benefit of providing launch assistance for short term rapid accelerations. Macro systems have considerably larger electrical components and provide a significant portion to the total drivetrain power. Component sizing and the operation logic is largely an optimization problem that is highly dependent on drive cycle. For long haul operations, large electrical systems are not favored due to their weight and costs. The benefits of regenerative breaking from stop and go behavior of city

driving are not applicable to highway long haul operation. The National Academies Press (NAP) found micro systems to offer long haul trucking the most benefit [8].

For larger hybrids, the two main configurations are series and parallel. These configurations can be further broken down into micro configurations such as pro or post transmission parallel. In the series configuration, the internal combustion engine (ICE) sends power to the electrical system, and the electrical system is directly connected to the drivetrain. The motivation behind series configurations is the ICE is able to run at its optimally efficient load while in operation. The fuel economy is more reliant on stop and go behavior than the parallel configuration. Because a larger motor is used, more energy can be recovered from regenerative breaking. A study that performed optimization of hybrid component in long haul operation showed an 8% decrease in fuel economy relative to the baseline diesel [9]. This decrease is attributed to the added losses due to the series configuration adding multiple energy conversions.

In the parallel configuration, the ICE and electrical system simultaneously send power to the drivetrain. This option has a smaller electrical system than series due to sharing the power requirement. The motivation to parallel configurations is to allow each component to operate in its preferred load. The electrical motor has its optimal efficiency at low loads while the ICE has its optimal efficiency at high loads. The ability to store energy from regenerative breaking for this configuration is less than series due to the smaller electrical motor. A study that performed optimization of hybrid components in long haul operation showed a 7% increase in fuel economy relative to baseline diesel [9].

Natural Gas

Interest in natural gas for heavy duty applications is driven by factors such as the potential for lower operating costs, compliance with tailpipe carbon dioxide (CO_2) emission requirements, and as a cost effective solution to ultra-low nitrogen oxides (NO_x) emissions. Natural gas has a 25% higher specific energy than diesel at 15 kWh/kg. The engine efficiency is around 5-10% less than a diesel engine due to necessity of spark ignition; however, compression ignition and its efficiency is possible if the fuel is blended with at least 10% diesel [8]. The spark ignition operation offers the benefit of a simpler three way catalyst exhaust system. According to the NAP, natural gas offers emission reductions of NO_x, carbon monoxide (CO), and sulfur oxides (SO_x) by 70%, 80%, and 97% respectively. There is literature debate on the greenhouse gas (GHG) reduction benefits. A 3% reduction in tailpipe emissions was shown by Cummings [8]. The cost to retrofit an existing diesel engine without a turbo charger is $7,000-$10,000 [10].

CNG is the most common option for onboard storage. Because it is a gas, CNG has a 75% lower energy density than diesel at 2.5 kWh/L. There are currently 872 CNG refueling stations across the US [11]. In January 2020, the national average price of CNG was 19% less than diesel

at $2.46/DGE [6]. Current tanks are designed to contain 250 bar; however, the advances of the hydrogen tanks will allow up to 700 bar. CNG has fast or timed refueling options. Fast fueling is typical for commercial refueling and generally takes on the order of 10 minutes and fills from high pressure tanks. This method induces heat of compression which causes less fuel to be stored in the tank. The timed fueling connects directly to a natural gas utility outlet. This method is used primarily by fleet owners over night and allows for a fuller fill.

LNG is a less common option than CNG. It has the advantage of a 176% higher energy density than CNG; however it has a 31% lower energy density than diesel at 6.9 kWh/L. There are currently only 62 refueling stations across the US [12]. The fueling time is very similar to diesel. The cryogenic storage at -162°C leads to increased storage costs and energy use. In January 2020, the national average price of LNG was 13% higher than CNG at $2.77/DGE; however, it was 9% lower than diesel [6].

Methanol

Methanol is easily produced, transported, and handled. It can be used in existing diesel infrastructure with minor modifications. In January 2020. The price of methanol was 7% cheaper than diesel at $2.83/DGE [6]. Methanol has 49% lower specific energy and a 58% lower energy density than diesel at 6.1 kWh/kg and 4.2 kWh/L respectively. The direct methanol fuel cell is the propulsion system considered for methanol. The fuel cell is hindered by the slow kinetics of the methanol oxidation reaction. This lowers the power density of the cell making it very large. It is also hindered by methanol crossover. Methanol can pass through the fuel cell membrane from anode to cathode, resulting in up to 10% wasted fuel and reduced efficiency. Reported efficiencies widely vary based on operating conditions; however, they are generally under of 30%. Moore et al demonstrated a maximum efficiency of 35% [13]. The exhaust of contains CO_2; however, other exhaust components from diesel such as NO_x, SO_x, and PM are absent. Further research on electrode kinetics and membrane selectivity is needed and is currently being explored by the Roman and Johnson groups at MIT.

Hydrogen

A hydrogen powered truck is part of the portfolio of options for the advancement of zero carbon emissions. Hydrogen as an energy carrier is particularly interesting in the long haul scenario due to its 236% high specific energy (40kWh/kg) than diesel. This enables trucks to travel further with less fuel weight. Hydrogen however, has a 78% lower energy density (2.2 kWh/L) than diesel. In addition, the fuel cell option can provide overnight hotel electrical loads. This eliminates the need for electrical power generation from idling traditional diesel trucks.

The most widely expected hydrogen powertrain system to penetrate the market is the polymer

exchange membrane fuel cell (PEMFC). The input fuel for this system is hydrogen and oxygen (air). The output is water, making this option a zero tail-pipe emitter. The Department of Energy (DOE) is one of the biggest contributors to research and development of hydrogen fuel cells for vehicular application.

Infrastructure, or the lack thereof, is among hydrogen's biggest obstacle to becoming a reality in transportation. Some of the infrastructure is already in place because hydrogen has long been used in industrial applications, but it's not sufficient to support widespread consumer use of hydrogen as an energy carrier. In the United States, there have been efforts to establish hydrogen fuel networks for light duty vehicles, mainly in the San Francisco and Los Angeles areas in California. As of mid-2019, there were 41 open stations with 36 planned stations, 12 of which are in the Northeast [14]. None of these stations are suitable for heavy duty trucks. Nikola Motors is pioneering the way for long haul fuel cell electric vehicles. They expect to release their line of hydrogen trucks in 2023. The company plans to build a network of 700 truck stop-size hydrogen fuel stations across the U.S. and Canada by 2028 [15].

Biofuels

The end biofuel product is very similar to fossil fuels. The liquid products can easily be integrated into the established diesel distribution and fueling infrastructure. The two biofuels considered in this study for class 8 heavy duty operation was biodiesel and renewable diesel. Biodiesel is produced by transesterification to make fatty acid methyl esters and glycerin. The glycerin co-product can be used to make soaps and other products. Biodiesel is commonly blended with diesel to form B100 (pure biodiesel), B20, B5, and B2. B20 is the most common and blends up to B20 can be used as a drop in fuel for 80% of OEMs [16]. Biodiesel is a well established fuel that has been in the market since the 1990s. Biodiesel development in the US was motivated by the 1970's oil embargo and incentivized to increase energy security. Pure biodiesel has a lower energy density than diesel at 9.3 vs 10.0 kWh/L [17]. The national average price in January 2020 for B20 and B100 were 2.93 and $4.00/DGE respectively [6].

Induced land use change (ILUC) can have significant environmental impacts depending on the type of land converted and literature is not consistent. Converting rainforests, peatlands, savannas, or grasslands, to produce food crop-based biofuels could ultimately produce more carbon than conventional diesel life cycle emissions. Converting land releases CO_2 as a result of burning or microbial decomposition of organic carbon stored in plant biomass and soils. Fargione et al. refer to this as the carbon debt [18]. They calculated how large biofuel carbon debts are and how many years are required to repay them for four different biodiesel cases of native habitat conversion. They studied palm diesel from Indonesia/Malaysia tropical rainforests and peatland rainforests, as well as soybean biodiesel from Brazilian tropical rainforests and Cerrado grasslands. Biodiesel produced

in Indonesia and Malaysia from clearing peatland rainforests was found to be the highest with a payback time of 423 years and the Brazilian Cerrado was the lowest at 37 years. For developing first generation biofuel technologies, this study shows any strategy to reduce GHG emissions that causes land conversion from native ecosystems to cropland is likely to be counterproductive.

For many biofuels, the required land area can be a barrier to widespread adoption. The most common biodiesel fuelstock, soybeans, has one of the lowest yields at 66 gallons of biodiesel per acre [19]. Using the Energy Information Agency (EIA) 2020 energy outlook class 8 annual vehicle miles traveled, one third of the US land area would be required to sustain the heavy-duty trucking sector. Biodiesel from algae has been proposed to alleviate the issue of land requirement due to it much higher yields estimated to be 10,000 gallons of biodiesel per acre. However, no large-scale algae farms are currently at scale.

Chapter 2

Development of a long-haul drive cycle based on real-driving data and its application in a diesel powertrain simulation

This work is finished and is currently being submitted to Transportation Research Part D: Transport and Environment. Special thanks is given to Moritz Koellner for assisting with writing and constructing the USLHC8 drive cycle and to IAV for providing the engine maps needed to model the diesel engine.

2.1 Introduction

While climate change poses an ever-increasing challenge for the world, the transportation sector brings additional barriers to reducing carbon dioxide emissions, particularly for heavy-duty trucking [1]. Heavy-duty freight trucks are responsible for approximately 30% of the highway transportation emissions even though they only represent about 5.5 % of vehicles on the road [2]. Heavy-duty trucks are also the backbone of US freight, as they account for 71 % of freight deliveries [3]. The corresponding on-road freight energy consumption has been consistently increasing over the last decades and is expected to grow even further in the future [4, 5].

The fast growth of heavy transport, which relies heavily on diesel engines, has motivated regulations intended to reduce both NO_x and CO_2 emissions. For instance, the approved California Air Resources Board (CARB) NO_x regulations in the U.S. foresee a 90 % reduction by 2027, compared to the US10 baseline [6]. In Europe, the proposal from the Consortium for ultra Low Vehicle Emissions (CLOVE) strengthen NO_x limits for the Euro VII heavy-duty vehicle legislation. These efforts in lowering emissions have also uncovered challenges in the context of heavy-duty engine developments.

Different alternative powertrains are being explored to answer the crucial question: how can road freight emissions be cut to net-zero carbon by 2050 while at the same time facing a growing transportation demand? The complexity of this question presents a challenging dilemma for the transportation sector: neither the scientific community nor large auto manufacturers have reached a consensus on which powertrain will be the best solution for the future of the long-haul sector. This lack of consensus has impacted decision-making among stakeholders. For example, policymakers are hesitant on large-scale incentives because an excessive bias towards one technology option could hinder the market penetration of competing technologies. However, these competing technologies might turn out to be a significantly better solution in the long run. Moreover, investors typically avoid substantial uncertainty, which makes it even more difficult for manufacturers to carry the burden of research and development costs for a multitude of different possible future powertrain solutions. Lastly, truck operators are uncertain which powertrains to purchase for their fleet to comply with future regulations and customer sustainability demands.

Comparative analyses of alternative powertrains has been performed to clarify the path to decarbonize the long-haul transport [7–9], primarily from economic and environmental criteria. While these comparisons have provided insights into the trade-offs of switching from diesel-based to cleaner technologies, comprehensive assessments with focus on long-haul trucking operation are still limited, particularly for the US freight operation. This makes it more difficult to evaluate technologies in an apple-to-apple basis when it comes to different vehicle models, design attributes, assumptions, and driving patterns that are unrepresentative of the national long-haul operation [10].

A representative long-haul class 8 drive cycle is then an essential prerequisite for an accurate assessment of suitable alternative powertrains. In general terms, a drive cycle consists of a series of data points that describe a vehicle speed trace over time. Drive cycles are the main input for most simulations determining on-road energy consumption and emissions. Also, drive cycles influence the sizing, and therefore performance requirement of the powertrain components. The purpose of this study is twofold:

1. Develop a characterization of long-haul freight operation in the form of a drive cycle and associated supplementary parameters.

2. Using the results from 1, establish a benchmark to conventional long-haul trucking on the basis of fuel consumption, GHG emissions, and total cost to society (TCS), for comparison with alternative powertrains in the present, midterm, and longterm.

This paper is organized as follows. Section 2.2 provides a literature review on drive cycles currently used to model long-haul operation. This section also gives background on comparative analyses of different powertrains and current research gaps. Section 2.3 outlines the methodology followed for the drive-cycle construction, vehicle-level simulation, emissions and TCO analysis. Results are presented in section 2.4. The paper concludes with section 2.5, outlining final remarks, limitations and future directions.

2.2 Literature Review

In the reviewed literature on heavy-duty truck emissions modeling in the USA, six commonly used drive cycles were identified for long-haul trucking. Namely:

1. Highway Fuel Economy Driving Schedule (HWFET)

2. Heavy-Duty Diesel Truck Cruise Mode (HHDDT)

3. Northeast States Center for a Clean Air Future Long-Haul Cycle (NESCCAF)

4. US06 Supplemental Federal Test Procedure

5. Heavy-Duty Urban Dynamometer Driving Schedule (HDUDDS)

6. NREL long-haul cycle

A graphic representation of the six driving cycles is shown in Figure S1. These are used for simulating highway duty cycles; however, they have significant shortcomings in terms of long-haul applications on the basis of distance traveled, duration, vehicle speed and road grade distributions, and driving behavior.

The drive cycle's length and duration determine the size and weight of the energy storage on board the truck. Energy storage sizing considerations are especially important for alternative powertrains such as battery and fuel cell electric trucks that suffer from low energy density. Except for the National Renewable Energy Laboratory (NREL) long-haul cycle, all cycles reviewed are too short in distance and duration to represent long-haul driving. They range from 6 to 103 miles, and from 10 to 114 minutes. The NREL long-haul cycle on the other hand is too long, consisting of 935 miles traveled in more than 19 hours. This length and duration would only be appropriate for slip seating operations, in which multiple drivers successively operate a single truck. While slip seating is a unique operational mode of long-haul driving, it has limited significance for long-haul because it requires very complex and costly logistic given a shortage of truck drivers in the US. [11, 12].

A drive cycle's vehicle speed and road grade distributions are directly related to a vehicle's tractive power demand and, consequently, to the fuel economy and powertrain component sizing. The Highway Fuel Economy driving schedule (HWFET), Heavy-duty Urban Dynamometer Driving Schedule (HDUDDS) and Heavy-duty Diesel Truck Cruise Mode drive cycle (HHDDT) are limited to vehicle speeds ranging up to 60 mph and thus lack the higher speeds driven in many states. This leads to an underrepresentation of the national average power demand. The Northeastern States Center for a Clean Air Future driving schedule (NESCCAF) is a modified version of the HHDDT that is designed to have higher vehicle speeds and longer driving time. However, the additional driving time is generated by adding modal segments that do not contain the transience that is representative of real driving. Therefore, modal segments also underestimate power demand due to the absence of accelerations. Of the six drive cycles discussed, only the NREL long-haul and NESCCAF cycle account for road grade. Even if the total elevation changes over a given driving profile were to be negligible, information about the road grade would still be of great importance to determine the instantaneous power demand which defines the performance requirements for the powertrain sizing. While the NESCCAF cycle contains a road grade profile, it is synthetically contrived to oscillate between -3% and 3% road grade and does not represent a realistic road grade profile. The NREL long-haul cycle represents a particular continuous driving event and thus only accounts for a single set of vehicle, driver and route characteristics. This significantly limits its representativeness to the aggregate national average long-haul driving profile. Due to the lack of a representative long-haul driving pattern, light-duty drive cycles including the HWFET and US06 are sometimes used for highway driving. This leads to a significantly higher power demand because of the increased number of acceleration events for light-duty vehicles. Hence, a more realistic drive cycle for long-haul driving is necessary to accurately determine road freight emissions for long-haul class 8 trucks. This need was also expressed by the US Environmental Protection Agency (EPA) in its report on GHG Certification of Medium- and Heavy-Duty Vehicles [13].

Studies on powertrain simulation and performance analysis are widely available in the literature. For example, Lee et al. [14] conducted a well-to-wheel (WTW) analysis of the emissions for

conventional diesel and H-FCET over a range of Class 2b through Class 8b trucks. They derived the truck fuel consumption from vehicle dynamic simulation using the Autonomie model and an adjusted version of EPA/NHTSA test cycles. Langshaw et al.[15] also compared two different fuel options, diesel and LNG in the context of food freight with a large UK Food Retailer as a case study. They estimated the GHG emissions, TCO and TCS using real data of duty cycles that were recorded by the food retail company. This data corresponded to measurements in fuel consumption and distance traveled for diesel and LNG vehicle fleets, which was then translated into vehicle energy efficiencies. Recently, Lajevardi et al.[9] analyzed several options for conventional and alternative short-haul and long-haul drivetrains over different scenarios of infrastructure deployment. To model fuel consumption, they used in-house models for these drivetrains with drive cycles that represent freight operation in British Columbia.

This literature review on powertrain emissions and TCO revealed some research gaps. First, very few studies compare powertrain performance in the mid and long term. This is particularly relevant because technology adoption and maturity could overcome the current limitations of clearer long-haul trucks, leading to more competitive options over conventional diesel. While some works made efforts to fulfill this gap, they are focused on other regions such as a Canada's province [9], under very different scenarios from the US. trucking sector. Second, few works provide apple-to-apple comparisons that help reach a consensus on the best options for decarbonizing the heavy transport [14]. Finally studies used transient and cruise cycles that are too short to fully represent the entire freight operation.

The first purpose of this paper is therefore to develop a new drive cycle that better represents heavy-duty long-haul operatio by modeling vehicle speed and road grade traces based on the national average long-haul class 8 truck driving profile. This new drive cycle may aid universities, companies, and other research institutions without access to proprietary drive cycles. Specifically, the drive cycle may provide a more realistic representation of long-haul class 8 truck traffic to improve powertrain simulation models. Second, this work will contribute to the literature through a comparative analysis of different powertrains in an apple-to-apple basis. In this study, diesel is covered as a benchmark and is defined in the context of U.S. long-haul trucking. In future studies, alternative powertrain and fuel combinations will use the diesel benchmark to assess their current and future viability.

2.3 Methods

2.3.1 Defining Long Haul

Regional Haul vs. Long Haul

In the context of freight operations, the duty cycles of class 8 trucks can be classified into regional-haul and long-haul. Long-haul operation was distinguished from the regional-haul duty cycle on

the basis of trip distance and average vehicle speed. Table 2.1 lists different values for long-haul driving distances and speeds available in the literature. Based on the reviewed literature, the class 8 long-haul truck operation was defined for distances of at least 250 mi with a minimum average vehicle speed of at least 40 mph.

Table 2.1. Parameters defining long-haul operation

Parameters	**Values**	**Units**	**Reference**
Minimum daily trip distance	>300	mi	NACFE [16]
	190	mi	[17]
	220-250	mi	[18]
	250	mi	This work
Minimum average vehicle speed	41.1	mph	[19]
	40	mph	This work
Vehicle lifetime	10	years	[6, 20, 21], this work
	5	years	[22]
	3	years	[23]
Vehicle miles traveled	120,000	mi/year	[22]
	1,500,000	mi/lifetime	[7]
	1,000,000	mi/lifetime	[24]
	104,000	mi/year	[25]
	91,506	mi/year	[26]
	52,000-108,000	mi/year	[20, 27], this work
Maximum driving hours	11	hours	[28]
Daily range	750	mi/day	[29, 30]
	600	mi/day	[16], this work
	587	mi/day	(J. Gregorio, personal communication, September 5, 2021)

Long-haul fraction of class 8 market

Data on the US. truck population from the Vehicle Inventory and Use Survey (VIUS) was used to determine the fraction of long-haul operation within the class 8 truck population. Two different approaches were considered. The first approach distinguishes the tractors with sleeper cabs as long-haul, as they allow operation without returning to home base or depot. The second approach was based on daily driving range greater than 250 miles per day. To this end, the LNG data in miles per year was translated into daily miles using the number of months operated, 30.4 days per month conversion factor, and 60/70-hour week constraints determined by the Federal Motor Carrier Safety Administration [28]. The daily ranges are depicted in Figure S2, which shows that 25% of class 8 trucks are used for long-haul operation.

Vehicle lifetime

This work considers the entire useful vehicle life of an average class 8 tractor. After their first-use in long-haul operations, long-haul tractors typically have a second-use phase as regional- or short-haul trucks. The latter applications have lower requirements in terms of engine performance and uptime in between service intervals because of their shorter distances and driving durations. The repurposing of trucks is an established market process that is financially incentivized and will very likely continue to take place in the future. Consequently, the long-haul use-phase should not be analyzed in isolation from secondary use when regarding emissions. In the reviewed literature, there are very consistent assumptions establishing the length of the vehicle lifetime at 10 years (see Table 2.1). In this work, the vehicle lifetime was therefore defined at 10 years. This longer lifetime assumption instead of first-use period enabled better comparison of alternative powertrains in terms of in-use emissions, replacement and durability, however, the secondary use will feature different driving characteristics compared to long-haul driving.

Vehicle Miles Traveled

The vehicle miles traveled (VMT) parameter was defined per year of operation within the entire vehicle life of 10 years to represent both first-use and second-use operation characteristics. These values derived from the VIUS dataset for class 8 sleeper cabs [20] and are available in Table S1. The average VMT per year over the vehicle life is 87,200 miles and the cumulative VMT after ten years is 872,000 miles [20, 27].

Daily Range

With respect to the legal limits for truck operation, a drive cycle length of 600 miles was chosen, which is also consistent with estimations of the North American Council for Freight Efficiency

(NACFE) and other works summarized in Table 2.1. This value is also supported by the VIUS daily range distribution given in Figure S2.

2.3.2 Drive cycle development

In general, the drive cycle presented in this paper was developed by first determining the characteristics of the national average driving profile and then generating a driving pattern from real data that best describes these features. Figure 2.1 shows a schematic representation of the steps followed for the drive cycle construction from the raw NACFE Run on Less Regional Roadshow (ROLR) [16]. Brief descriptions of each step are provided below; however more details are available in the supplementary material.

Assessment feature selection

The matching of the real driving data to the national average driving profile was done on the basis of selected assessment features. The vehicle speed, road grade and daily range were prioritized over a set of seven driving characteristics that also included vehicle acceleration, powertrain idle time, number of stops and absolute elevation change. The prioritization criteria was based primarily on data availability and the impacts of each assessment features on the powertrain energy demand, and therefore GHG emissions [31].

Target feature vector definition

The target feature vector described the national average values of long-haul truck driving for the chosen assessment features of vehicle speed and road grade. This vector was constructed from five different publicly available datasets, namely:

1. NACFE Run on Less 2017 Roadshow ROL17 [16]
2. NACFE Run on Less Regional ROLR [32]
3. US Bureau of Transportation Statistics (BTS) Freight Analysis Framework [33]
4. Oak Ridge National Laboratory Heavy Duty Cycle Project (HTDC)
5. NREL Commercial Fleet Vehicle Operating Data (Fleet DNA) [34]

A summary of each dataset in regards to assessment features is given in Table S2. While each dataset encompasses several states in the US, combinations of these datasets into one national average vehicle speed distribution were tested as shown in Figure S3. The selected target for vehicle speed derives from the combination of 70% HTDC, 20% ROL17, 5% ROLR and 5% filtered Fleet DNA.

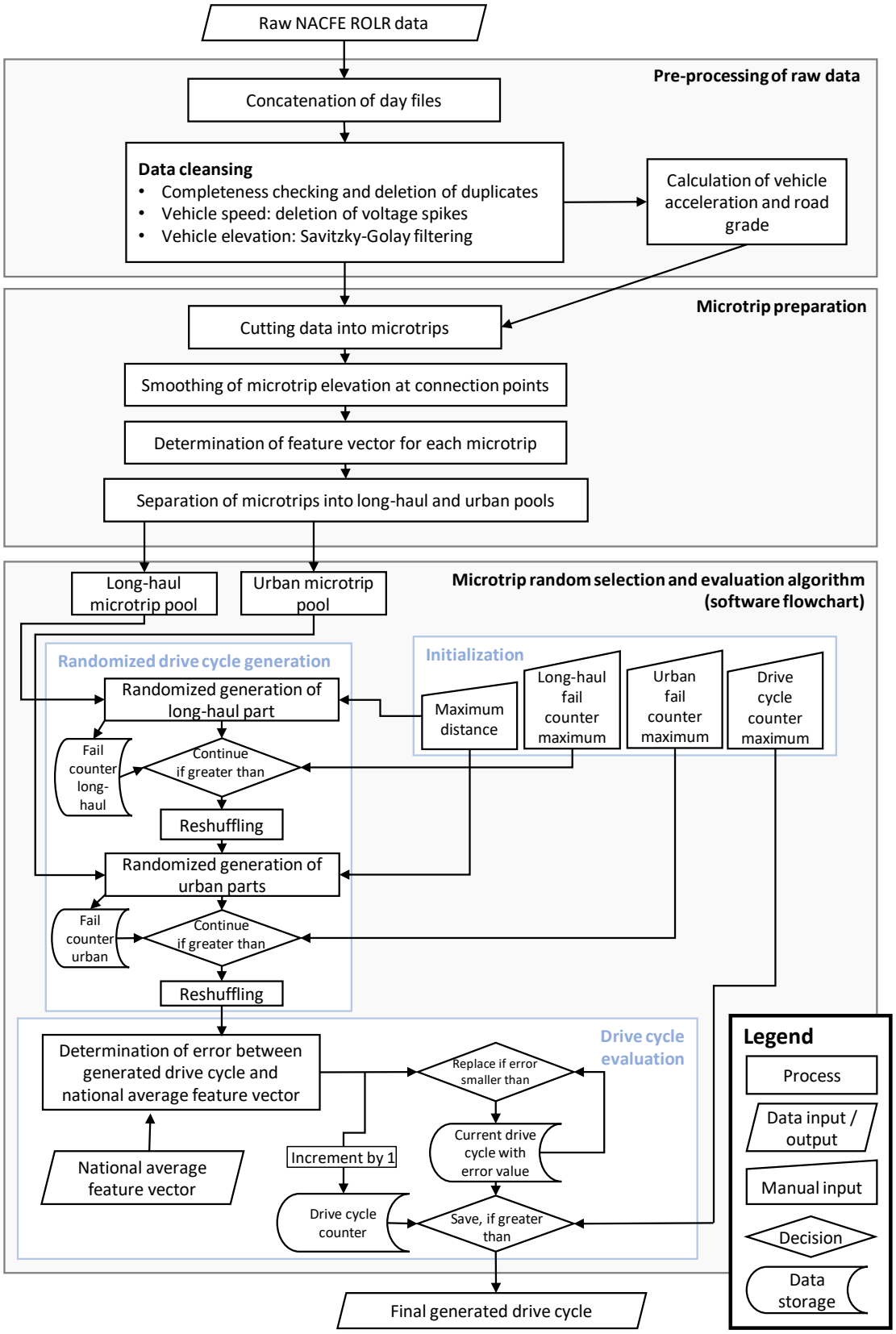

Figure 2.1. Flowchart of the drive cycle generation process

The road grade target was determined from the activity-weighted, distance-based cumulative distributions of absolute road grade introduced by the NREL with the TomTom database [35]. A single national average road grade vector was generated from these distributions at different truck speed limits using the share of each speed limit to the national average highway system, which derived from the truck speed limit map shown in Figure S4. To obtain the final target road grade vector, the relative frequencies of single road grade distribution were divided into negative and positive road grade intervals. This was done in order to ensure a uniform distribution. The resulting target vector for vehicle speed and road grade is given in Table S3.

Drive cycle generation

As shown in Figure 2.1, the drive cycle was generated through three major steps: pre-processing of raw data, microtrips preparation, microtrip random selection, and drive cycle evaluation. A detailed explanation of each step is given in the supplementary material. The data pre-processing step covers data cleansing to remove unrealistic, incomplete and duplicate datapoints. The data quality of elevation signals was also validated by denoising with the Savitzky-Golay filter. The microtrip preparation step includes cutting the ROLR data at the points with zero vehicle speed and acceleration, which leads to a set of microtrips. The elevation at these connecting points was smoothed to ensure that the resulting road grades were equal to zero. The feature vector for each microtrip was also generated and finally, the microtrips were classified into highway and urban using the criteria from Table S4. For the microtrip random selection and evaluation step, an algorithm was developed and consists of three main processes framed in light blue boxes. Namely, these main processes are initialization, randomized drive cycle generation and evaluation. In the initialization, manual inputs determining the generation process are defined. Then, drive cycles are randomly generated. Through the evaluation step, each resulting drive cycle is compared to the national average driving profile. The drive cycle with smallest error was selected and named as USLHC8.

The validation of the USLHC8 cycle was performed through a two-sample KS test with the cycles reported in the literature. This was done to determine the degree of similarity and thus the representativeness relative to the defined national average driving profile for each drive cycle. In addition, a drive cycle named as control was generated with a slightly altered algorithm to serve as a control for the generation methodology.

2.3.3 Diesel heavy-duty truck model for fuel economy

A diesel internal combustion engine truck (D-ICET) model was constructed using the software GT-Suite to serve as a baseline and compare alternative powertrains to in future research. The USLHC8 serves as the main input for D-ICET model simulations. In general, a tractive power demand is calculated from the drive cycle's vehicle speed and road grade and is met by the powertrain. The

output of the model is the fuel economy, which can then be used to calculate GHG emissions and costs.

Description of diesel truck model components

An overview of the D-ICET model is given in Figure 2.2. The main model components are the vehicle body, wheels, trailer, engine, engine control unit, transmission and transmission control unit. The driveline is contained within the vehicle and trailer blocks. The original template for a conventional truck was obtained from the GT-DRIVE+ package and its components were edited to suit the objectives of the research project. A brief description of each component modeled is given below.

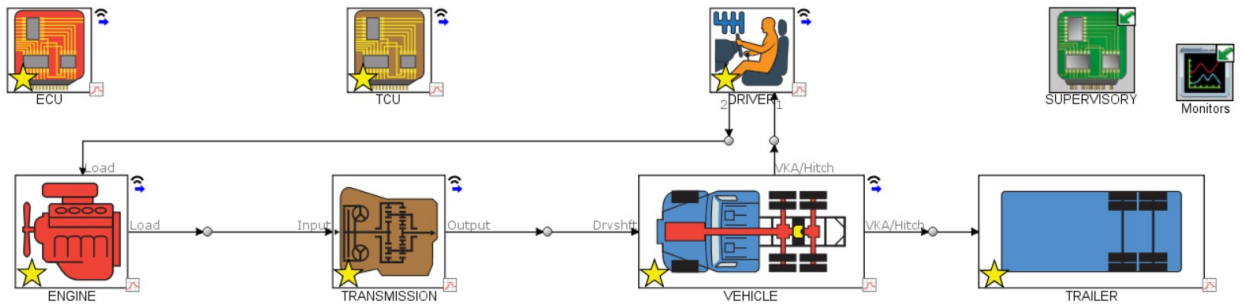

Figure 2.2. Diesel model overview

The heavy-duty diesel engine was modeled using engine map-based approach. Thus, no detailed, predictive simulation of the air path, the combustion process, or NO_x emissions is carried out, but steady-state engine maps are used to describe e.g. the engine performance, friction and fuel consumption characteristics. The baseline engine map used for the model represents a contemporary heavy-duty diesel engine, and the engine maps were obtained through collaboration with IAV GmbH. The selected, 12 L class heavy-duty diesel engine features charge air cooled turbocharging, high pressure EGR and has peak torque of 2600 Nm and rated power of 370 kW. An overview of the engine properties is presented in Table 2.2.

An overview of the steady state engine behavior regarding selected parameters is presented in Figure S18. The calibration of the engine has been conducted to maximize the brake efficiency values while considering the engine-out NO_x emissions targeting current, US10 / Euro VI emissions limits. Accordingly, the peak brake efficiency of the engine is 44 %, which is reached at 1200 RPM and at 200 kW. In this operation range moderate EGR rates are used and the resulting engine-out NO_x emissions are 10 g/kWh.

The appropriate size of the engine was determined by the engine power and torque requirements over the USLHC8 drive cycle. Simulations across the USLHC8 were limited to no more than a 1 mph average absolute error. The output space of these simulations is depicted in Figure S7. Based

Table 2.2. Specification of selected HD diesel engine

Engine feature	Value
Displacement	12 L class
Number of cylinders	6
Number of valves	4 per cylinder
Compression ratio	18.5:1
Injection system	Direct injection, common rail
Charging system	Turbocharged, charge air cooled
Exhaust gas recirculation (EGR)	Cooled, high pressure EGR
Maximum brake torque	2600 Nm between 1100 and 1300 RPM
Rated power	370 kW at 1600 RPM

on this figure and the 99th percentile requirements, the engine max power and torque requirements was determined to be least 350kW and 2000Nm.

A conventional US10 / Euro VI exhaust aftertreatment system (EAT) consists of a diesel oxidation catalyst, a particulate filter, an urea doser, a selective catalytic reduction aftertreament system (SCR) catalyst and an ammonia slip catalyst. An EAT system of this kind has a significant throttling effect downstream the turbine and, thus, increases the pressure level after the turbine – typically leading to a drop in break thermal efficiency (BTE). Although an EAT system model is not directly included in the Diesel Truck Model, its negative effect on brake thermal efficiency is considered in the engine maps (e.g. regarding BTE). Furthermore, using the above mentioned EAT layout ensures compliance with US10/Euro VI emission limits as shown also by the authors in previous works [36–38].

The engine control unit is implemented to increase fuel economy by mediating engine idling and fuel cutting. Fuel cut occurs one second after coasting and fuel resume occurs at 700 RPM. Fuel cut also occurs at 2000 RPM to keep the engine from rotating past its max speed.

Power auxiliaries are modeled to generate a negative torque on the engine and include the A/C, pumps, and fans. The average auxiliary power is 5 kW over the USLHC8. An 18-speed manual transmission based on the Eaton Heavy-Duty Super 18 is used in this study. The gear efficiency is assumed constant across all gears and is 0.97. The clutch's maximum static torque is rated at 3000Nm. The transmission control unit (TCU) was implemented in GT-Suite using the TCU-Manual template and functions to execute the shifting schedule.

The average curb weight of long-haul class 8 tractors was defined as 19,500 lb by adding the fuel weight [39] to the average dry tractor weight of 17,500 lb from [40]. This is consistent with standard heavy-duty sleeper tractors such as the 2011 Freightliner Cascadia 133 [41]. The average payload for class 8b trucks was defined as 40,600 lb using the most recent dataset from the SmartWay program [42].

The parameters, aerodynamic drag coefficient and projected frontal area, were defined as 0.6 [25, 43, 44], and the projected frontal area was defined as 9.2 m2 [44, 45] for an average long-haul class 8 tractor-trailer. The rolling resistance coefficient was assumed to be independent of the vehicle powertrain and defined as 0.007 in accordance with the NAP [46]. Similar values are reported by Zhao et al. [47].

Shifting Optimization

Simulations were designed to optimize fuel economy with performance as a constraint. The goal for the shifting strategy is therefore to operate the engine in its most efficient region. Two approaches were considered in designing the shifting strategy. The first approach is based on constant RPM upshifting and downshifting. Downshifting was explored between 600 and 1000 RPM, while upshifting, ranged from 1600 to 2000 RPM. The second approach considered GTSuite's built-in shift schedule generator, which optimizes shifting by considering acceleration potential and fuel economy in each gear at various vehicle speeds through static analysis.

With a shifting strategy set, the final drive and transmission gear ratios were optimized to further improve the fuel economy. Top gear ratios were chosen to optimize over due to the nature of long-haul driving cruising at high vehicle speeds for the majority of operation. The number of top gear ratios was determined using k means clustering for RPM, velocity, torque, and power over the drive cycle. Using the elbow method, the minimum number of clusters and therefore minimum number of top gears was chosen.

A case sweep over the top transmissions and final drive ratios was performed to obtain an output space of fuel economies. The highest fuel economy from these results was used to find the initial point for optimization while ensuring a global optimum from the optimizer.

Projected fuel economies

This study considers the powertrains of heavy-duty long-haul trucks in three different scenarios: present, mid and long term. Future fuel economy is based on the current simulated value, and increases proportionally to the increase in engine peak efficiency and added fuel economy of the waste heat recovery (WHR) system.

The current baseline for comparison of engine peak efficiency is 44% . The mid-term peak BTE is assumed to be 55% and is based on the Department of Energy (DOE) project, SuperTruck II [48]. A BTE of 60% is assumed for the long term and is based on projections set by the Department of Energy as stated in their 21st Century Truck Partnership [49], although efficiencies as high as 66.9% have been modeled in the most ideal scenarios [50].

2.3.4 Diesel truck emission modeling

This study considers greenhouse gas emissions produced during the fuel production process, well-to-pump (WTP), and emissions from combusting the fuel as the vehicle operates, pump-to-wheel (PTW). The entire process consisting of fuel production and vehicle operation is known as WTW, and is a primary output of this study.

The Greenhouse Gases Regulated Emissions and Energy Use in Technologies Model (GREET) is the primary tool used to calculate WTP emission intensities. GREET allows for the customization of production pathways. Ultra-low sulfur diesel #2, renewable diesel, and biodiesel20 (BD20) are considered in this study. All fuel pathways consider emissions from agricultural impacts, land use change, feedstock and co-product transportation, fuel production, fuel distribution, storage and fuel use. The fuel use (PTW) value for diesel is derived from the EIA carbon dioxide emission coefficient at 10.19 $kgCO_2eq/gal$ [51], however this value is offset by carbon fixation for biofuels during the feedstock growing process.

The WTW emissions in gCO_2eq/mi are therefore calculated as the sum of WTW and WTP deriving from Equations 2.1 and 2.2.

$$WTP = 3.79\frac{ED \times EI}{FE} \tag{2.1}$$

$$PTW = \frac{CI}{FE} \tag{2.2}$$

Where ED is energy density in kWh/L, EI is emission intensity calculated by GREET in gCO_{2eq}/kWh, FE is the fuel economy in mi/gal, and EC is the emission coefficient of diesel fuel in $kgCO_{2eq}/gal$.

2.3.5 Diesel Truck Total Cost to Society Model

This study uses a TCS analysis to combine operating cost, capital cost and the social cost of GHG emissions. A conservative discount rate of 7% is used and based on recommendations by the White House's Office of Management and Budget [52]. Assumptions for each cost consideration vary by year and are included in the present, mid term, and long term. More details about the techno-economic estimates are provided in the supplementary information.

Operating Cost

The operating cost is broken down into labor, maintenance & repair, fuel, permits, licenses and insurance. Table 2.3 lists the cost data for these parameters based on survey data from The American Transportation Research Institute (ATRI) [53]. Detailed equations for total operating cost estimates are given in the supplementary information. The fuel cost for the present scenario was based on the retail price on highway of the ultra-low sulfur diesel by 2020 [54]. For the mid and the long

term, the diesel cost was taken from the EIA Annual Energy Outlook projections out to 2050 [55]. The present-day cost of renewable diesel was taken from the plant gate cost and the addition of the average distribution cost reported by NREL [56]. As for biodiesel BD20, the fuel cost was based on the DOE's report on alternative fuel price published in 2020 [57]. Taxes and subsidies are excluded from the total cost to society because taxes and subsidies are internal transfers; therefore, they do not contribute to the TCS.

Table 2.3. Operating and capital cost parameters

Item	Values in each scenario			Unit	Reference
	Present	Mid-term	Long-term		
Aftertreatment cost	5782	7297	9118	USD	[58, 59]
Engine price density	34.62	46.41	51.37	USD/kW	[60]
Fuel tank cost	6.00	6.00	6.00	USD/kg	[21]
Maintenance and repair	0.14	0.14	0.14	USD/mi	[53]
Labor	0.69	0.69	0.69	USD/mi	[53]
Tolls	0.03	0.03	0.03	USD/mi	[53]
Permits and licenses	0.02	0.02	0.02	USD/mi	[53]
Insurance	0.07	0.07	0.07	USD/mi	[53]
WHR system (15 kW)	5900	5900	5900	USD	[61]
18-speed automated manual transmission	10250	10250	10250	USD	[62]
Diesel cost	1.99	2.73	3.13	USD/gal	[54, 55]
Renewable diesel cost	3.14	4.31	4.94	USD/gal	[56]
Biodiesel BD20 cost	2.53	3.47	3.98	USD/gal	[57]

Capital Cost

The capital cost considers the engine, aftertreatment, transmission, waste heat recovery, fuel tank, and glider manufacturing costs. Special attention is given to powertrain components that are assumed to experience major change as time progresses, such as the engine and aftertreatment. A manufacturing cost for the engine as a function of engine peak power was derived by Argonne's Energy Systems Division in collaboration with the International Council on Clean Transportation (ICCT) [63]. Cost increases due to efficiency are taken into consideration and are shown in Figure S10b. The region defined by the first slope considers the EPA/ NHTSA's suggestions for fuel economy improvements based on the Phase II Rule requirements [64]. The region defined by the second slope is internally derived by Argonne National Lab [60].

The aftertreatment system cost is based on a manufacturing cost analysis performed by the ICCT [58]. For the present-day scenario, the aftertreatment cost as function of power is depicted in Figure S10a. While future emission regulations are uncertain, this paper assumes that the medium and long-term efforts to improve aftertreatment are primarily to meet Euro VII limits.The estimated incremental cost of the aftertreatment system for these scenarios is found in [59]. Particularly for the long-term scenario, two SCR-configuration was assumed for the Euro VII emission control system.

Cost of GHG emissions

The future damages of CO_2 emissions are typically translated into economic terms through metrics such as the abatement cost, carbon tax and social cost of carbon (SCC) [65]. Values available in the literature for these metrics are depicted in Figure S11. In this work, the SCC metric was used to estimate the present monetary value of the GHG emissions from each powertrain option over years. The TCO has been predominantly used for climate policies and regulations in the U.S., and to define zero-emissions credits in states such as Illinois and New York [66, 67]. This metric is calculated through integrated models that predict CO_2 emission trajectories over time and its relationship with economic growth, which refer to climate and socio-economic modules in modular frameworks, respectively. They also determine the climate damages associated to these emissions within the damage module and translate them into present values using rates defined within the discounting module [68]. While the TCO is highly dependent on parameters such as time preference, discount rates, and climate sensitivity, it offers a clarifying baseline to underpin cost-benefit analysis of climate actions. In this work, the SCC values are chosen based on estimates from the U.S. Government for the years 2020 through 2050 [69]. Therefore, the social cost of a metric ton of CO_2 is 51, 62 and 85 in 2020 dollars for the present, mid and long term using an average discount rate of 3%.

2.4 Results & Discussion

2.4.1 Drive Cycle Development

Figure 2.3 displays the KS statistics values for the USLHC8 and the drive cycles from the literature. The USLHC8 shows a significantly higher representativeness relative to the defined national average driving profile when compared to all other considered drive cycles in terms of both vehicle speed distribution and the road grade distribution. Regarding the vehicle speed, USLHC8 showed a lower KS test value than HHDDT, HWFET and NESCCAF by approximately 44, 12 and 32%, respectively. The NESCCAF is the only other drive cycle in consideration consisting of both a vehicle speed and road grade trace.

The control drive cycle was selected in particular because it achieves a vehicle speed KS score

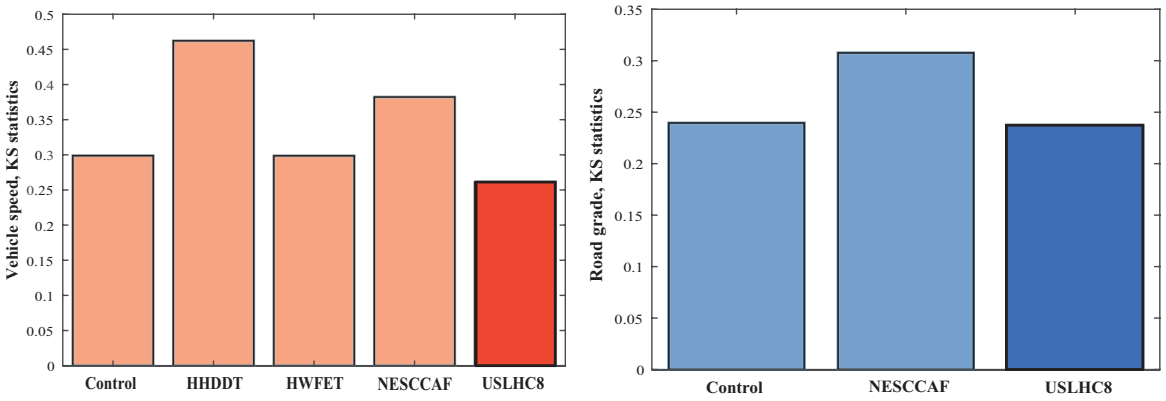

(a) Vehicle speed

(b) Road grade

Figure 2.3. Comparison of KS test for different drive cycles

very similar to the HWFET KS score. The HWFET cycle has the second-best vehicle speed KS score after the USLHC8. The control cycle has an error value of 1.1775, which is about 122 % greater than the USLHC8 error value of 0.5311. Yet, the control cycle has a vehicle speed KS score that is just as good as the next best drive cycle from the literature. The road grade KS score of the control cycle is even about 23 % lower than the NESCCAF KS score. After running the microtrip randomization and evaluation algorithm more than 50 times, the resulting error values only deviated from each other by less than 5%. Therefore, a 122 % increase in the error value is an extremely unlikely result of the algorithm. This proves a very high robustness of the presented methodology in terms of generating drive cycles with a high degree of representativeness relative to the defined national average driving profile. Moreover, the generated degrees of representativeness are consistently higher than those of drive cycles from the literature.

The selected final drive cycle "US Long-Haul Class 8" (USLHC8) is shown in Figure 2.4, and compared with other drive cycles in Table 2.4. The USLHC8 covers a total distance of 599.43 miles, which is over seven times longer than the NESCCAF cycle. It has an average vehicle speed of 55.56 mph, similar to the average vehicle speed of the defined national average driving profile at 60 mph. USLHC8 achieved a maximum vehicle speed of 70.87 mph, which along with the NESCCAF, is the closer value to the limit of 80 mph in the national average profile. The total driving time at 10 hours and 47 minutes (38840 seconds) is slightly below the maximum legal driving window of 11 hours.

The USLHC8 exhibits a distinguished segment of urban driving at either end. These segments show significantly more acceleration and deceleration as well as lower speed driving. Both urban segments are similar in length at about 2,000 seconds. The urban driving in each segment includes short and interrupted highway sections which model metropolitan traffic and the changing of highways. The remaining long-haul segment in the middle consists of prolonged highway driving which

is only interrupted by very few stops. These may represent stops necessary for refueling or the truck operator's personal needs. For the most part, the long-haul segment exhibits steady driving. Two long-haul segments of USLHC8 cover highway speeds at about 55 mph and one segment comprises of driving at about 65 mph. The last long-haul segment of USLHC8 also accounts for more transient long-haul driving towards the end of the cycle ranging from about 40 mph to about 70 mph.

Most USLHC8 road grade values are between -3% and +3%. However, there are also road grade values up to -6% and +6%. Most of these high values are part of urban segments where more extreme grades may be more common than on the highway.

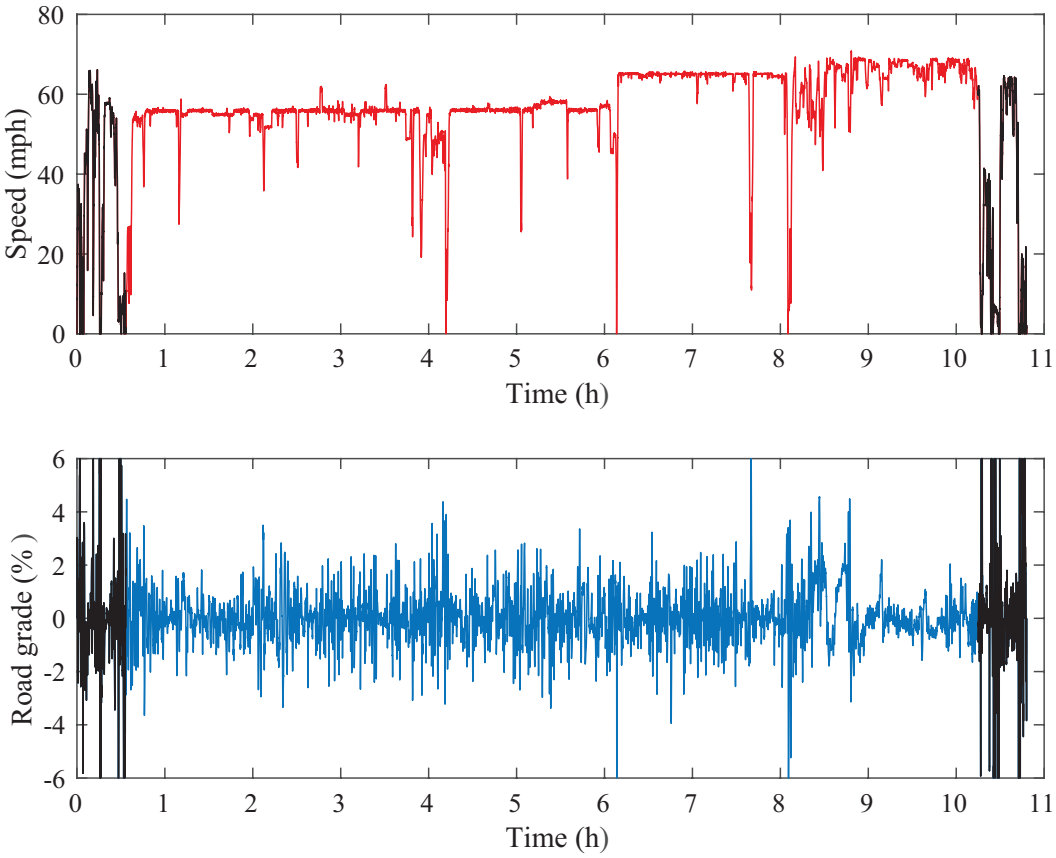

Figure 2.4. Long-Haul Class 8 Drive Cycle (USLHC8). Urban segments are shown in black, highway speed is shown in red, and highway grade is shown in blue.

Despite these differences between USLHC8 and drive cycles from the literature, it must also be noted that the overall spread in between the drive cycles is not too large. The USLHC8 vehicle speed KS statistic is about 1.8 standard deviations away from the mean of the literature drive cycle KS statistics. Consequently, it can be concluded that the deviation of USLHC8 from literature drive cycles is within reasonable limits.

Table 2.4. Properties of USLHC8 and drive cycles commonly used in the literature

Drive cycle	Vehicle speed KS statistic	Road grade KS statistic	Distance (miles)	Time (s)	Average vehicle speed (mph)	Maximum vehicle speed (mph)
HHDDT	0.4622	n.a.	23.07	2084	39.86	59.3
NESCCAF	0.3822	0.3076	72.51	6830	38.22	70.2
HWFET	0.2986	n.a.	10.26	765	48.3	59.9
USLHC8	0.261	0.237	599.43	38840	55.56	70.87

2.4.2 Diesel heavy-duty truck model

The engine power distribution over the UCLHC8 drive cycle is shown in Figure S18 and is typically within the range of 70-170 kW. From this power map, the red lines underline the envelop for the majority of potential engine operating points. The red envelop corresponds to one standard deviation from the mean of the engine power distribution. The maximum fuel economy occurs at 1200 RPM, according to the efficiency map.

Shifting optimization

The RPM upshifting and downshifting approach led to fuel economies of up to 7.33 mpg, achieved when upshifting at 1600 RPM and downshifting at 600 RPM. Figure S6 depicts the fuel economy ranges at different RPM. The second approach using GT-Suite resulted in fuel economy of 7.45 mpg. The generated shift schedule is provided in Figure S7. Because this method resulted in higher fuel economy and satisfied performance constraints, this shifting schedule was used in the final model.

For the case sweep, the top three gears along with the final drive ratio were selected according to the elbow point (see Figure S8). The output space of this optimization is presented as a histogram given in Figure S9. The highest fuel economy obtained from the case sweep was 7.49 mpg for a final drive, 16th gear, 17th gear, and 18th gear ratios of 3.1, 0.9, 0.86, and 0.75 respectively. These values served at the initial guess for the optimization and ranges for optimizer variables included ± 0.1 of these values. The optimization was a maximization of fuel economy under the constraint of 2.0 mph average error over the drive cycle. The optimization resulted in an optimized fuel economy value of 7.51 mpg at gear ratios of 3.04, 0.82, 0.75, and 0.71 for final drive, 16th gear, 17th gear, and 18th gear ratios respectively (see Table S5). The operating points with a fuel economy of 6.82 mpg for the default Eaton-Super18 are show on the left and operating points with a fuel economy of 7.51 mpg using the optimized 18 speed transmission are shown on the right in Figure 2.6.

Table 2.5 compares fuel economy and average error of the USLHC8 and other cycles. The

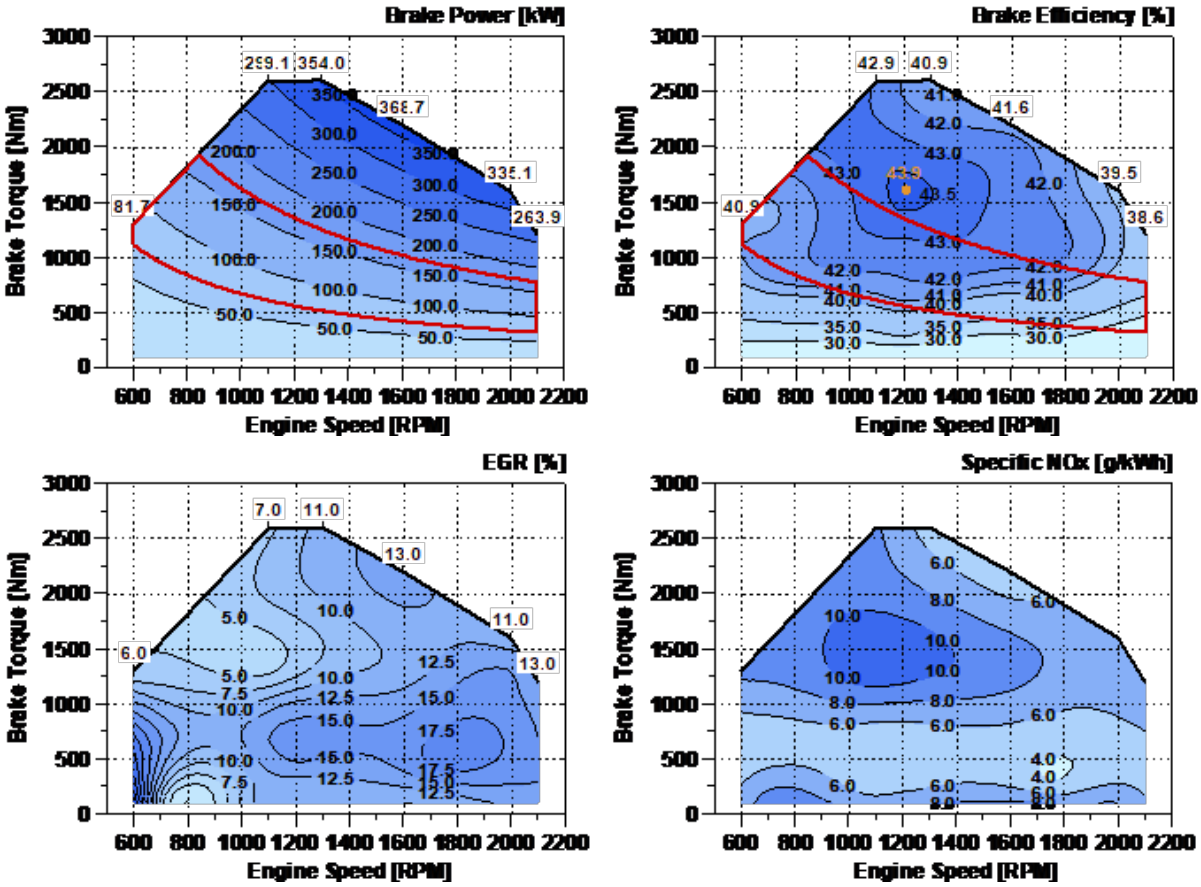

Figure 2.5. Power and efficiency map of the diesel engine

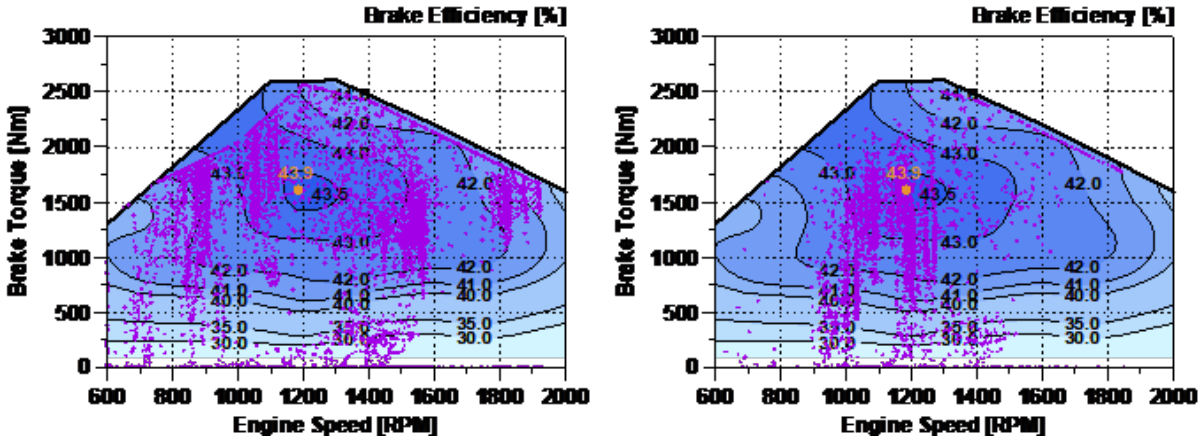

(a) 6.82 mgp **(b)** 7.51 mpg

Figure 2.6. Operating points for different fuel economies

USLHC8 shows the best fuel economy and second lowest error amongst the drive cycles considered in this study. The NESCCAF cycle has the second highest fuel economy and lowest error. Its artificially modal segments disregard transient power spikes and troughs leading to overly optimal performance and fuel economy; however, it is slightly worse in fuel economy than the USLHC8 since the gear ratios were optimized for the USLHC8. The NESCCAF cycle should only be used to derive an upper limit to long-haul fuel economy. The recent NREL cycle that was developed using the same ROL data as the USLHC8 cycle, exhibits nearly 7% lower fuel economy than the USLHC8 cycle and an average error over six time higher. The NREL cycle contains speeds primarily at 65 mph while the USLHC8 cycle contains a bimodal distribution for speeds of 55 and 65 mph. Higher speeds and an idling section likely account for the NREL cycle's decrease in fuel economy relative to the USLHC8 cycle. The HDUDDS significantly has the lowest fuel economy at 5.38 mpg. This is due to its stop and go driving behavior and lack of sustained highway driving. The HWFET has one of the model's highest errors, missing the cycles by an average of 1.96 mph. This is largely because it is a cycle developed for light duty vehicles with much higher acceleration potentials. This cycle should not be used for heavy-duty simulation; however, it has been due to the absence of long-haul cycles at sustained high speeds.

Table 2.5. Model fuel economies over literature drive cycles

Drive cycle	Fuel Economy (mpg)	Average Error (mph)
USLHC8	7.51	0.52
NREL	6.96	3.25
HDUDDS	5.38	1.68
NESCCAF	7.49	0.15
HWFET	7.20	1.96

Sensitivity Analysis

A sensitivity analysis was performed to test the vehicle under different conditions (see Figure 2.7). The payload was varied from 0 kg, representing an empty truck, to 27,200 kg, representing a fully loaded truck. The fuel economy without load and fully loaded was 9.95 and 6.41 mpg respectively. The drag coefficient represents a proportionality constant between velocity and air resistance and was varied between 0.5 and 0.7 with resulting fuel economies of 8.13 and 6.89 mpg respectively. Vehicle frontal area was also included and was varied from 8 m^2 to 10 m^2 with resulting fuel economies of 7.04 and 7.93 mpg respectively. Rolling resistance coefficient was varied between 0.006 and 0.008 with resulting fuel economies of 7.15 and 7.98 mpg respectively. Finally, road grade was excluded, as many drive cycles do not include road grade. Without road grade, the fuel economy

resulted in 7.53 mpg.

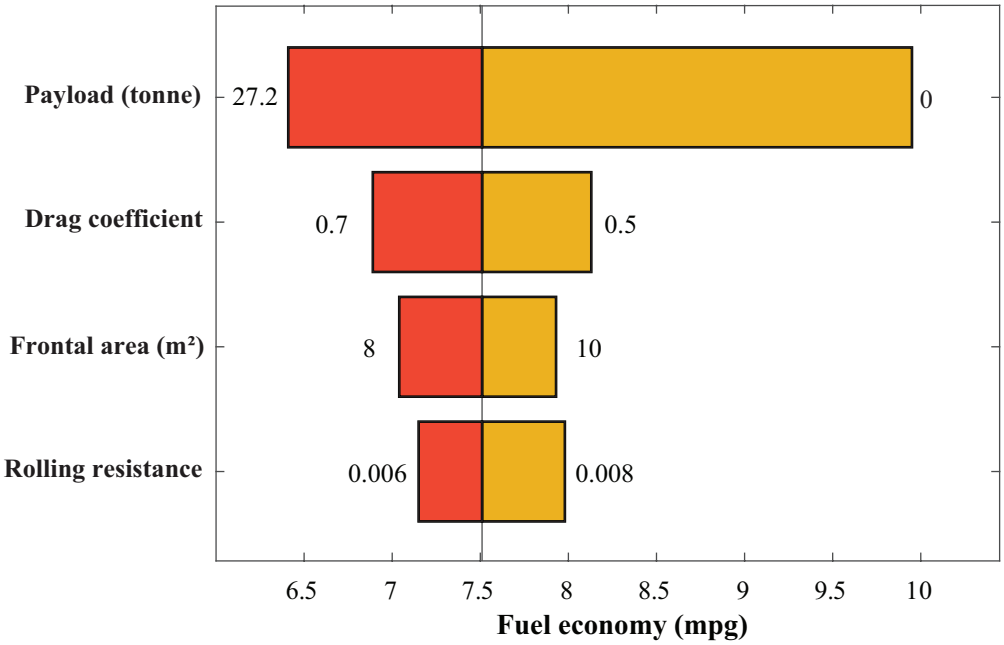

Figure 2.7. Effect of design parameters on fuel economy

Projected fuel economies

The calculated fuel economy for the present-day D-ICET model was 7.51 mpg. Future fuel economies are projected to be 9.59 and 10.46 mpg for the mid and long term, respectively. These increases are mainly due to engine improvements as other powertrain components such at the transmission already operate with efficiencies near unity. The heat recovery system added in the mid and long-term scenario improves fuel economy by powering the auxiliary load using waste heat. Similar improvements in the fuel economy of diesel long-haul trucks have been reach in the context of DOE's SuperTruck projects. For example, the Cummins-Peterbilt team reported fuel economies ranging between 9.2 and 10.7 mpg in real driving conditions, while the Daimler team achieved a higher fuel economy of 12.2 mpg [70]. Recent publications have also projected advances in present-day technologies that lead to higher freight efficiencies and better diesel engine performance. For instance, Tong et al.[71] estimated the fuel consumption of different designs for long-haul diesel trucks with modifications in empty vehicle weight, rolling resistance and frontal area. They reached fuel economies ranges between 4.1 and 7.0 mpg for current models, while the advanced design showed energy efficiencies between 4.9 and 8.9 mpg.

2.4.3 Well to Wheel Emissions

Figure 2.8 shows the emissions associated with fuel production (WTP) and fuel combustion during use (PTW) for the diesel long-haul truck. Using conventional diesel led to WTW emissions of 1507, 1180 and 1081 gCO_2eq/mi for the present, mid and long term, respectively. Renewable diesel has the lowest emissions followed by biodiesel (BD20). While renewable diesel serves as a low carbon option for the diesel powertrain, it is not zero emissions.

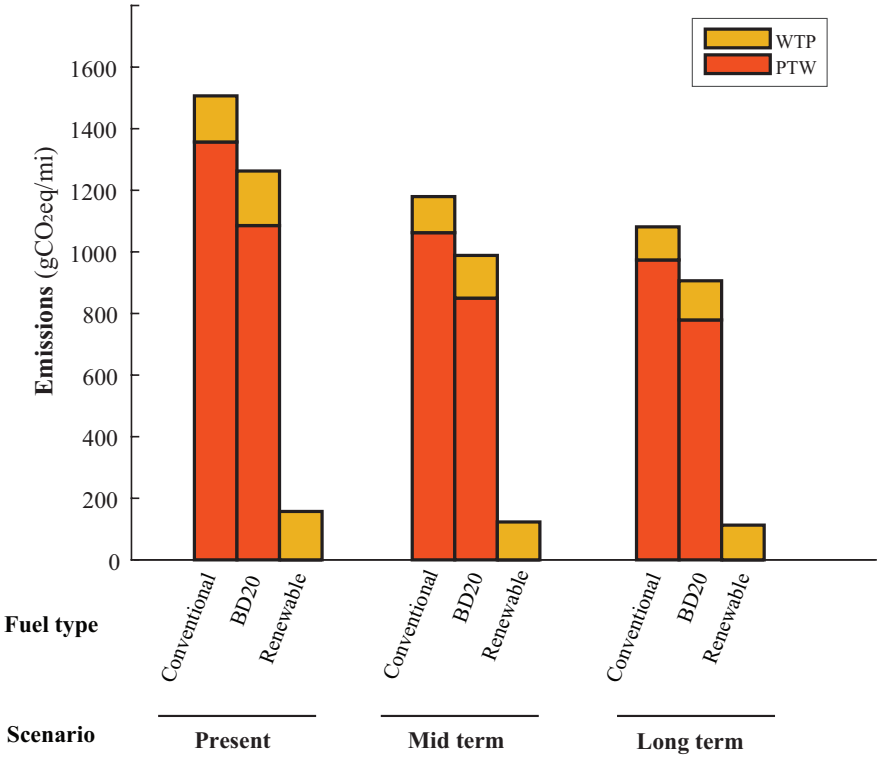

Figure 2.8. Total WTW emissions

The pump to wheel emissions are offset by carbon fixation during the fuel growing process, however the well to pump emissions associated with processing and transporting the fuel remain. Because WTP emissions remain, these emissions would have to be offset by other means to achieve economy wide zero emissions. Since WTW emissions are highly dependent on vehicle models, design attributes and drive cycles, a wide range of values is found in the literature for diesel powertrains. Liu et al.[72] derived WTW emission for different heavy and medium duty trucks following the driving patterns of three standard US. cycles from EPA and CARB. For the Class 8 long-haul trucks, the total GHG emissions reached 1846 g/mi, of which 1521 g/mi correspond to the vehicle use. Camuzeaux et al. [73] also compared the GHG emissions of diesel and natural gas heavy-duty trucks using three different engine configurations. One of these engine configurations is commercially designed for long-hauling and reached WTW emissions of close to 2000 gCO_2eq/mi. In the context of the UK freight operation, Langshaw et al.[15] estimated WTW emissions above 1000 gCO_2eq/mi for

both diesel and LNG engines, with PTW emissions contributing the most to the total environmental performance of these powertrains.

2.4.4 Total Cost to Society

The capital cost for the present, mid-term, and long term slightly increase in time and are roughly $125,400, $137,000, and $140,500 (see Figure 2.9). The glider makes up the majority of the capital cost at $95,000 and was included to achieve total amounts. However, the analysis focused on powertrain components and their potential over time. The largest powertrain cost is attributed to the engine.

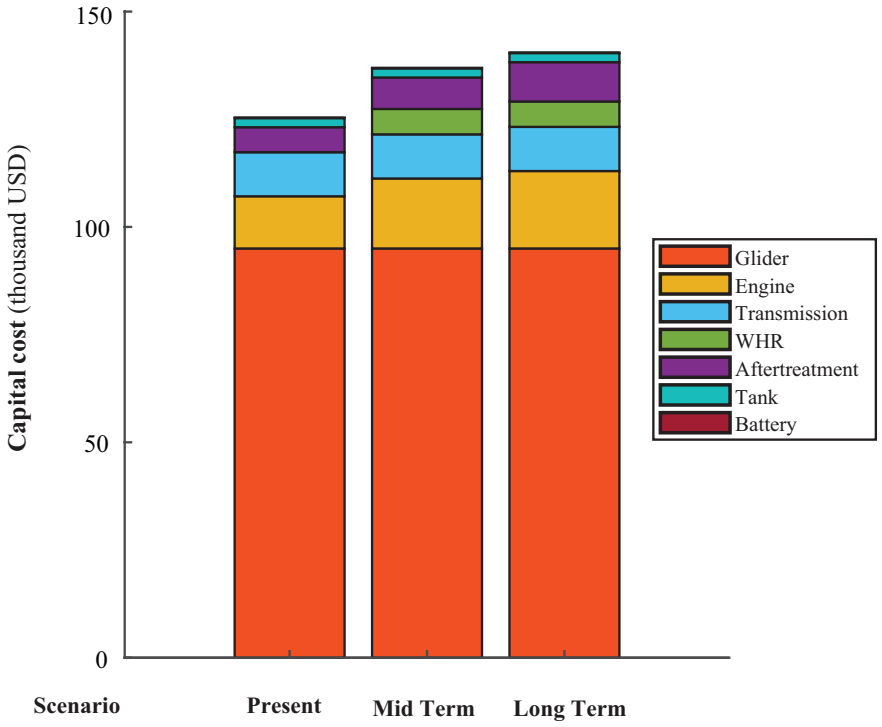

Figure 2.9. Capital costs

The engine costs roughly $12,000 in 2020 and increases to nearly $18,000 in the mid term projection. This increase is due to technology improvements to increase fuel economy and emission requirements [74]. The waste heat recovery system increases fuel economy by using wasted heat generated by the engine to generate electricity to power the auxiliary electronics. The waste heat recovery system increases the capital cost by 6,000. Also included in the capital cost are the fuel tank, transmission, aftertreatment, and battery.

As shown in Figure 2.10, the operating cost for the time scenarios remains relatively constant and are roughly constant. Labor is the largest operating cost component followed by fuel, maintenance and repair, insurance, and fees. In the long term scenario, labor costs are expected to drastically decrease due to autonomous driving; however, the scope of this study is limited to powertrain and

fuel variations. The price of all fuels is expected to increase in time; however, the fuel economy increase from engine improvements offsets the fuel price increase. Renewable diesel leads to the largest operating cost for all time scenarios followed by diesel, and BD20.

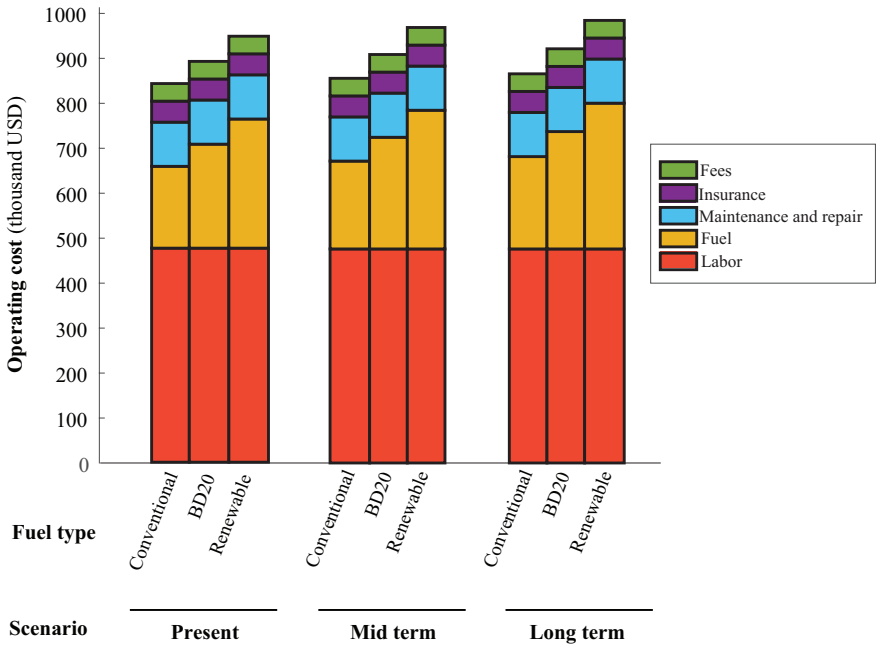

Figure 2.10. Operating costs

Figure 2.11 shows the total cost to society of the diesel powertrain using the conventional and alternative fuels. While the carbon cost penalizes emissions more severely in the long-term, they are still insufficient to offset the higher operating cost when renewable diesel is used instead.

A recent comprehensive total cost of ownership analysis was performed by Argonne National laboratory. The results of this study are compared to Argonne's in Figure 2.12. The Argonne model considers additional costs relative to the MIT model including taxes and financing over time. Taxes are not included within the MIT model because the model will serve as a comparison baseline to alternative powertrains where future taxing methodologies are largely uncertain. When the MIT model is equipped with Argonne parameters, results are within 5% of each other. The MIT model with MIT parameters differs from the Argonne model with Argonne parameters by roughly 30%. Major differences in input parameters include the discount factor, fuel economy, and diesel fuel cost. The Argonne model used a discount factor of 3%, whereas the MIT model uses 7%. The fuel economy used within the Argonne model is nearly 15% lower than the MIT model. This difference is attributed to driving patterns as the Argonne model considered all class 8 trucks, while the MIT model focuses strictly on long-haul operation. Finally, the diesel cost in the Argonne model includes fuel taxes which constitutes 22% of the final diesel cost. The MIT model removes the diesel tax to allow comparison to alternative powertrain and fuel combinations.

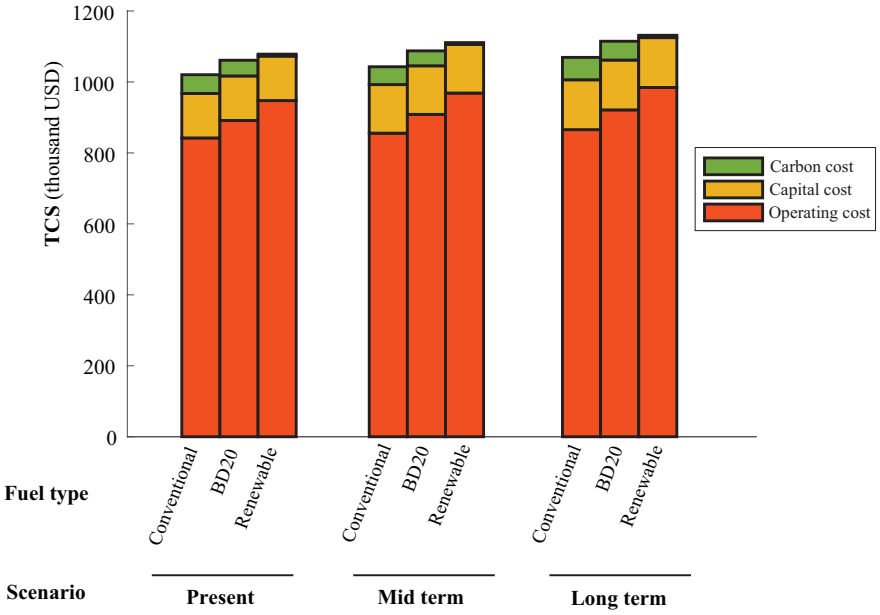

Figure 2.11. Total Cost to Society

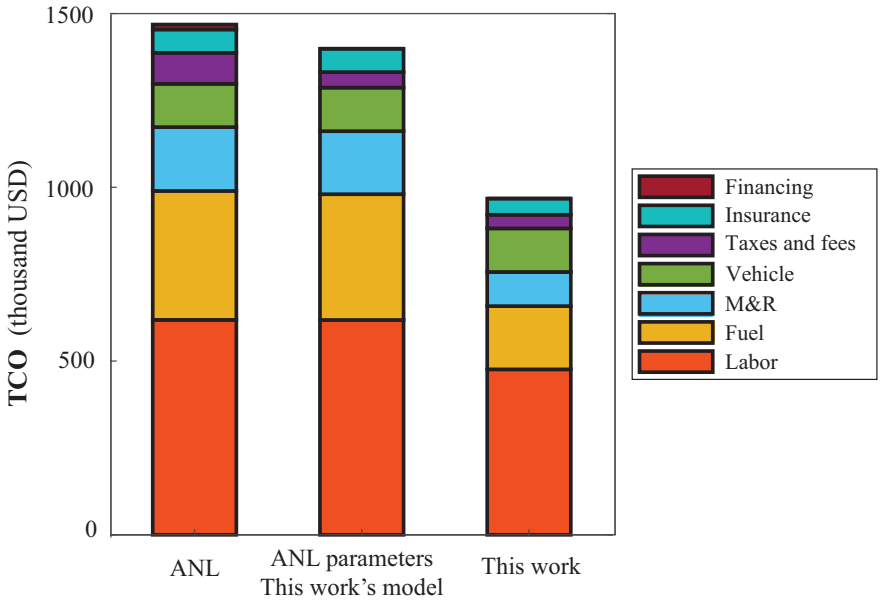

Figure 2.12. Comparison of TCO with other works

2.5 Conclusions

In this work, the US long-haul trucking was characterized through a set of performance metrics (e.g., daily range, driving hours, vehicle lifetime) and a representative drive cycle that describes real driving behaviors on the basis of vehicle speed and road grade. This drive cycle, named as USLHC8, is based on 58,000 miles of pre-processed real driving data from the Run On Less Regional dataset.

It covers a total distance of 599.43 miles with an average vehicle speed of 55.56 mph and a maximum vehicle speed of 70.87 mph. This drive cycle, along with data from a state-of-the-art diesel engine, were the main inputs in the system-level simulation of the powertrain. The total cost to society of the powertrain was analyzed for conventional diesel, renewable diesel, and biodiesel BD20 while projected under current, mid, and long-term scenarios. At the assumed social cost of carbon, the cost of the CO_2 emissions are not very large compared to the other costs in the long-haul trucking system. This suggests that the transition to a decarbonized long-haul trucking system may have to be driven by regulation and carbon taxes.This is similar to how other vehicle emissions are controlled primarily by standards on new vehicles.

While this work provides a comprehensive benchmark for diesel long-haul powertrains in terms of cost and greenhouse gas emissions, some limitations were identified. First, the simulation of the long-haul truck under real US. driving patterns was intended to represent the national average, and therefore, would not be representative of specific driving patterns state-wise. Second, the shift optimization during vehicle simulation was particularly for the USLHC8 drive cycle, therefore optimal performance would be different in real-world simulations with other cycles. Third, fuel costs are highly volatile for future scenarios and can be affected by political and economic instability, factors outside the scope of this paper.

In future directions, this benchmark for diesel powertrains will be compared to other powertrain options (e.g., hydrogen-powered engines and battery-electric trucks) on an apple-to-apple basis. These comparisons under different infrastructure build-out scenarios will provide insights into the competitiveness of powertrain options in the future and main drivers of this transition.

2.6 Appendix

Standard Drive Cycles

Figure S1 shows six drive cycles used on heavy-duty truck emissions modeling in the USA. The US EPA has been using the HWFET, US06 Supplemental Federal Test Procedure and (HDUDDS. The CARB HHDDT. The NESCCAF and the NREL also developed their own long-haul cycles.

Long-haul definition

The vehicle miles traveled for a 10-year life truck is given in Table S1. The daily range distribution for trucks with sleeper cab is depicted in S2

Drive cycle parameters

The target vector was defined according to the vehicle speed and absolute road grade distribution from Figure S3 and Figure S4. Descriptions of the datasets used for the target vehicle speed vector

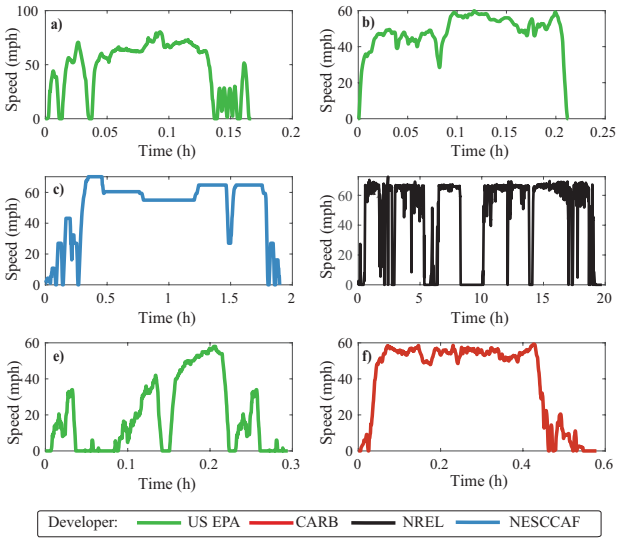

Figure S1. Standard drive cycles used for long-haul trucks: a) US06, b) HWFET, c) NESCCAF, d) NRTL, e) HDUDDS, and f) HHDDT.Source:[75–78]

can be found in Table S2. The target vector is available in Table S3.

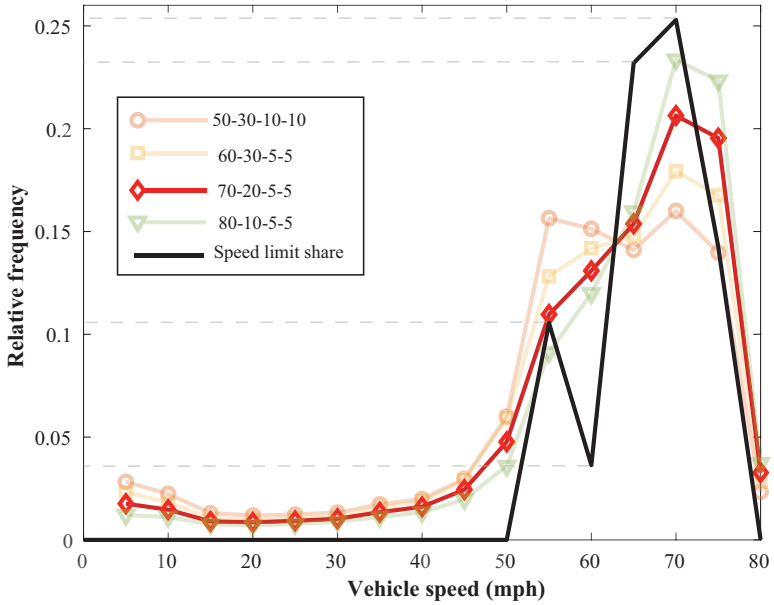

Figure S3. Vehicle speed distributions of different dataset combinations. Share distribution of HTDC (%)-ROL17 (%)-ROLR (%)-Fleet DNA (%). Selected distribution in red.

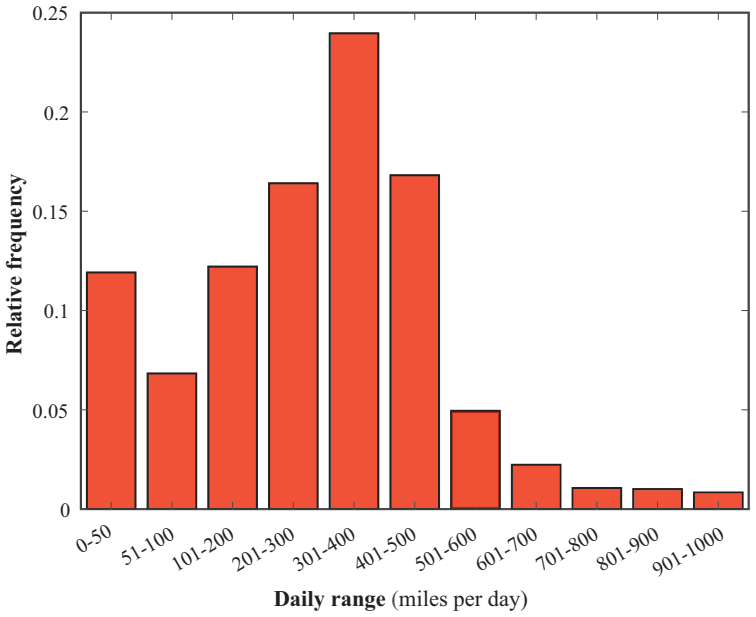

Figure S2. Daily range from VIUS mi/day considering months operated, 30.4 days in a month, and 60/7/34 work period, and sleeper cab. Adapted from [28]

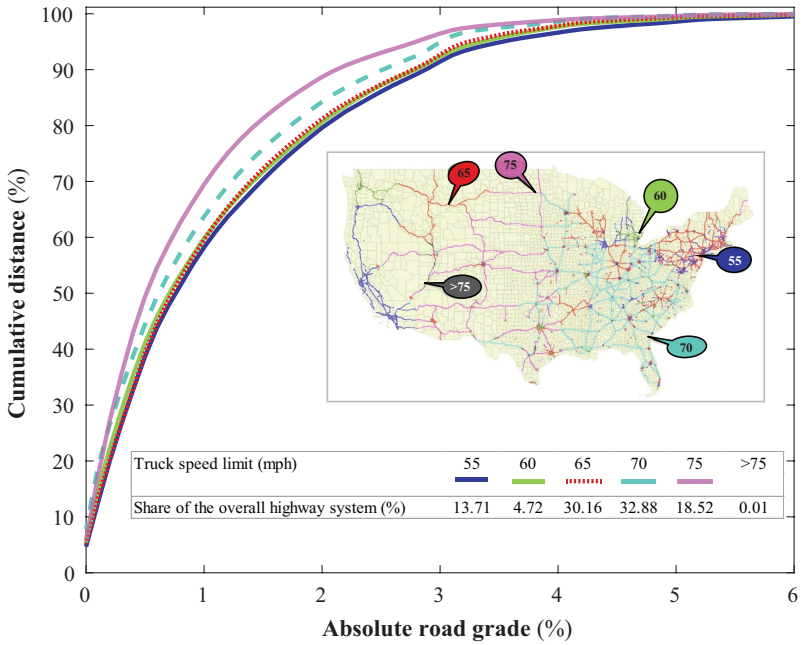

Figure S4. Activity-weighted, distance-based cumulative distribution of absolute road grade by truck speed limit. Adapted from:[13]

Table S1. Annual average vehicle miles traveled of long-haul class 8 trucks in the USA [79]

Year of vehicle life	Vehicle miles traveled
1	108,000
2	120,000
3	114,000
4	105,000
5	92,000
6	81,000
7	74,000
8	67,000
9	59,000
10	52,000

Table S3. Target vector for long-haul drive cycle construction

Target road grade vector				Target speed vector	
Interval (%)	Relative frequency	Interval (%)	Relative frequency	Interval (mph)	Relative frequency
[-6; -5)	0.000962	(0; 0.1]	0.079101	(0; 5]	0.017636
[-5; -4)	0.000524	(0.1; 0.2]	0.039151	(5; 10]	0.014692
[-4; -3.5)	0.0013954	(0.2; 0.3]	0.0341882	(10; 15]	0.009007
[-3.5; -3)	0.001678	(0.3; 0.4]	0.031951	(15; 20]	0.008556
[-3; -2.6)	0.005869	(0.4; 0.5]	0.030012	(20; 25]	0.00928
[-2.6; -2.3)	0.004532	(0.5; 0.6]	0.025255	(25; 30]	0.010288
[-2.3; -2)	0.00547	(0.6; 0.7]	0.020996	(30; 35]	0.013487
[-2; -1.8)	0.007702	(0.7; 0.8]	0.018812	(35; 40]	0.01611
[-1.8; -1.6)	0.008405	(0.8; 0.9]	0.017279	(40; 45]	0.024457
[-1.6; -1.4)	0.009555	(0.9; 1]	0.016175	(45; 50]	0.047686
[-1.4; -1.2)	0.011091	(1; 1.2]	0.013247	(50; 55]	0.10966
[-1.2; -1)	0.013247	(1.2; 1.4]	0.011091	(55; 60]	0.130886
[-1; -0.9)	0.016175	(1.4; 1.6]	0.009555	(60; 65]	0.15372
[-0.9; -0.8)	0.017279	(1.6; 1.8]	0.008405	(65; 70]	0.206397
[-0.8; -0.7)	0.018812	(1.8; 2]	0.007702	(70; 75]	0.195433
[-0.7; -0.6)	0.020996	(2; 2.3]	0.00547	(75; 80]	0.032708
[-0.6; -0.5)	0.025255	(2.3; 2.6]	0.004532		
[-0.5; -0.4)	0.030012	(2.6; 3]	0.005869		
[-0.4; -0.3)	0.031951	(3; 3.5]	0.001678		
[-0.3; -0.2)	0.034188	(3.5; 4]	0.001395		

Table S2. Overview of datasets considered for the target vehicle speed vector definition [32] [16] [80] [34]

Dataset	Description
ROL17	• 7 trucks over a period of 17 days. Over 50,107 miles of data collected • Average driving speed of 54 mph, very little time was spent at 68 mph or higher • Average mileage of 506 miles/day • Data collection with a focus on longer haul driving • Relatively good geographical coverage of the main long-haul freight routes of the US, but concentrated in the Midwest and Southeast of the US.
ROLR	• 10 trucks over a period of 18 days. Over 58,000 miles of data collected • Average driving speed of 53.21 mph, but significantly more zero-speed time and significantly higher number of stops in comparison to ROL17 • All trucks drove over 350 miles per day with an average mileage of 434 miles/day • Not a dedicated long-haul data collection. Focus on Regional-haul with more frequents stops and therefore more frequent acceleration events • Limited geographical coverage because of locally concentrated regional-haul scope.
HTDC	• 6 trucks over a period of 12 months. 637,558 miles of data collected • Average driving speed of 66.82 mph • Dedicated long-haul data collection • Very good coverage of the Southern and Eastern US, but no coverage of the West Coast of the US • Very good temporal coverage: captures seasonal variations
Filtered fleet DNA	• 12 trucks and 7247.4 miles of data collected. No information about the exact duration of the data collection period • Average driving speed of 45.57 mph • Dataset filtered to select long-haul driving, but not a dedicated long-haul data collection • Geographical coverage Heavy bias towards states on the West Coast of the US

Drive cycle construction

Data pre-processing: The Run on Less Regional (ROLR) dataset was selected because of its high-resolution data at 1 Hz for an interdependent set of variable speed and road grade. The raw data was provided under a collaboration agreement with the NACFE. A set of concatenated files for each truck was created for further data cleansing. This cleansing process includes the detection and correction of corrupt, coarse, or inaccurate data, which enables a more representative characterization of the long-haul cycles.

1. Remove duplicates and incomplete data: we excluded duplicate speed profiles and vehicle data lacking several important signals.
2. Remove unrealistic datapoints: Outliers representing the maximum possible OBD vehicle speed value of 255.99 km/h for an increment of only one second were removed from the dataset since the maximum vehicle speed in a realistic progression is 124.5 km/h. For values above 150 km/h, the datapoints were replaced by a linear interpolation of the previous and the subsequent error-free datapoints.
3. Check data quality of raw elevation signal: No extreme outliers were detected for the elevation signal, but noise. Hence, the Savitzky-Golay filter was applied to denoise the signals.

Acceleration and road grade estimation: The vehicle acceleration was calculated using the cleansed speed datapoints. The road grade (RG) was calculated from both elevation signal and vehicle speed signal. As shown in Equation S1, the road grade (%) derives from the difference in elevation (rise) divided by the difference in distance (run) between two sampling points.

$$RG(\%) = \frac{\Delta Elevation}{\Delta Distance} * 100 = tan\alpha * 100 \tag{S1}$$

Microtrips preparation: The microtrip based cycle approach was used for the construction of the drive cycle. These microtrips were prepared as follows:

1. Cutting of the ROLR data into microtrips: the datapoints with vehicle speed and acceleration of zero were used to define connecting points between consecutive microtrips. Based on these bounded points, the microtrips were cut from the ROLR data. All other datapoints were discarded.
2. Smoothing the microtrip elevation at connecting points: the elevation values were smoothed

at the connecting points to ensure that the resulting road grades were equal to zero. This leads to a more consistent sequence of microtrips and continuous road grade traces.

3. Determination of feature vector for each microtrip: the vehicle speed trace was integrated over time to obtain the total distance driven per microtrip. The average speed value was then estimated as the arithmetic mean of the vehicle speed trace. The relative frequency of each 5-mph vehicle speed interval was determined as the ratio of the total number of datapoints within a given interval to the total number of datapoints of the microtrip. Similarly, the relative frequency of the road grade intervals was calculated from the road grade trace of each microtrip.
4. Microtrips classification into long-haul and urban: the microtrips were separated into an urban pool representing the drive out of or into a metropolitan area and a long-haul pool representing the prolonged highway driving in between metropolitan areas. This distinction was made according to the criteria summarized in Table S4. All microtrips that could neither be classified as long-haul nor as urban were discarded.

Table S4. Classification criteria for long-haul and urban microtrips

Criteria	Value	Unit	Reference
Minimum long-haul distance	170	km	This work
Minimum average driving speed	40	mph	[19]
Driving time between stops	2	hours	(J. Gregorio, personal communication, Sept 5, 2021)
Complete stops on interstate	No	-	(J. Gregorio, personal communication, Sept 5, 2021)
Minimum urban distance	15	mi	This work
Total urban distance	30	mi	This work

Microtrips random selection: After the microtrip preparation process, an algorithm for the random selection and evaluation of microtrips was programmed and applied to the data. The randomized drive cycle generation process constructs drive cycles in two segments. First, the long-haul segment is generated with randomly selected microtrips from the long-haul microtrip

pool. In detail, microtrips are successively selected at random and their cumulative distance is calculated with each microtrip selection. If the sum of the current cumulative distance and the distance of the next microtrip candidate exceeds the maximum distance for the long-haul segment, the long-haul fail counter is incremented by one. The maximum long-haul segment distance is equal to the maximum total distance subtracted by the initialized urban distance. If the fail counter is greater than the initialized maximum fail counter value, the generation of the long-haul segment is terminated. It is important to consider that the described optimization for a maximum distance leads to a bias of shorter microtrips towards the end. Therefore, all microtrips of the segment are randomly reshuffled before they are concatenated. Analogous to the long-haul segment, the urban segments are generated at either end of the long-haul segment. Microtrips are also successively selected at random and then randomly added to either the beginning or the end of the already generated long-haul segment. The urban fail counter is incremented by one if adding the distance of the next candidate microtrip would exceed the maximum total distance. Microtrips from the urban pool are excluded from the process if their distance is greater than 50 % of the remaining distance until the initialized maximum. This was done after initial trial runs to increase the efficiency of the algorithm and to prevent the urban segment from consisting of only very few and long microtrips. Again, the generation of the urban segment is terminated when the maximum value of the urban fail counter is exceeded and then the generated segment is reshuffled. The urban segments are created last because the urban microtrips are significantly shorter than the long-haul microtrips. Consequently, the urban segment has a higher variability and is more adaptable to converge towards the target feature vector and towards the defined maximum distance.

Drive cycle evaluation: Through this step, each resulting drive cycle is compared to the national average driving profile. The deviation of each feature in the microtrips from the target vector is estimated and used to calculate the absolute error of the entire drive cycle. The contribution of each microtrip to the absolute error was time-weighted. Since the complete target vector accounts for 63 features, namely, distance, average vehicle speed, 16 vehicle speed distribution intervals and 44 road grade distribution intervals, weighting factors were introduced to account for the relative importance of each feature to the error. In this work, the weighting factors for distance feature, vehicle speed and road grade were set at 0.1,0.54 and 0.36, respectively. Based on these weights, a single error value is obtained for each generated drive cycle using the Euclidian norm of the weighed deviation vector. Finally, the drive cycle with smallest error was selected, and was named as USLHC8 (i.e. US Long-Haul Class 8 drive cycle).

Truck modeling

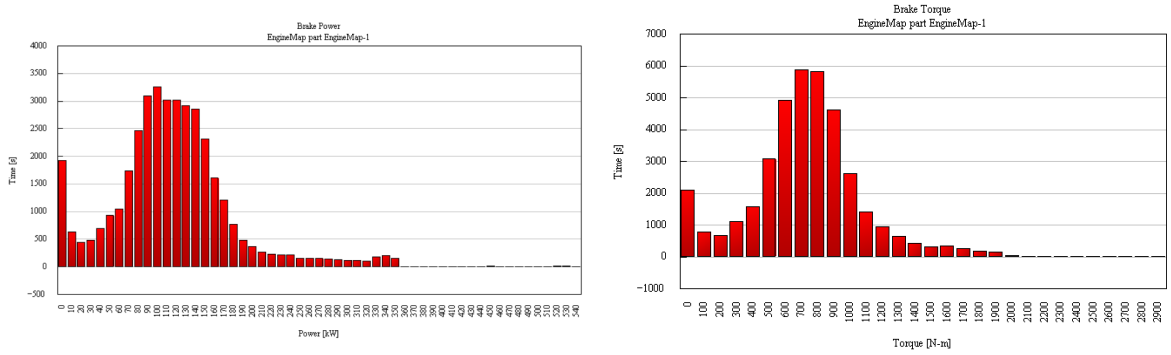

Figure S5. Output space for engine sizing

Shifting optimization

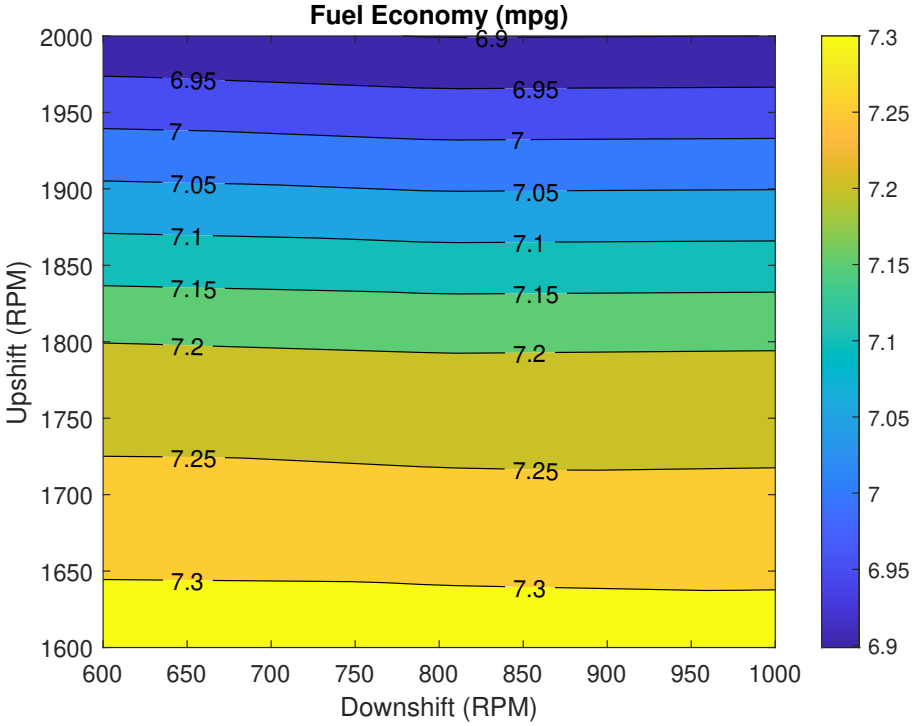

Figure S6. Effect of gear shift strategies on fuel economy

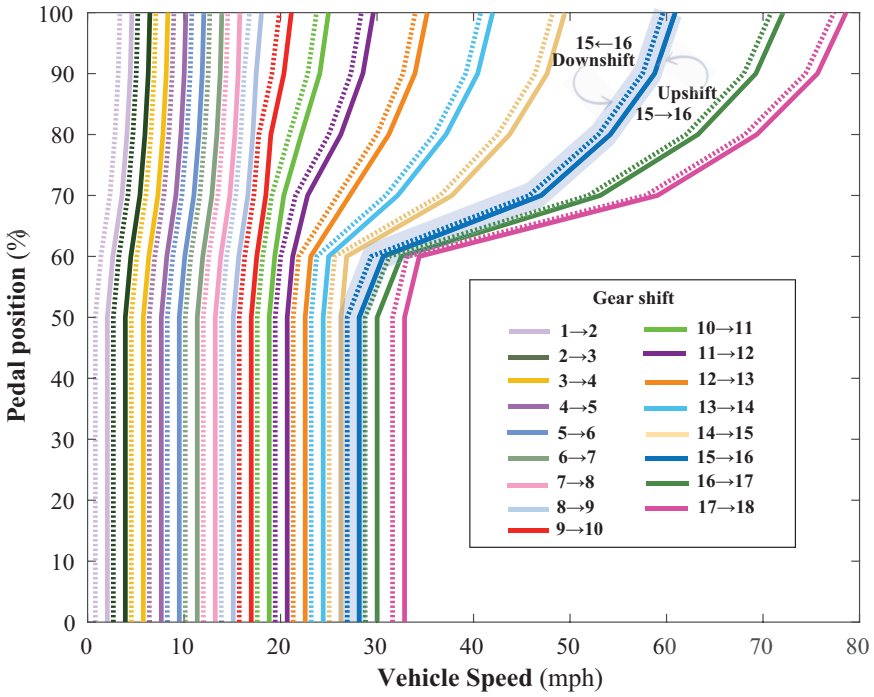

Figure S7. Shift schedule generation. Downshifting in dotted lines

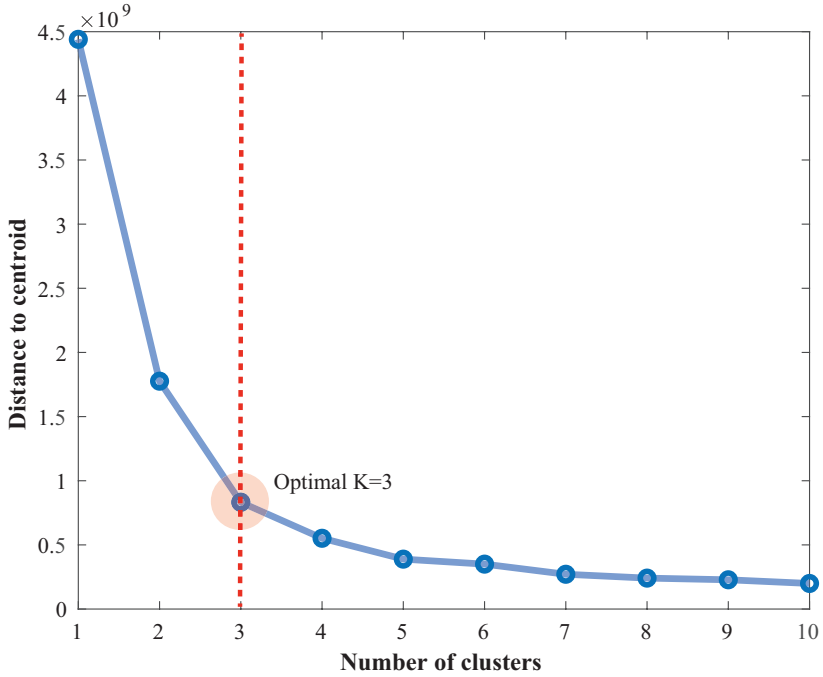

Figure S8. Optimal number of clusters using elbow method

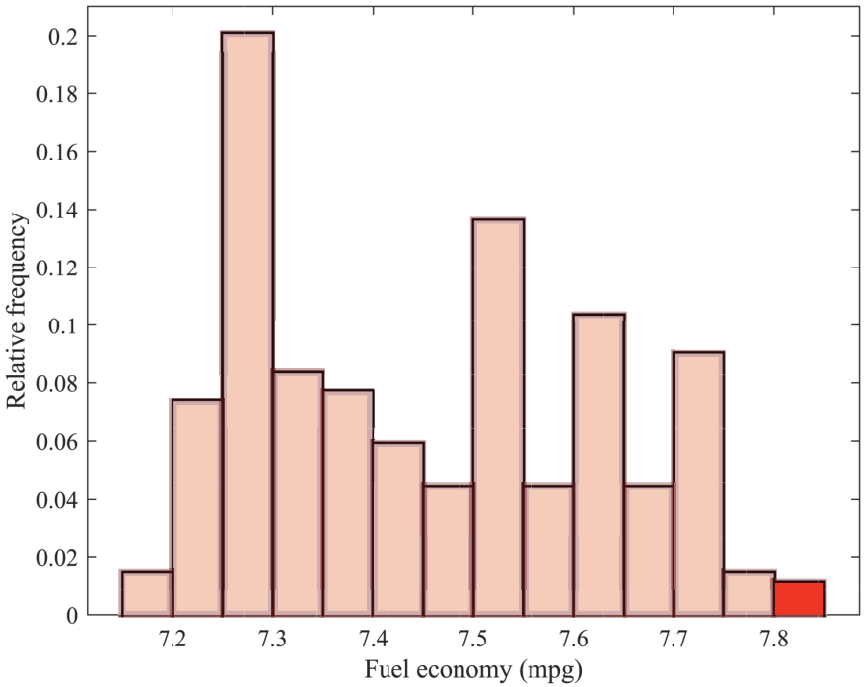

Figure S9. Output space of fuel economies in case sweep

Table S5. Optimization results for sweep case

Variable	Minimum	Maximum	Optimized
Final drive ratio	2.9	3.9	3.04
16th gear	0.8	1.1	0.82
17th gear	0.65	0.9	0.75
18th gear	0.55	0.8	0.71

Total Cost of Ownership Model

Discount rate: The discount factor is calculated according to equation

$$DF = \left(\frac{1}{1+DR}\right)^{yr} \tag{S2}$$

Where DF is the discount factor, DR is the discount rate, and yr is the year

Operating cost: The operating cost considers labor, maintenance & repair, tolls, permits & licenses, fuel and insurance. The cost of these components per mile travelled was translated to

total operating costs using the VMT per year and the discount factor as given in Equation S4.

$$Operating\ Cost = \$_{Labor} + \$_{M\&R} + \$_{Tolls} + \$_{Permits\&Licenses} + \$_{Fuel} + \$_{Insurance} \tag{S3}$$

$$Operating\ Cost_i = \sum_{yr=1}^{10} \left(\frac{\$}{mi} \times VMT_{yr} \times DF_{yr} \right) \tag{S4}$$

Capital cost: The capital cost considers engine, aftertreatment, transmission, waste heat recovery, fuel tank, and glider manufacturing costs. The total capital cost is given by Equation 4.1.

$$Capital\ Cost = \$_{Engine} + \$_{aftertreatment} + \$_{Transmission} + \$_{WHR} + \$_{Tank} + \$_{Glider} \tag{S5}$$

The manufacturing costs for the engine and the aftertreatment system are depicted in Figure S10

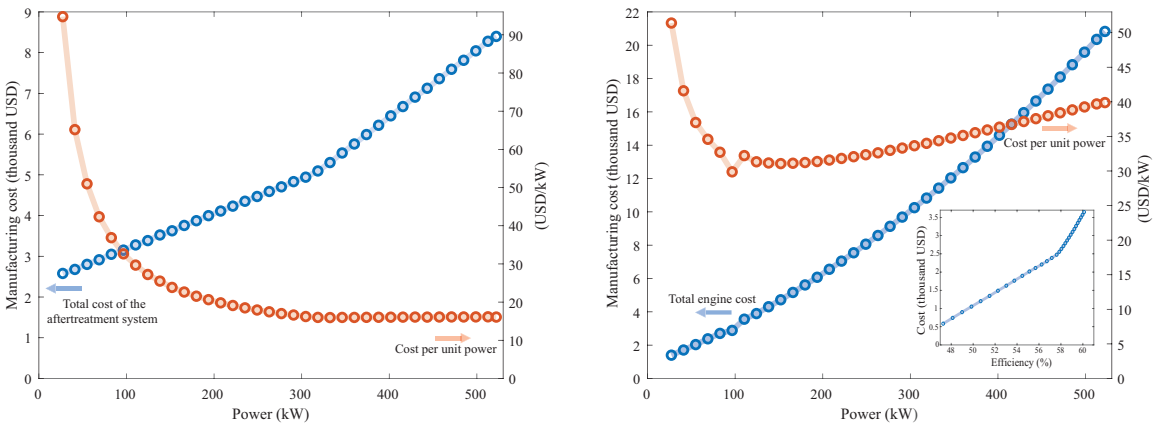

(a) After-treatment **(b)** Engine

Figure S10. Manufacturing cost as function of power demand

Carbon cost: Figure shows literature values for the social cost of carbon, abatement cost and carbon tax.

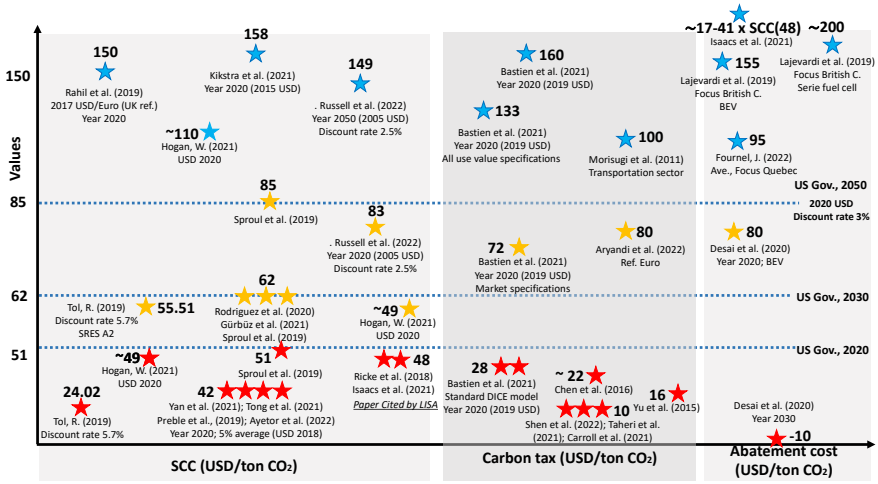

Figure S11. Literature values for cost of GHG emissions

2.7 references

(1) Agency, U. E. P. Sources of Greenhouse Gas Emissions, 2018.

(2) Davis, S. C.; Boundy, R. G., *Transportation Energy Data Book: Edition 37.2*, 2019.

(3) Of Transportation. Bureau of Transportation Statistics, U. D. 2017 CFS Preliminary Data. U.S. Department of Transportation, 2018.

(4) Framework, F. A. FAF Trend - Over Time (1997 - 2045), 2012.

(5) Of Transportation Statistics, B. National Transportation Statistics 9/4/19 Update, Shares of U.S. Energy Consumption and other categories, 2019.

(6) Board, C. A. R. Heavy-Duty Omnibus Regulation, 2021.

(7) Leistner, P.; Lozanovski, A.; Dingel, O.; Erath, M. *Environmental impact of various CO_2 neutral long-haul heavy- duty powertrains*; 2020.

(8) De la Pena, A. G.; Davendralingam, N.; Raz, A. K.; DeLaurentis, D.; Shaver, G.; Sujan, V.; Jain, N. Projecting adoption of truck powertrain technologies and CO2 emissions in line-haul networks. *Transportation Research Part D: Transport and Environment* **2020**, *84*, DOI: 10.1016/j.trd.2020.102354.

(9) Lajevardi, S. M.; Axsen, J.; Crawford, C. Simulating competition among heavy-duty zero-emissions vehicles under different infrastructure conditions. *Transportation Research Part D: Transport and Environment* **2022**, *106*, 103254.

(10) Lajevardi, S. M.; Axsen, J.; Crawford, C. Examining the role of natural gas and advanced vehicle technologies in mitigating CO2 emissions of heavy-duty trucks: Modeling prototypical British Columbia routes with road grades. *Transportation Research Part D: Transport and Environment* **2018**, *62*, 186–211.

(11) Association, A. T. Truck Driver Shortage Analysis 2019. *American trucking association* **2019**.

(12) Burks, S. V.; Monaco, K. Is the U.S. labor market for truck drivers broken? *Monthly Labor Review* **2019**, *2019*, 1–21.

(13) Wood, E.; Duran, A.; Kelly, K. EPA GHG certification of medium- and heavy-duty vehicles: Development of road grade profiles representative of US controlled access highways. *SAE International Journal of Fuels and Lubricants* **2016**, *9*, DOI: 10.4271/2016-01-8017.

(14) Lee, D. Y.; Elgowainy, A.; Kotz, A.; Vijayagopal, R.; Marcinkoski, J. Life-cycle implications of hydrogen fuel cell electric vehicle technology for medium- and heavy-duty trucks. *Journal of Power Sources* **2018**, *393*, 217–229.

(15) Langshaw, L.; Ainalis, D.; Acha, S.; Shah, N.; Stettler, M. E. Environmental and economic analysis of liquefied natural gas (LNG) for heavy goods vehicles in the UK: A Well-to-Wheel and total cost of ownership evaluation. *Energy Policy* **2020**, *137*, DOI: 10.1016/j.enpol.2019.111161.

(16) Mihelic, R.; Schaller, D.; Park, Y.; Otto, K.; Roeth, M.; Rondini, D. *Run on Less Regional Report*; North American Council for Freight Efficiency, 2020.

(17) Damasky, J. In. 2019.

(18) Freight, G. G. Long-Haul, 2021.

(19) Boriboonsomsin, K.; Johnson, K.; Scora, G.; Sandez, D.; Vu, A.; Durbin, T.; Jiang, Y. *Collection of Activity Data from On-Road Heavy-Duty Diesel Vehicles Collection of Activity Data from On-Road Heavy-Duty Diesel Vehicles FINAL REPORT*; University of California at Riverside, Center for Environmental Research and Technology, 2017.

(20) Burnham, A.; Gohlke, D.; Rush, L.; Stephens, T.; Zhou, Y.; Delucchi, M. A.; Birky, A.; Hunter, C.; Lin, Z.; Ou, S.; Xie, F.; Proctor, C.; Wiryadinata, S.; Liu, N.; Boloor, M. Comprehensive Total Cost of Ownership Quantification for Vehicles with Different Size Classes and Powertrains. *U.S. Department of Energy, Argonne National Laboratory* **2021**.

(21) Moultak, M.; Lutsey, N.; Hall, D. *Transitioning to zero-emission heavy-duty freight vehicles*; The International Council on Clean Transportation, 2017.

(22) Vijayagopal, R.; Prada, D. N.; Rousseau, A.; Suarez, L. Y. T. Fuel Economy and Cost Estimates for Medium- and Heavy-Duty Trucks. *U.S. Department of Energy, Argonne National Laboratory* **2019**.

(23) Kuhn, M. *Valuation of Fuel Economy of Medium Duty/Heavy Duty Vehicles*; Ricardo Inc. Detroit Technical Center, 2017.

(24) Mauler, L.; Dahrendorf, L.; Duffner, F.; Winter, M.; Leker, J. Cost-effective technology choice in a decarbonized and diversified long-haul truck transportation sector: A U.S. case study. *Journal of Energy Storage* **2022**, *46*, DOI: 10.1016/j.est.2021.103891.

(25) Zhao, H.; Wang, Q.; Fulton, L.; Jaller, M.; Burke, A. *A Comparison of Zero-Emission Highway Trucking Technologies*; U.C. Davis, Sustainable Transportation Energy Pathways Institute, 2018.

(26) Murray, D.; Glidewell, S. *An Analysis of the Operational Costs of Trucking: 2019 Update*; American Transportation Research Institute, 2019, pp 1–48.

(27) Zabelsky, T.; Miller, J.; Detlefsen, R.; Fitzpatrick, B.; Stoudt, D.; Sessamen, B.; Brown, R. *2002 Economic Census: Vehicle Inventory and Use Survey*; U.S. Census Bureau, 2004.

(28) Administration, F. M. C. S. Summary of Hours of Service Regulations. https://www.fmcsa.dot.gov/regulations/hours-service/summary-hours-service-regulations.

(29) Pietras, F.; Ermer, M.; Simon, M.; Guttmann, B. Trends in the truck & trailer market. *Roland Berger* **2018**.

(30) Marcinkoski, J.; Vijayagopal, R.; Adams, J.; James, B.; Kopasz, J.; Ahluwalia, R. DOE Advanced Truck Technologies: Technical Targets for Hydrogen-Fueled Long-Haul Tractor-Trailer Trucks. *Electrified Powertrain Roadmap* **2019**.

(31) Kollner, M. C. *Drive Cycle Development and Parameter Definition for the Assessment of Powertrain Options for Long-Haul Class 8 Trucks in the USA*; Technische Universitat Berlin, 2021, pp 1–133.

(32) Park, Y.; Roeth, M.; Rondini, D.; Schaller, D.; Wachtel, B. *Run on Less Report*; North American Council for Freight Efficiency, 2018, pp 1–55.

(33) Capps, G.; Franzese, O.; Knee, B.; Lascurain, M. B.; Otaduy, P. *Class-8 Heavy Truck Duty Cycle Project Final Report No. ORNL/TM-2008/122*; Oak Ridge National Laboratory, 2008.

(34) Walkowicz, K.; Kelly, K.; Duran, A.; Burton, E. Fleet DNA Project Data, 2019.

(35) N.V., T. TomTom ADAS Map, 2021.

(36) Rauch, H.; Kovacs, D.; Rezaei, R.; Strots, V.; Kah, S.; Wille, A. In. 2018.

(37) Kovacs, D.; Mennig, M.; Rezaei, R.; Bertram, C. Holistic Engine and EAT Development of Low NOx and CO2 Concepts for HD Diesel Engine Applications. *SAE International Journal of Advances and Current Practices in Mobility* **2020**, *3*, 320–336.

(38) Rauch, H.; Rezaei, R.; Weber, M.; Kovacs, D.; Strots, V.; Bertram, C. In. SAE International: 2018; Vol. 2018-September.

(39) Sher, E., *Handbook of air pollution from internal combustion engines. Pollutant formation and control*, 1st Edition; Academic Press: 1998.

(40) Of the National Academies, N. R. C. *Technologies and approaches to reducing the fuel consumption of medium- and heavy-duty vehicles*; 2010, pp 1–234.

(41) ExpressLease, P. 2011 Freightliner Cascadia 113, 2021.

(42) Agency, U. E. P. SmartWay Program, 2021.

(43) Guensler, R.; Yoon, S.; Feng, C.; Li, H.; Jun, J. *Heavy-Duty Diesel Vehicle Modal Emission Model (HDDV-MEM) Volume I: Modal Emission Modeling Framework*; U.S. Environmental Protection Agency Office of Research and Development, 2005.

(44) Of Science Engineering, T. N. A.; Medicine. *Reducing Fuel Consumption and Greenhouse Gas Emissions of Medium- and Heavy-Duty Vehicles, Phase Two*; 2019, pp 1–380.

(45) Partnership, 2. C. T. *Roadmap and Technical White Papers*; 21st Centrury Truck Partnership, 2013, pp 1–145.

(46) Transportation Research Board and National Academies of Sciences Engineering and Medicine, *Reducing Fuel Consumption and Greenhouse Gas Emissions of Medium- and Heavy-Duty Vehicles, Phase Two: Final Report*; The National Academies Press: Washington, DC, 2019.

(47) Zhao, H.; Burke, A.; Miller, M. Analysis of Class 8 truck technologies for their fuel savings and economics. *Transportation Research Part D: Transport and Environment* **2013**, DOI: 10.1016/j.trd.2013.04.004.

(48) Of Energy, U. D. Super Truck 2. https://www.energy.gov/eere/vehicles/articles/supertruck-2-paccar.

(49) Partnership, 2. C. T. *Research blueprint*; 2019, pp 1–19.

(50) Caton, J. A. Maximum efficiencies for internal combustion engines: Thermodynamic limitations. *International Journal of Engine Research* **2018**, *19*, 1005–1023.

(51) Administration, U. E. I. Carbon Dioxide Emissions Coefficients. https://www.eia.gov/environment/emissions/co2_vol_mass.php.

(52) Of Management, O.; Budget. Discount Rates for Cost-Effectiveness Analysis of Federal Programs. **2020**.

(53) Williams, N.; Murray, D. *An Analysis of the Operational Costs of Trucking: 2020 Update*; American Transportation Research Institute, 2020, pp 1–53.

(54) Administration, U. E. I. Weekly Retail Gasoline and Diesel Prices. https://www.eia.gov/dnav/pet/PET_PRI_GND_DCUS_NUS_A.htm.

(55) Administration, U. E. I. Annual Energy Outlook 2021 with projections to 2050. https://www.eia.gov/outlooks/aeo/data/browser/#/?id=12-AEO2021%5C&region=0-0%5C&cases=ref2021%5C&start=2019%5C&end=2050%5C&f=A%5C&linechart=~ref2021-d113020a.32-12-AEO2021%5C&map=%5C&ctype=linechart%5C&sourcekey=0.

(56) Laboratory, N. R. E. Diesel Fuel. https://atb.nrel.gov/transportation/2020/diesel_fuel.

(57) Of Energy, U. D. *Clean Cities Alternative Fuel Price Report, January 2020*; 2020.

(58) Posada, F.; Chambliss, S.; Blumberg, K. Costs of Emission Reduction Technologies for Heavy-Duty Diesel Vehicles. *The International Council of Clean Transportation (ICCT)* **2016**, 39.

(59) Pierre-Louis, R.; Rodriguez, F. *Estimated cost of diesel emissions control technology to meet future Euro VII standards*; 2021.

(60) Laboratory, A. N. ANL-MDHD Vehicle Simulation. https://www.autonomie.net/pdfs/ANL-MDHD%20Vehicle%20Simulation%20Report.pdf.

(61) Norris, J.; Escher, G. *Heavy Duty Vehicles Technology Potential and Cost Study*; Ricardo Energy & Environment, 2017.

(62) Lajevardi, S. M.; Axsen, J.; Crawford, C.; Lajevardi, S. M.; Axsen, J.; Crawford, C.; Lajevardi, S. M.; Axsen, J.; Crawford, C.; Lajevardi, S. M.; Axsen, J.; Crawford, C.; Lajevardi, S. M.; Axsen, J.; Crawford, C. Comparing alternative heavy-duty drivetrains based on GHG emissions, ownership and abatement costs: Simulations of freight routes in British Columbia. *Transportation Research Part D: Transport and Environment* **2019**, *76*, DOI: 10.1016/j.trd.2019.08.031.

(63) Stephens, T.; Vijayagopal, R.; Dwyer, M.; Birky, A.; Rousseau, A. *Vehicle Technologies and Fuel Cell Technologies Office Research and Development Programs: Prospective Benefits Assessment for Medium-and Heavy-duty Vehicles*; Argonne National Laboratory, 2019, pp 1–53.

(64) Agency, U. E. P.; Administration, N. H. T. S.; of Transportation, D. Greenhouse Gas Emissions and Fuel Efficiency Standards for Medium- and Heavy-Duty Engines and Vehicles-Phase 2. https://www.federalregister.gov/documents/2016/10/25/2016-21203/greenhouse-gas-emissions-and-fuel-efficiency-standards-for-medium--and-heavy-duty-engines-and.

(65) Wagner, G.; Anthoff, D.; Cropper, M.; Dietz, S.; Gillingham, K. T.; Groom, B.; Kelleher, J. P.; Moore, F. C.; Stock, J. H. *Eight priorities for calculating the social cost of carbon*; 2021, pp 548–550.

(66) Carleton, T.; Greenstone, M. *Updating the United States Government's Social Cost of Carbon*; Energy Policy Institute at the University of Chicago, 2021, pp 1–42.

(67) Fairley, P. States Are Using Social Cost of Carbon in Energy Decisions, Despite Trump Opposition. https://insideclimatenews.org/news/14082017/states-climate-change-policy-calculate-social-cost-carbon/.

(68) Ricke, K.; Drouet, L.; Caldeira, K.; Tavoni, M. Country-level social cost of carbon. *Nature Climate Change* **2018**, *8*, 895–900.

(69) On Social Cost of Greenhouse Gases, I. W. G. *Technical Support Document: Social Cost of Carbon, Methane, and Nitrous Oxide Interim Estimates under Executive Order 13990*; 2021, pp 1–44.

(70) Gao, Z.; Smith, D. E.; Daw, C. S.; Edwards, K. D.; Kaul, B. C.; Domingo, N.; Parks, J. E.; Jones, P. T. The evaluation of developing vehicle technologies on the fuel economy of long-haul trucks. *Energy Conversion and Management* **2015**, *106*, 766–781.

(71) Tong, F.; Jenn, A.; Wolfson, D.; Scown, C. D.; Auffhammer, M. Health and Climate Impacts from Long-Haul Truck Electrification. *Environmental Science and Technology* **2021**, *55*, 8514–8523.

(72) Liu, X.; Elgowainy, A.; Vijayagopal, R.; Wang, M. Well-to-Wheels Analysis of Zero-Emission Plug-In Battery Electric Vehicle Technology for Medium- And Heavy-Duty Trucks. *Environmental Science and Technology* **2021**, *55*, 538–546.

(73) Camuzeaux, J. R.; Alvarez, R. A.; Brooks, S. A.; B. Browne, J.; Sterner, T. Influence of methane emissions and vehicle efficiency on the climate implications of heavy-duty natural gas trucks. *Environmental Science and Technology* **2015**, *49*, 6402–6410.

(74) ANL. *Fuel Economy and Cost Estimates for Medium and Heavy Duty Trucks*; Argonne National Laboratory, 2019, pp 1–41.

(75) Agency, U. E. P. Vehicle and Fuel Emissions Testing: Dynamometer Drive Schedules. https://www.epa.gov/vehicle-and-fuel-emissions-testing/dynamometer-drive-schedules.

(76) Dieselnet. Heavy Heavy-Duty Diesel Truck (HHDDT) Schedule. https://dieselnet.com/standards/cycles/hhddt.php.

(77) Wenli, Y. Heavy Duty Diesel Vehicle Exhaust PM Speciation Profiles. https://ww2.arb.ca.gov/speciation-profiles-used-carb-modeling.

(78) For a Clean Air Future; ICCT International Council on Clean, N. N. S. C. *Heavy-Duty Long Haul Combination Truck Fuel Consumption and CO 2 Emissions*; 2009.

(79) Burnham, A.; Gohlke, D.; Rush, L.; Stephens, T.; Zhou, Y.; Delucchi, M. A.; Birky, A.; Hunter, C.; Lin, Z.; Ou, S.; Xie, F.; Proctor, C.; Wiryadinata, S.; Liu, N.; Boloor, M. Comprehensive Total Cost of Ownership Quantification for Vehicles with Different Size Classes and Powertrains. *U.S. Department of Energy, Argonne National Laboratory* **2021**.

(80) Capps, G.; Franzese, O.; Knee, B.; Lascurain, M. B.; Otaduy, P. *Class-8 Heavy Truck Duty Cycle (Report No. ORNL/TM-2008/122)*; tech. rep. December; 2008.

Chapter 3

Is a hydrogen economy the solution to decarbonizing long-haul trucking?

The work on hydrogen powertrains is currently being finished and will soon be submitted for publication. Special thanks is given to Kariana Moreno Sader for her assistance in document preparation and the hydrogen costing analysis. Also, to IAV for their continued support in providing professional advice to model the hydrogen powertrains.

3.1 Introduction

Efforts in decarbonizing the heavy-duty transport though different low and zero-emission vehicle technologies have highlighted the need for strategic decisions about the transition to cleaner options. These decisions are grounded around comparative evaluation of powertrains over a wide range of factors including economic, technological, environmental, social and political [1]. When it comes to technological factors, vehicle efficiency, technology maturity and availability of refuelling infrastructure play a key role. From a technoeconomic standpoint, comparisons across technologies are based on vehicle cost (i.e. Total Cost of Ownership), fuel cost and refuelling infrastructure cost, among others.

Recent studies have highlighted the merits of heavy-duty trucks running on hydrogen as an option to achieve net zero targets in the US, Table 3.1. The increasing research efforts around these power technologies have led to studies involving their technical, economics and emissions performance. Further, these studies compare hydrogen trucks with other emission-free options and its diesel counterpart.

Table 3.1. Recent publications on hydrogen-powered trucks

Reference	Context	Hydrogen Technology	Technical	Economic	Emissions
[2]	USA	FCEV	✓	x	x
[3]	USA	FCEV	✓	x	x
[4]	USA	FCEV	✓	✓	x
[5]	USA	FCEV	✓	x	✓
[6]	USA	FCEV	✓	x	x
[7]	Canada	FCEV	✓	✓	✓

The technical performance of trucks powered with hydrogen fuel cells (H-FCET) across different truck categories, which include long-haul trucks, was addressed by Kast et al.[2]. They modelled and simulated H-FCET trucks under real world driving patterns using the Fleet DNA database and Autonomie software. This work was mainly focused on the on-board needs for a set of truck categories given transient fuel demands from the drive cycles. In a later publication, those authors examined mass and space constraints of the on-board storage system that meet daily range requirements, but using shorter drive cycles from the California Air Resource Board (CARB) [3].

Mauler et al. [4] evaluated the competitiveness of fuel cell electric trucks (H-FCET), battery electric trucks (BET) and conventional diesel trucks (D-ICET) under different present-day and future scenarios of technology maturity. While this study revealed that BETs outperformed H-FCETs in many scenarios, H-FCETs were shown to be more cost-competitive for trip distances >600 km (360 miles). Mauler et al.'s fuel consumption models were based on the fuel cell efficiency, the distance travelled, and the work done by the truck. This was performed without accounting for

transient fuel demand associated with on-highway driving patterns.

Lee et al. [5] also studied the fuel consumption of H-FCET, as well as the associated emissions. They developed vehicle dynamic simulations using the Autonomie software and real-world driving data. The transient fuel consumption was based on an adjusted EPA/National Highway and Traffic Safety Administration (NHTSA) method extended to fuel cells. Standard drive cycles in cruise and transient mode were used by the authors as an input for the simulations, however, these cycles only represent an small portion of the entire driving patterns in freight operations.

Forrest et al. [6] assessed the feasibility of both battery electric and fuel cell electric trucks considering technological factors such as charging and refueling availability, powertrain efficiency and miles travelled. The feasibility was analyzed in terms of the capability of the given technology to meet the requirements in vehicle miles travelled (VMT) for a given truck category. This study revealed that for class 8 trucks, H-FCETs outperform BETs because they can cover a larger fraction of the VMT than BETs with home base charging.

Lajevardi et al. [7] used in-house models for different powertrains for short and long haul duty cycles (e.g. battery electric, fuel cell, diesel, CNG and hybrid architectures). These models considered on-road fuel consumption according to the drive cycles characteristics of British Columbia in Canada. Along with techno-economic aspects, this work was intended to compare the competitiveness of these technologies under different scenarios of infrastructure deployment for refueling and charging stations. Lajevardi et al. found that in scenarios where the hydrogen refueling infrastructure is rapidly deployed, H-FCETs would grab most of the market share of long-haul trucks (but not in scenarios with slow deployment). This study used a relatively high discount rate of 15%, which makes replacement batteries for BET significantly more attractive than in scenarios assuming a lower discount rate.

Hydrogen Supply Chain Review

A hydrogen powered fleet of trucks would create a large increase in demand forhydrogen. A review of hydrogen supply and outlook is presented in the context of vehicular application with emphasis on production from renewables and carbon capture. Technologies in the hydrogen supply chain (production, delivery and refueling) have been extensively examined to drive the transition to a hydrogen economy.

Current hydrogen production produces significant CO_2 emissions, however there are options to reduce and ultimately eliminate emissions. In 2018, global emissions from hydrogen production reached 830 MtCO_2eq/yr, which is greater than the combined total emissions of Indonesia and the United Kingdom. carbon capture, utilization, and storage (CCUS) can be used in steam methane reformation (SMR) to reduce carbon emissions by up to 90% for a cost of \$80/tCO_2 [8]. The EIA estimates the current hydrogen production via SMR with CCUS in the United States costs \$1.50/kgH_2 (compare with \$1.00/kgH_2 for SMR without CCUS). There are several variants of low-

greenhouse hydrogen production from natural gas, each with slightly different costs and emissions, but mostly in the range of the EIA number. In the zero emission scenario, hydrogen can be produced from water via electrolysis. This production pathway is still in it's early stages, however with decreasing costs of solar and wind renewable electricity, the EIA estimates hydrogen production in the distant future to cost under $\$1.60/kgH_2$ in promising areas such as Patagonia, New Zealand, Northern Africa, the Middle East, Mongolia, most of Australia, parts of China, and the United States [8].

Wickham et al. [9] developed an optimization model for H_2 supply chain to meet the hydrogen demands of the transport sector, particularly for fuel cell electric vehicles. Authors evaluated a set of technologies for hydrogen production including electrolysis and steam methane reformation with carbon capture and sequestration (SMRCCS); for transmission and distribution, they considered new pipelines, trucks, re-purposing gas distribution networks and blending. This work also accounts for purification technologies to deliver high-purity hydrogen at refueling stations. The cost optimal configuration resulted to be SMRCCS, new transmission pipelines, re-purpose of gas distribution networks and on-site purification at refueling stations, which led to a hydrogen cost of £6.18 per kg at the pump in Great Britain.

In this research domain, Li et al. [1] evaluated different hydrogen supply chain networks covering SMR, coal gasification, biomass gasification, and central electrolysis. Both liquid and gaseous pathways for hydrogen delivery and refueling were also considered. The optimal configuration derives from emission and economic-based assessments, revealing potential trade-off between technologies over optimized levelized cost of hydrogen (LCOH) and global warming potential (GWP). This work illustrates the applicability of the modelling framework with a case study in France, in which the lowest LCOH was estimated at 18.6 €/kg H_2 with a GWP intensity of 3.68 kgCO_2/kg H_2.

Frank et al.[10] estimated well-to-wheel (WTW) emissions for production and delivery options supporting the current market of fuel cell electric vehicle (FCEV) and future expansion scenarios. They used techno-economic analysis to screen feasible options in liquid and gaseous pathways. Emissions were calculated through the GREET (Greenhouse gases, Regulated Emissions, and Energy use in Technologies) model in the US context and considers electricity variations across regions. Energy consumption of delivery components such as liquefiers and compressors derived from the Hydrogen Delivery Scenario Analysis Model (HDSAM) tool. Under future capabilities for green hydrogen production, the authors found that emissions are 4 to 20 times lower than those of conventional internal combustion engines, which was significantly dependent on the delivery technology implemented.

3.2 Methods

3.2.1 Scale of Hydrogen Demand

The demand of hydrogen for heavy-duty long-haul trucking in the US was analyzed under three deployment scenarios for hydrogen-based powertrains. The time-based scenarios include the present-day, mid-term and long-term. The following scale analysis is based on alternative heavy duty sale volumes in accordance with scenario year. Data for heavy duty truck production rates are obtained from the EIA annual energy outlook 2019 [11] and scaled by 25% to represent the long-haul fraction of the heavy duty truck market. Present and mid-term scenario years are assumed to be a prototype era and have small alternative heavy duty truck sales. In the midterm, alternative powertrains are assumed to have initial market penetration and larger sale volumes. In the long term, alternative truck sales are assumed to take over the market and account for its entirety. This equates to a market share of 100% when assuming vehicle retirement after 10 years and an average of 87,000 miles traveled per vehicle per year. The results of this analysis are shown and discussed in section **??**.

The model uses heavy-duty class 8 truck production predictions to 2050 by the EIA and this study's alternative truck production rates that align with scenario previously discussed. The governing equation for how many alternatives trucks are present in a given year is given by equation 3.1

$$\frac{dN_{alt}}{dt} = r(t)_{alt}^{produced} - r(t)_{alt}^{retired} \tag{3.1}$$

Where, N_{alt} corresponds to the number of alternative trucks, and r_{alt} represents the rate of alternative trucks being either produced or retired. The retirement rate, given in equation 3.2, is the production rate shifted by the lifetime of the vehicle multiplied by a Heaviside function to switch it on after a lifetime has passed for the first trucks produced.

$$r(t)_{alt}^{retired} = r(t - t_{retired})_{alt}^{produced} \cdot H(t - (t_0 + t_{retired})) \tag{3.2}$$

The production rate is constructed using the scenario years 2019, 2030, and 2050 to account for the present, mid term, and long term assumed production levels of 1000, 10000, and 100000 units/yr. These production rates are then scaled such that by 2050, 100% of truck production is alternative to align with COP targets of significantly decarbonized world by 2050.

With the number of alternative trucks, the total hydrogen demand is found using vehicle miles traveled per truck and fuel economy according to equation 3.3.

$$H_{2,Demand} = \frac{N_{alt} \cdot VMT}{FE} \tag{3.3}$$

3.2.2 Cost of hydrogen

The hydrogen cost alone can determine the competitiveness of H_2-powered trucks against the D-ICET and all other alternative powertrains. Because of its significance, the cost to produce and distribute hydrogen was extensively studied using the H2A [12] and HDSAM frameworks [13]. A overview of the hydrogen pathways modeling is given in Figure 3.1.

A total of nine hydrogen production pathways were considered using three types of technology and distributed and central delivery locations. This study considers natural gas feedstocks processed by SMR variations, water feedstocks processed by electrolysis with various sources of electricity, and coal feedstocks processed by gasification with carbon capture and sequestration. This study aims to compare these processes and suggest viable production methods in a hydrogen based heavy-duty trucking market. Each feedstock and production method are evaluated based on cost, GHG emissions, and practicality.

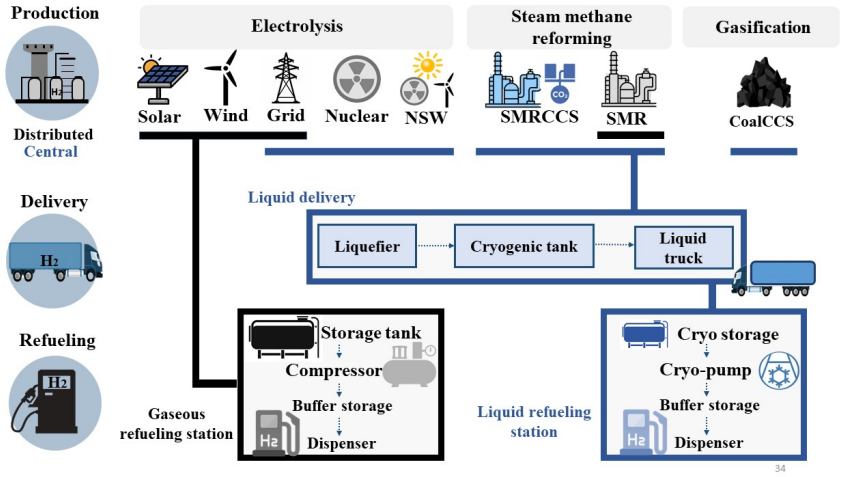

Figure 3.1. Overview of the hydrogen pathways modeling

Cost of H_2 production

We used hydrogen analysis (H2A) framework to estimate hydrogen production cost as it incorporates the technical design of a production plant with an economic discounted cash flow model. H2A includes an analysis for present and future scenarios and considers 2015 and 2040 technology, respectively [12]. The present H2A models were used for this study's present scenario and the future H2A models were used for the midterm and long term scenarios.

SMR: Three SMR processes were examined in this study and include centralized without CCUS, distributed SMR without CCUS, and centralized SMR with CCUS. Emissions can be reduced in the SMR process by capturing up to 90% of the carbon; however, this introduces the need for significant infrastructure development in carbon sequestering. Finally, distributed SMR without

carbon capture was included in the analysis in an attempt to avoid costly delivery associated with traditional central SMR plants. Carbon capture and sequestration for distributed SMR was not explored due to the insurmountable impracticality of transporting the carbon from a refueling station to a sequestration site. More information on SMR can be found in the supplementary information.

Natural gas price, capacity factor, and utility prices heavily influence hydrogen production prices based on H2A sensitivity analysis results, and are therefore of interest in production analysis. The price of natural gas and electricity are obtained from EIA's 2019 annual energy outlook [11]. Electricity was costed considering EIA's industrial values. The capacity factor was left at H2A defaults. Because SMR is a developed process, capacity factors are not predicted to change in time. The base case values for each scenario are given in Table S1. Other values are available in S2.

Electrolysis: Different electricity sources (i.e., solar, wind, nuclear, and grid) for central and distributed production plants. A combination of nuclear, solar, and wind (NSW) was also explored to utilize a high capacity factor from nuclear when solar and wind electricity generation is inoperable. A table of electricity cost, capacity factors, and electrolyzer cost for the base case is given in Table S4. Electricity price cost inputs and their ranges are based on literature values for the levelized cost of energy. Industrial transmission costs, using the EIA's 2019 annual energy outlook, are added to central and grid-based plants. Solar and wind current baseline values and future values and their ranges are used from NREL's Annual Technology Baseline (NRELATB) database [14], while current ranges are obtained from Lazard [15]. Central nuclear baseline values are obtained from the NRELATB database, however the ranges are obtained from International Energy Agency (IEA)'s projected costs of generating electricity study. The levelized cost of energy's lower bound for central nuclear considers long term operation by lifetime extension as define in the IEA report [8]. The central nuclear upper bound is derived considering a 10% increase relative to baseline values. Grid based electricity cost values are obtain from the EIA's annual energy outlook 2019 and ranges consider 10% deviations. The NSW plant averages the levelized cost of energy for wind, solar, and nuclear using weights derived by constituent capacity factors according to equations S1 and S2

In this study, capital costs for electrolyzers are based on total production volumes and consider economies of scale. Production volumes are obtained from considering the yearly hydrogen demand, plant design capacity, operating factor, and plant life according to equation 3.4. The hydrogen demand is a function of year and is derived in section 3.2.1. The Hydrogen and Fuel Cell Technology Office (HFTO) manufacturing analysis is used to obtain the installed capital cost of the electrolyzers (Figure S7). The referenced HFTO manufacturing analysis was for 1MW systems, that are most similar to distributed configurations. Relative to central plants, distributed plants have higher balance of plant (BOP) costs. To account for this, the default H2A capital cost ratios for stack and BOP were taken into consideration. H2A analysis shows the central BOP to stack capital cost ratio to be 0.65 and 1.7 for distributed. Analysis considering same stack MW volumes results in a central

cost ratio to distributed cost ratio of 0.66. As such, HFTO manufacturing cost analysis values were scaled to derive central installed system capital cost values. The results of the electrolyzer costing are given in S8.

$$Electrolyzers\ built\ (\frac{Number}{year}) = \frac{yearly\ demand \cdot MW}{Plant\ design\ capacity \cdot Operating\ factor \cdot Plant\ life} \quad (3.4)$$

Cost of H_2 delivery

The hydrogen delivery cost was estimated using the HDSAM V3.1, developed by the Argonne National Laboratory [13, 16]. This tool translates market demand parameters into a detailed hydrogen delivery infrastructure costing through techno-economic and manufacturing data [17]. While the HDSAM tool was originally conceived for Light Duty Vehicles (LDV), this work extends its use for Heavy-duty Vehicles (HDV) by introducing input parameters that are characteristic of HDV, such as fuel economy and miles travelled per road mile.

HDSAM enables users to define parameters, such as market scenarios, market penetration, transmission/distribution mode, production volume and dispensing rate. The input parameters used in this work are given in Table 3.2. The market penetration is derived from the hydrogen scale demand analysis (section 3.3.1). The average capacity of H_2 refueling stations was defined in accordance with the forecast demand of alternative long-haul trucks and the number of stations in rural interstate highways. We assumed the existing truck stop facilities to serve as refueling stations while alternative the heavy-duty truck (HDT) rollout grows and penetrates the market. Details of the parameter estimates and delivery cost results are given in the Supplementary Information (section **??**).

Cost of H_2 refueling

This work determines the cost of dispensing hydrogen through the Heavy-duty Refueling Station Analysis Model (HDRSAM), an Excel-based tool developed by the Argonne National Laboratory. This tool sizes station components according to market parameters and anticipated design features such as fuel cell-heavy duty fleet size and station type. The input parameters for HDRSAM are defined in Table 3.3. More details are also provided in section **??**. The dispensing cost relies on the average capacity of the refueling stations and the number of trucks that can be refueled per day. All trucks are assumed to carry up to 80 kg hydrogen on-board. The fleet size was estimated at 6, 29 and 37 long-haul trucks per day for the present, mid and long term scenario. The profiles of these trucks being fueled per hour in each scenario are depicted in Figure S15, which are based on

Table 3.2. Input parameters for hydrogen delivery cost

Parameters	Present	Midterm	Longterm	Units	Reference
Market penetration	1	5	100	%	This work
Refueling station capacity	0.5	2.5	3	ton/day	This work
Production volume	low	low	high	-	This work
Market		Rural interstate		-	This work
Real after-tax discount rate		7		%	This work
Analysis Period		30		years	HDSAM
Annual Vehicle Distance Traveled in highway		51770		millions of miles	[18]
Total US rural interstate highway length		33,061		mi	[13]
Ave. HDV Miles Traveled/Rural Interstate Hwy mile		4300		mi/day per mi-highway	This work

the Chevron profile for Friday [19, 20]. These profiles also served to estimate the number of hoses required in peak hours, impacting the overall dispenser cost. While the present-day scenario only requires one hose, two hoses were needed for larger refueling stations in the mid and long term.

Refueling stations with on-site hydrogen production

Refueling stations with on-site hydrogen production need additional storage to accommodate hourly demands as well as scheduled and unplanned outages. Since gaseous hydrogen is supplied from the electrolyzer to the station, the gaseous 700-bar cascade dispensing pathway was selected. Three different storage requirements were analyzed: storage to supply hourly demands and the compressor suction side needs, additional storage to accommodate a two-day reserve, and storage for 10 days that considers both planned and unplanned outages. The 10-day reserve provides a level comparison with centralized facilities because 10 days of outage per year are also accounted by HDSAM for supply side variations [21]. No geological storage availability was assumed in this work.

For the first case, the storage capacity comes from the resulting accumulation of H_2 over the day as hydrogen is produced and consumed according to daily profiles. The daily profiles for on-shore

Table 3.3. Input parameters for hydrogen refueling cost

Parameters	Present	Midterm	Longterm	Units	Reference
Fleet size	6	29	37	# trucks	This work
Production volume	low	low	high	-	This work
Number of hoses	1	2	2	#	This work
After-tax Discount Rate		7		%	This work
Dispensing option		700 bar via cryogenic pump		-	This work
Fueling rate		7.2		kg/min	This work
Vehicle fill time		11		min	HDRSAM
Annual utilization		80		%	This work

wind and solar are depicted in Figure S16. For Cases 2 and 3, the storage capacity was based on the average dispense per day that must be maintained during the outage. More information as well as results for the refueling analysis can be found in section 3.5.

3.2.3 Fuel consumption models

Technical models for the H-ICET and H-FCET were developed to assess the viability of replacing the diesel internal combustion engine. The vehicle-level simulations were performed in GT-Suite software using the USLHC8 drive cycle (Figure 3.2) as input. This drive cycle was developed in Part 1 from real driving data, enabling more representative fuel consumption models for the US freight operation. An overview of the models are given in Figures 3.3 and 3.4.

Hydrogen combustion fuel consumption model

The hydrogen combustion truck model uses a hydrogen spark ignition engine for the propulsion system and is modeled using map-based methodology (Figure 3.3). This engine model applies a holistic, model-based approach using coupled engine and EAT models [22]. During the development, a system-level optimization was carried out targeting emission limits of upcoming regulatory requirements. The 1D hydrogen engine model features IAV's in-house developed and widely published predictive hydrogen combustion model [23–25]. Specifically, submodels are developed to predict the laminar flame speed and knock occurrence. The combustion model was validated using single-cylinder test results. In addition, a calibrated NO_x model was developed and based on the extended Zeldovich mechanism and is coupled with the hydrogen combustion model. The transient thermal behavior (thermal inertia, heat transfer properties, etc.) of the engine cyclinders and the air path system (including the TC group) are taken into account. The engine specifications are summarized in Table 3.4. Further descriptions of the model development methodology and a detailed overview of the approach can be found in [22].

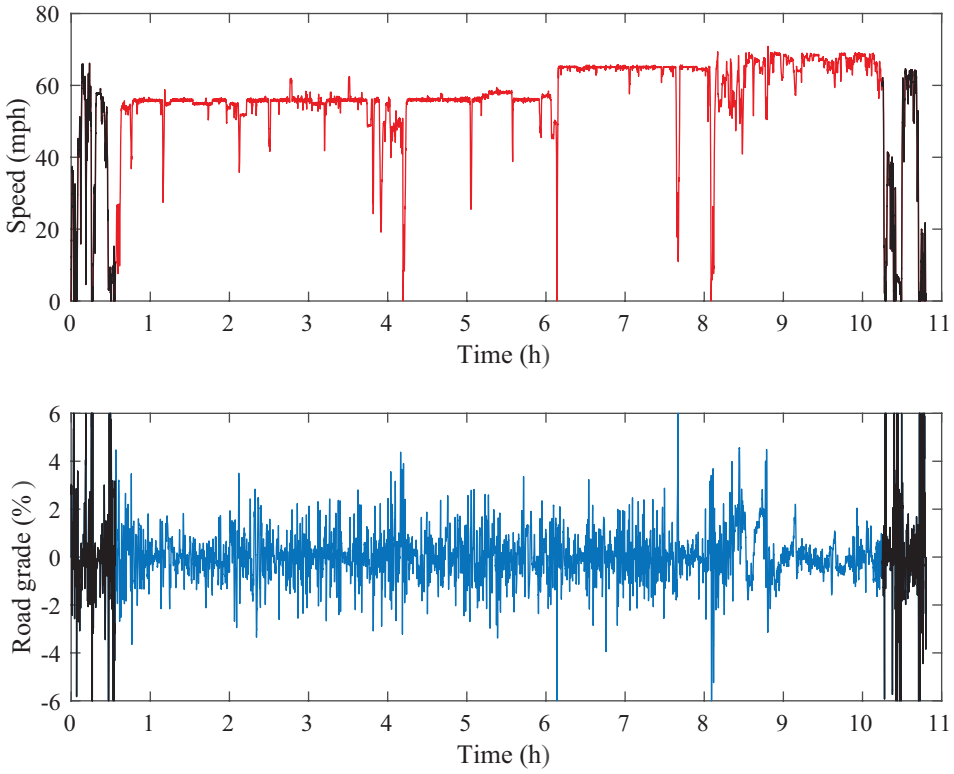

Figure 3.2. Drive cycle for long-haul trucking USLHC8

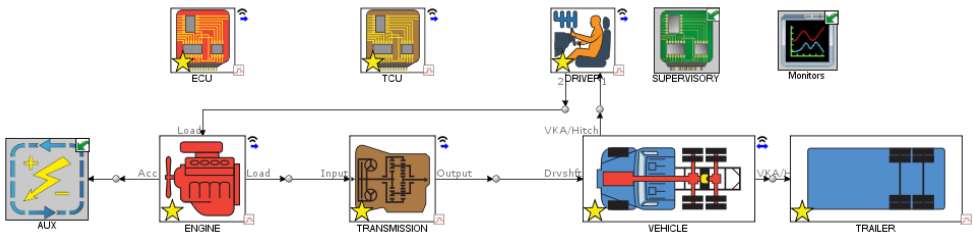

Figure 3.3. Hydrogen internal combustion engine truck (H-ICET) model overview

Engine Operation Optimization

Shifting plays a large role in vehicle performance and fuel economy. The nature of long haul constitutes driving within a small window of high speeds and therefore a small window of power requirements. A power envelope representing one standard deviation of the engine power requirement over the USLHC8 cycles is shown in Figure S19. An ideal shifting strategy operates the engine closest to its peak efficiency while maintaining performance output requirements.

A shift schedule was generated using GT's built-in shift schedule generator. This method optimizes shifting by considering acceleration potential and MPG in each gear at various speeds through static analysis in which involves the static calculation of the tractive force exerted on the vehicle.

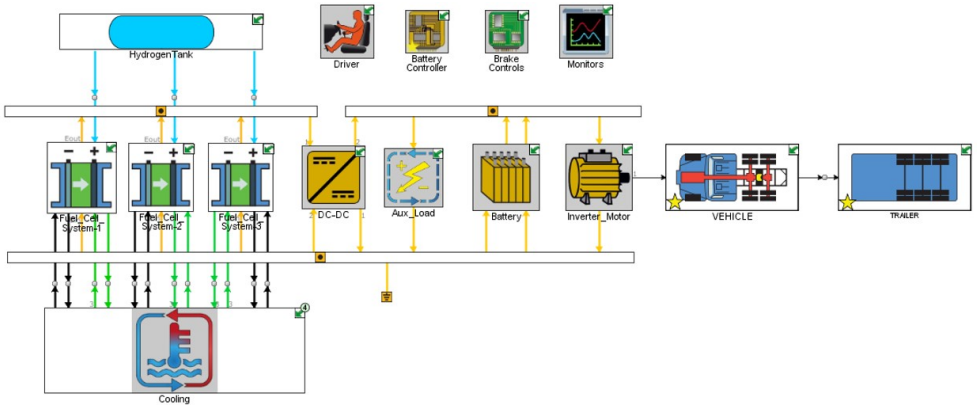

Figure 3.4. Overview of the H-FCET vehicle architecture

Table 3.4. Powertrain input specifications

Components	**Specifications**	
Engine	Displacement	12-liter class
	Number of cylinders	6
	Number of valves	4 per cylinder
	Compression ratio	11.5:1
	Injection system	Direct injection
	Charging system	VTG turbocharged, charge air cooled
	EGR	Cooled, high pressure EGR
Transmission	Speed	18
Storage Tank	Pressure	700 bar

Parameters considered in shift schedule generation include minimum engine speed following upshift, percentage of max load following upshift, minimum offset between successive upshifts, downshift hysteresis offset, and engine speed and break mean effective pressure (BMEP) at best fuel economy point.

With a shifting strategy set, the final drive and transmission gear ratios were optimized to further improve the fuel economy. Because optimizing over 18 transmission gears would result in unreasonable computation times, only a select few were used. Top gear ratios were chosen to optimize over due to the nature of long-haul driving cruising at high speeds for the majority of operation. Gear ratios determine where the engine torque and speed points lie on the engine map under the influence of power demand and vehicle speed. Therefore, the number of top gear ratios was determined using k means clustering for rpm, velocity, torque, and power over the drive cycle. Using the elbow method, the top three gears along with the final drive ratio were chosen for optimization.

To find the initial point for optimization and to ensure a global optimum from the optimizer, a case sweep over the top three transmission gears and final drive ratios was performed the establish

an output space of fuel economy. The input variable ranges explored are given in Table S8. After filtering the output space to only include an average drive cycle error less than 1 mph, the highest fuel economy point was chosen as the initial guess for the optimizer. The optimized parameters are given in Table S8.

Hydrogen fuel cell electric hybrid

The H-FCET model is a physical based model and an overview of the GT-Suite model is shown in Figure 3.4. This model contains three fuel cell stacks that are the primary power supply, a battery pack to handle transient power demands, a DC-DC converter to regulate system voltage, a motor to convert electrical to mechanical power, a cooling system to maintain the temperature of the powertrain components, and a hydrogen tank to supply fuel. Relevant vehicle's component attributes are given in Table 3.5.

Table 3.5. H-FCET powertrain components and their attributes

Component	H-FCET-HEV	H-FCET-PHEV
Fuel Cell	350 kW peak power 64% peak efficiency	300 kW peak power 64% peak efficiency
Air Compressor	18.2 kW	18.2 kW
DC-DC Converter	95% constant efficiency	95% constant efficiency
Motor	1100 kW peak power 98% peak efficiency	1100 kW peak power 98% peak efficiency
Hydrogen tank	700 bar type 4 gas storage vessel 72 kg storage	700 bar type 4 gas storage vessel 65 kg storage
Cooling system	Radiator with fan WCAC Cooling jacket for heat generating components	Radiator with fan WCAC Cooling jacket for heat generating components
Battery	100 kWh 98% peak efficiency	430 kWh 98% peak efficiency

The fuel cell stack is modeled considering physical mechanisms leading to voltage losses (Eq. S4). Mechanisms contributing to voltage loss included in this analysis are activation, mass transport, and ohmic, as given in Eq. S5.

The fuel cell's performance was tuned to match 2017 Toyota Mirai data by optimization of model input parameters to match the Mirai's efficiency curve. Mira data was obtained from Argonne National Lab (ANL) [26] and contained current density sweeps for anode and cathode pressures, flow rates, efficiencies, and voltages. A benchtop model was created in GT-Suite to simulate the

fuel cell under the conditions described by Argonne sweeps (Figure S20 & S22). The input variables optimized over include the springer coefficient, catalyst loading density , open circuit voltage loss, and electrode porosity. The resulting efficiency curve is given in Figure S21. The fuel cell stack model operates up to 1.8 A/cm^2 until the performance plummets. A peak efficiency of 64% occurs at a current density of 0.05 A/cm^2. The anode and cathode pressures range from 0.5 to 1.5 bar, peaking at higher current densities. Temperature was held constant at 80°C during the validation.

With the fuel cell stack parameters set, the hydrogen and air recirculation systems were implemented. The blue lines in Figure 3.5 represent the hydrogen circulation system. The hydrogen system is a forward pressure system, using a valve after the tank to dictate the pressure of the anode. Hydrogen enters the system at the tank pressure. An inlet valve is equipped with a controller to establish an inlet hydrogen pressure of 2 bar at the fuel cell stack. Fed hydrogen is consumed within the stack on the first pass; however, an outlet recirculation stream serves to recycle unreacted hydrogen. A purge stream is included to release the buildup of inert nitrogen. The purge stream valve is design to open when hydrogen mass fraction falls below 0.3. A pump is implemented to recirculate the hydrogen and is actuated to maintain an anode stoichiometric ratio (SR) of five.

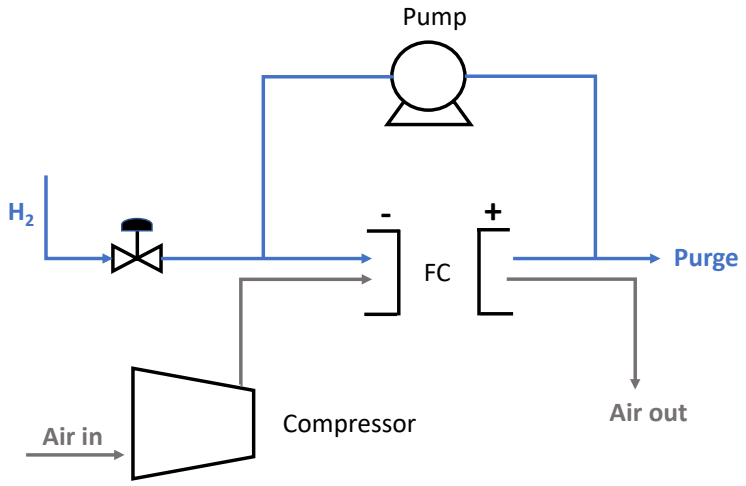

Figure 3.5. A diagram of the fuel cell system including the stack, hydrogen recirculation system, and air flow system

The black lines in Figure 3.5 represent the air flow's path. The air system is a backward pressure system using a valve to build up pressure from exhaust. Air is brought in at ambient conditions and compressed to a target pressure where it then passes through the charge air cooler where it is heated up or cooled down to meet the target fuel cell temperature. A humidifier is used to increase the humidity of the entering air. The humidified charged air enters the fuel cell where the oxygen is consumed and the remaining gas is rejected to the exhaust. A humidity set point of 0.8 was used.

The compressor was designed according to its pressure ratio and air mass flow rate. The SR is a design variable used to control the flow rate of the compressor relative to the consumption rate of oxygen at the cathode. The design point of the air compressor is designed such that the mass flow rate enables the SR to be slightly higher than unity at high current densities. Higher SRs are used at lower currents to prevent the compressor from surging. The equation used to model the system is given as below:

$$SR = \frac{O_2 mass\ flow\ rate\ into\ cathode}{O_2\ mass\ consumption\ rate} = \frac{4\ m_{air}^{compressor}\ X_{O_2}^{air}\ F}{i\ N_{cell}\ A\ MW_{O_2}} \tag{3.5}$$

Where $m_{air}^{compressor}$ is the design mass flow rate for compressor, $X_{O_2}^{air}$ is the mass fraction of O_2 in air, F is the Faradays constant, i is the current intensity, N_{Cells} is the number of cells in stack, A is the area of stack, MW_{O_2} is the molecular weight of O_2.

A cooling system was implemented to control the temperature for the fuel cell, DC-DC converter, electric machine, and battery (Figure 3.6). The cooling system serves to target a fuel cell stack operating temperature of 80°C. The system is comprised of a water charge air cooler (WCAC) for each fuel cell stack, a radiator equipped with a fan, and coolant jackets that encase each fuel cell stack. The coolant is a 50/50 mixture of ethylene glycol and water.

A starting point in the cooling circuit is post fuel cell stack. Coolant is heated from cooling the stack and its temperature must be lowered back to the coolant set point temperature. From the stack, coolant flows to the WCAC. The WCAC brings inlet air to its target temperature. When compression across the cathode compressor is high, it will cool down the air to prevent it from exceeding the boiling point of water and reducing the relative humidity. When the compression is low, it will warm the air and improve the kinetics of the fuel cell. From the WCAC, the coolant flows through a valve that allows a fraction of the coolant to go to the radiator and a certain fraction to bypass the radiator in to control the coolant temperature. Large amounts of required cooling favor more coolant passing through the radiator. The radiator cooling system gets bypassed if the coolant is colder than its set point. Once the coolant passes through the radiator, it is cooled using convection by an air flow rate through the grille of the truck or a fan. The air flow rate through the grill is dependent on vehicle speed and the fan's blowing rate is dependent on the required remaining cooling rate needed by the radiator. From the radiator, coolant flows to the fuel cell stack. The fuel cell stack is encased by a coolant jacket which allows the colder fluid to pass over the hot fuel cell, completing the circuit.

The attributes of the cooling system components are given in Table S10. The cooling system power auxiliaries include the radiator, fan and coolant pump. The battery cooling plate, DC-DC converter, cooler, and motor are modeled as lumped mass thermal models. The temperature profile is assumed uniform throughout the mass. A mass and surface area are assumed for each cooling component.

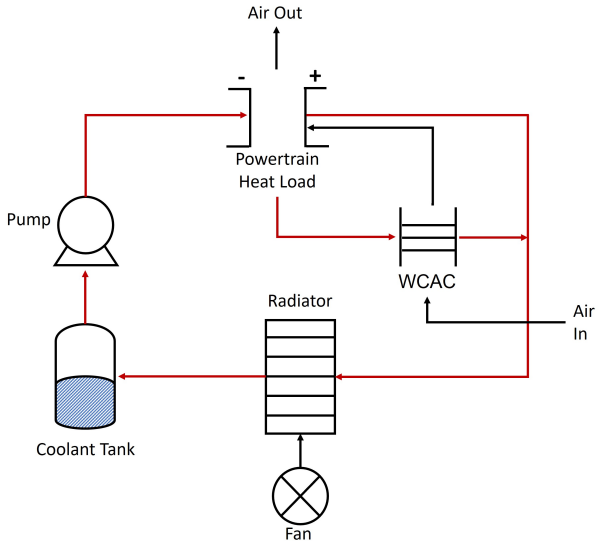

Figure 3.6. Schematic representation of the cooling system. Red lines represent the coolant circuit and black lines represent air flow systems.

The battery pack is a Thevenin electrical-equivalent model that is based on open-circuit voltage and internal resistance. Data used to model open circuit voltage and internal resistance can be found in Figure S23. Additional battery model specifications are given in Table S11. The battery management system limits the voltage and current passing through the battery. Battery limits for voltage and current are provided here based on the C-rate and the number of cells in series and parallel.

The motor is a map-based model that uses efficiency, positive and negative torque maps (Figure S25). The motor is oversized to achieve the torque and vehicle speed requirements. A much smaller motor can be used in conjunction with a transmission. The transmission allows the motor's max speed to be reduced due to the presence of gears. While the transmission allows the motor's max speed to be reduced, the motor's max torque should consider the torque requirements over its operational duty. Future work will consider powertrain architectures that contain smaller motors coupled with a transmission.

Powertrain Component Sizing and Architecture

The fuel cell was optimized on the basis of powertrain architecture and peak power sizing to improve fuel economy and reduce the total cost of ownership. In general, fuel cells experience their peak efficiency at low loads. Larger systems tend to have higher average efficiencies over a drive cycle; however, large systems can be hindered by capital costs and weight penalties. Architectures explored in this study include the plug-in and non-plug-in hybrid electric.

The H-FCET hybrid powertrain architecture is parallel such that the battery and fuel cell

can directly supply the motor with electrical power. The powertrain is designed to be fuel cell dominant with a large fuel cell to provide the majority of the power demand. The battery is sized to predominantly provide the transient power demands during moments. The plug-in parallel hybrid has the same energy management logic as the non-plug-in parallel hybrid. The difference between the two is the battery size. Because the plug in starts the day with a full charge, an initial SOC of 0.9 was used along with larger batteries in the sizing sweep.

The energy management scheme for the hybrid architecture is given in Figure 3.7. The power management states for the considered architectures are fuel cell off, normal operation, battery charging, and battery super charging. In the off state, the fuel cell idles at 10kW and supplies no power to the battery or motor. Under normal operation state, the fuel cell supplies the majority of the power demand. For the battery charging state, the fuel cell supplies power to the motor and charges battery at 20kW. For the battery super charging state, the fuel cell supplies power to motor and charges battery at 40kW. The parameters associated with the transitions to each state are given in Table S9.

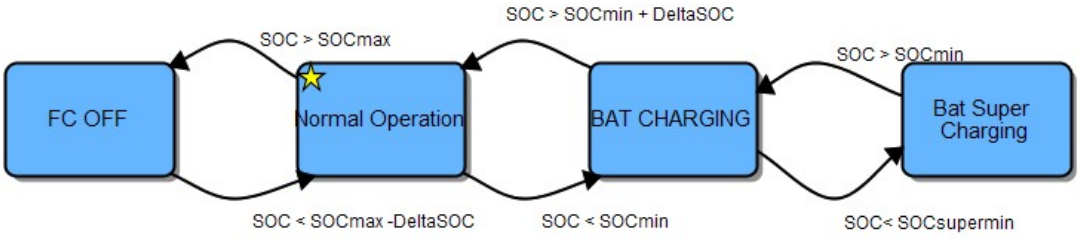

Figure 3.7. Energy management transition states for the H-FCET

The fuel cell and battery sizing were optimized over the total cost of ownership by sweeping over the number of cells in the fuel cell stack and the number of parallel cells in the battery. The battery and fuel cell sizes considered are 300-900kW and 25-1250kWh, respectively.

Projected Fuel Economies

This study considers the powertrains of heavy-duty long-haul trucks in three different scenarios: present, mid and long term. Future fuel economy is based on the current simulated value, and increases proportionally to the increase in the propulsion system's peak efficiency. In the case of the combustion engine future fuel economy is further improved by the addition of a waste heat recovery system.

The current baseline for comparison of engine peak efficiency is 43% according to the IAV hydrogen combustion engine maps. Future H-ICET efficiencies are based on diesel combustion engine projections. The mid-term peak BTE is assumed to be 55% and is based on the DOE project, SuperTruck II. A BTE of 60% is assumed for the long term and is based on projections set

by the Department of Energy as stated in their 21st Century Truck Partnership [27].

The hydrogen fuel cell base line peak efficiency is 64% according to the efficiency curve (see Figure S21). Future hydrogen fuel cells efficiencies are based on the hydrogen fuel cells technology office's future projections and are 68% and 72% for the midterm and longterm scenarios, respectively [28].

3.2.4 Total Cost to Society

The TCS was calculated using a discounted cash flow for each scenario year considered. The TCS considers a total cost of ownership along with emission damage to society by incorporating the SCC. Production volumes associated with economies of scale were considered for major cost components. Previous work by the authors established the methodology and associated parameters for a discounted cash flow in the context of long-haul trucking. The discount rate was set at 7%, while vehicle lifetime was 10 years. The vehicle miles travelled was a function of year with an average of 87,000 mi per year.

The TCO portion of the TCS is broken into capital and operating cost components. The capital cost is the sum of the manufacturing costs for each powertrain component. Powertrain components considered include, the glider, hydrogen combustion engine, fuel cell system, fuel tank, electric motor, DC-DC converter, transmission, and battery. Because the fuel cell and the hydrogen tank dominate the capital costs and are not currently produced at scale, manufacturing volumes are considered based on model year market penetration (section 3.2.1). The operating cost is comprised of driver salary, fuel, tolls and fees, insurance, maintenance and repair, and permit and licenses. A summary of capital and operating cost parameters is given in Table 3.6.

3.2.5 Well-to-Wheel Emissions

This study considers greenhouse gas emissions produced during the fuel production process, WTP, and emissions from combusting the fuel as the vehicle operates, PTW. The entire process consisting of fuel production and vehicle operation is known as WTW, and is a primary output of this study. In the present term, central SMR without carbon capture is the selected technology because it accounts for nearly all present-day hydrogen generated in the United States. The midterm scenario uses central SMR with carbon capture because the carbon capture has been shown to add minor complexity and costs and an established technology, however it drastically reduces emissions by 90%. The longterm scenario imagines a world with net zero emissions. To achieve this, only renewable electrolysis was considered in the longterm.

The pump to wheel emissions for the hydrogen powertrains is zero due to the absence of carbon within the propulsion reactions. The hydrogen combustion engine has the potential to produce emissions due to the oil seeping into the combustion chamber. This is a small amount compared to

Table 3.6. Capital and operating cost parameters in 2020 USD

Parameter	Present	Mid Term	Long Term	Unit	Source
Glider	95,000	95,000	95,000	USD	[29]
Battery	132	100	80	USD/kWh	BatPac [30]
Motor	13	13	13	USD/kW	[31]
Fuel Cell	283	90	69	USD/kW	[32]
Tank	566	533	473	USD/kgH_2	[33]
Power Electronics (DC-DC)					
Transmission	10,000	10,000	10,000	USD	[34]
Electricity	0.133	0.128	0.117	USD/kWh	[35]
Hydrogen	12.24	6.64	5.83	$/kg	[35]
Maintenance and Repair	0.09	0.09	0.09	USD/mi	[36]
Labor	0.69	0.69	0.69	USD/mi	ATRI
Tolls	0.03	0.03	0.03	USD/mi	ATRI
Insurance	0.07	0.07	0.07	USD/mi	ATRI
Battery Replacement	75,000	75,000	75,000	cycles	USCAR
Fuel Cell Replacement	20,000	25,000	30,000	Hours	[28]

the emissions associated with combusting diesel fuel and is assumed to be zero for simplicity. From the WTP emissions, the WTW emissions are calculated using the vehicle's fuel economy.

3.3 Results & Discussion

3.3.1 Scale of Hydrogen Demand

The total annual hydrogen demand for the present, midterm, and long-term scenarios are found to be 0.01, 0.30, and 6.8 billion kg H_2 as shown in Figure 3.8. This is roughly half of the 2020 hydrogen demand in the US **[STATISTA2020]**. Hydrogen demand is most sensitive to the assumed long haul fraction of the heavy-duty truck market. Market penetrations resulting from this scale were 1%, 5% and 100%, respectively. Detailed trends in total number of alternative trucks expected to deploy are available in Figure S1.

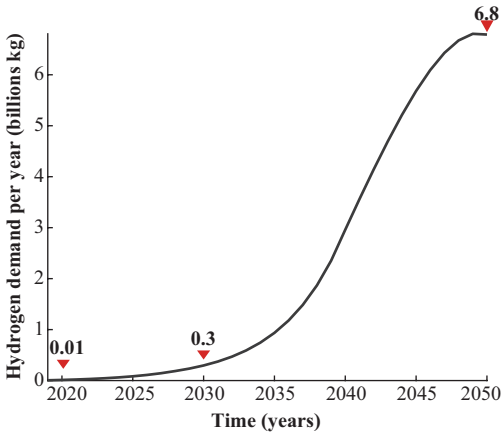

Figure 3.8. Hydrogen demand over time

3.3.2 Cost of Hydrogen

The hydrogen costing analysis accounts for production, carbon capture and sequestration, distribution, and refueling costs and the results are shown in Figure 3.9. The present day scenario shows values ranging from a maximum of $30.17/kg for solar distributed electrolysis to a minimum of $7.84/kg for distributed SMR. The technology standard today is centralized SMR and is selected for the present-day scenario used in this study. The results of this study calculate SMR central hydrogen to range from $10.37/kg to $16.67/kg with a base case value of $12.24/kg. These values do not consider retail markup and are therefore comparable to the average price of vehicular hydrogen sold in California for $16.51/kg. SMR benefits from cheap production costs, however delivery accounts for over half of the costs in centralized plants. Amongst other technologies in the present, electrolysis is the most expensive regardless of electricity source and location with an average present-day scenario cost of $16.53/kg. This is largely due to the high production costs in the present as electrolyzers have not reached scale. Coal gasification with carbon capture has an intermediate cost of $13.46/kg. For the case of central versus distributed plants in the present scenario, there seems to be no clear distinction, however distributed plants for their respective technology average slightly cheaper. The cheaper refueling cost of central plants is offset by the addition of an expensive delivery cost. Distributed plants average 2.2% and 10.1% cheaper than central plants for electrolysis and SMR technologies, respectively.

The midterm scenario tells a similar story to the present-day scenario, however the production pathways begin to distinguish themselves from each other. The cost of hydrogen in the midterm is significantly cheaper than the present-day and ranges from $18.56/kg for distributed grid-based electrolysis to $4.17/kg for distributed SMR. The midterm technology selected for this study is centralized SMR with carbon capture and sequestration. This technology ranges from $6.27/kg to $7.85/kg with a base case value of $6.45/kg. Electrolysis continues to be the most expensive technology with an average cost of $9.23/kg, however the distributed wind plant does have lower

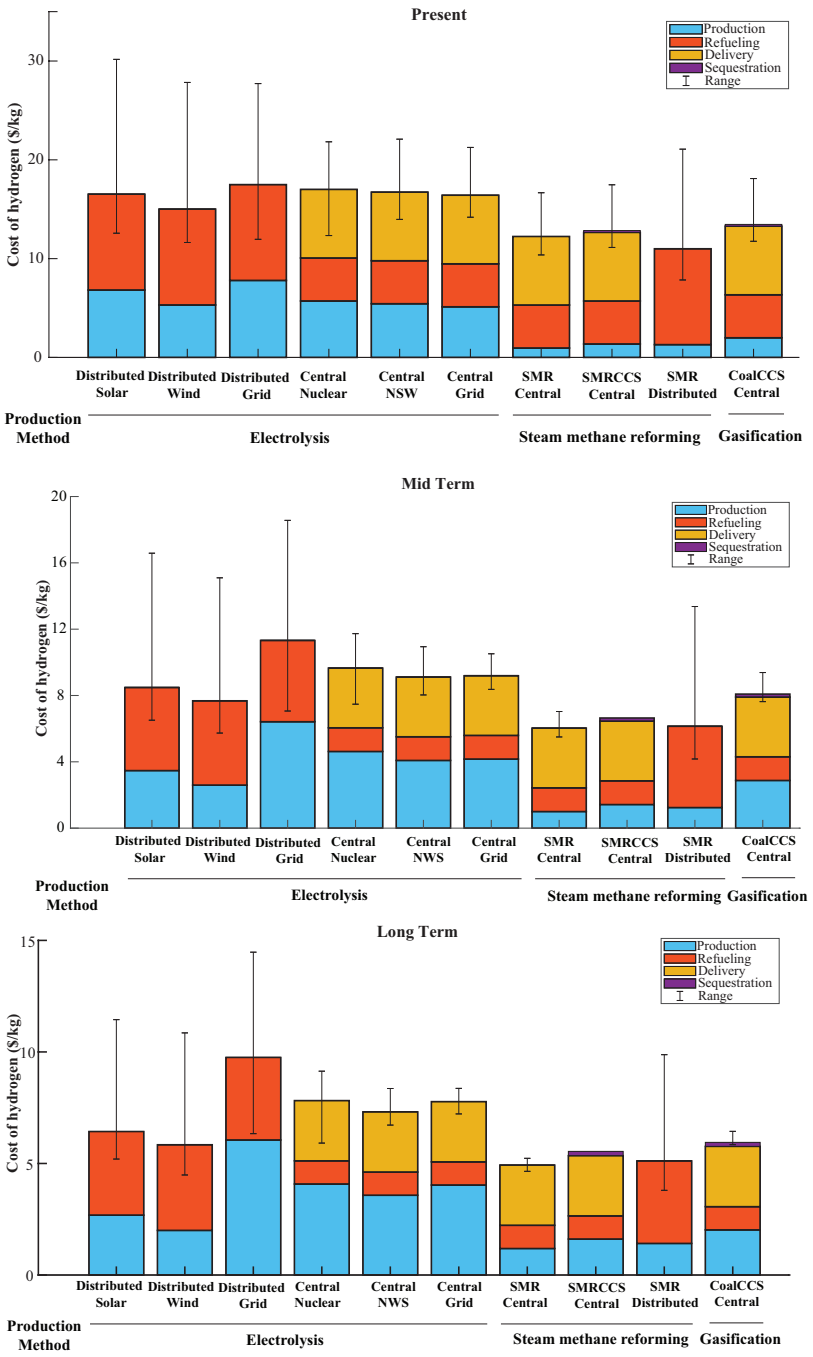

Figure 3.9. Total cost of hydrogen in present, mid term and long term scenario

costs than the coal plant at $8.09/kg. SMR continues to be the lease expensive option. Again, there is no clear winner between central or distributed plants, however the distributed electrolysis plants show more variation.

Again, the longterm scenario trends look very similar to the present and midterm scenarios, however scale has been met and costs are lower ranging from $14.47/kg for distributed grid-based electrolysis to $3.79 for distributed SMR. The longterm technology selected for this study are the

renewable pathways with no carbon emissions and include electrolysis with electricity produced from either solar or wind. Because it is likely both options will be needed and largely depend on geographic location, an arithmetic average was taken. Renewable electrolysis in the longterm ranges from $4.84/kg to $11.14/kg with a base value of $6.14/kg. Even at scale, electrolysis is the most expensive technology, however it becomes comparable to both SMR and coal gasification with averages of $5.20/kg and $5.95/kg, respectively. The distributed electrolysis from renewables shows significant advantage over the central electrolysis plants.

3.3.3 Fuel Economy and Powertrain Component Sizing

The fuel economy sweep for the H-ICET is given in Figure 3.10. The H-ICET fuel economy ranges from 6.41 to 6.74 mi/kg depending on the gear ratio configuration. Because sizing of the gear ratios does not have any tradeoffs when considering the TCS, no further optimization is necessary. The highest fuel economy directly relates to the lowest TCS, therefore the present-day fuel economy for the H-ICET is set at 6.74 mi/kg. The resulting fuel economies for the mid and long-term are 7.48 and 8.6 mi/kg respectively.

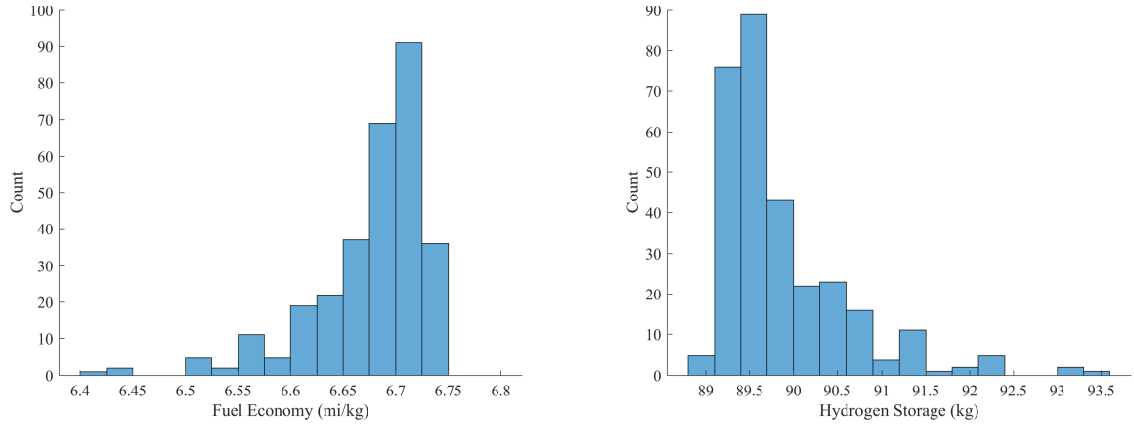

Figure 3.10. H-ICET fuel economy and hydrogen storage considering various gear ratios

The influence of battery and fuel cell size on fuel economy and hydrogen storage for the H-FCETHEV is shown in Figure 3.11. The fuel economy of the H-FCETHEV is most sensitive to the size of the fuel cell. The fuel economy increases with increasing fuel cell size, because fuel cells operate more efficiently at low loads. However, this trend is not linear and has diminishing gains, which is exhibited by the increased spacing between fuel economy contours. In the case of the H-FCETHEV, the battery size affects the fuel economy at smaller battery sizes before the fuel economy becomes independent of battery size. This is because at large battery sizes, the increased storage is not utilized. The amount of useful battery energy storage is highly dependent on energy management logic and the duty cycle. Duty cycles with large amounts of braking energy

dissipation can benefit from larger batteries. Once the battery is fully charged, any more energy from breaking will not be recovered and therefore lost. This scenario suggests increasing battery size would improve fuel economy. In addition, energy management logic that is dynamic over the entirety of the battery's SOC will increase the fuel economies sensitivity to battery size. The energy management logic in this study discharges the battery until a 0.3 **SOC!** (**SOC!**). From there, the fuel cell slightly begins to charge the battery and will stop when the battery reaches 0.4 **SOC!**. In the absence of excess regenerative breaking, an **SOC!** greater than 0.4 will not be achieved and therefore a significant portion of the battery energy storage will be wasted. In a HEV configuration, an ideal battery size would provide all the transient energy needed the fuel cell could not, while at the same time, being just large enough to recover all the energy from regenerative break. The fuel economy which minimizes the TCS is chosen for the present-day scenario and is 7.56 mi/kg. The amount of on-board hydrogen storage needed for this configuration is 72.4 kg.

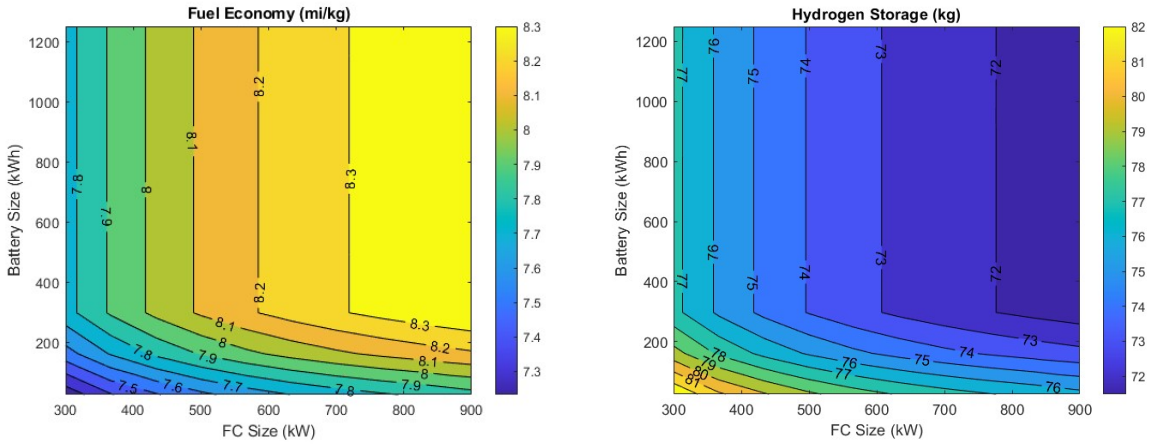

Figure 3.11. H-FCETHEV fuel economy and required hydrogen storage considering various battery and fuel cell sizes.

The influence of battery and fuel cell size on fuel economy and hydrogen storage for the hydrogen fuel cell electric truck (plug in hybrid) (H-FCETPHEV) is shown in Figure 3.12. The hydrogen fuel economy is sensitive to both the fuel cell and battery size. The electricity fuel economy is provided because the PHEV must purchase and consume electricity. Increasing the PHEV's battery size is shown to largely increase the hydrogen fuel economy. This is because electricity serves as a secondary propulsion source. Because the battery is assumed to start at a full charge each day, larger batteries use more electricity to propel the vehicle per shift, causing more electricity and less hydrogen to be consumed. Increasing the fuel cell size has marginal returns at low battery sizes and becomes more significant at larger battery sizes. This is primarily because the large fuel cells operate more efficiently at these high loads of providing the tractive power demand and the power demand to charge the battery. Small fuel cells would be operating at their peak power to provide these demands, causing them to be at the low end of their efficiency curves. The present-day fuel

economies that minimize the present day TCS and are 9.46 mi/kg and 2.03 mi/kWh. The amount of on-board hydrogen storage needed for this configuration is 63.4 kg.

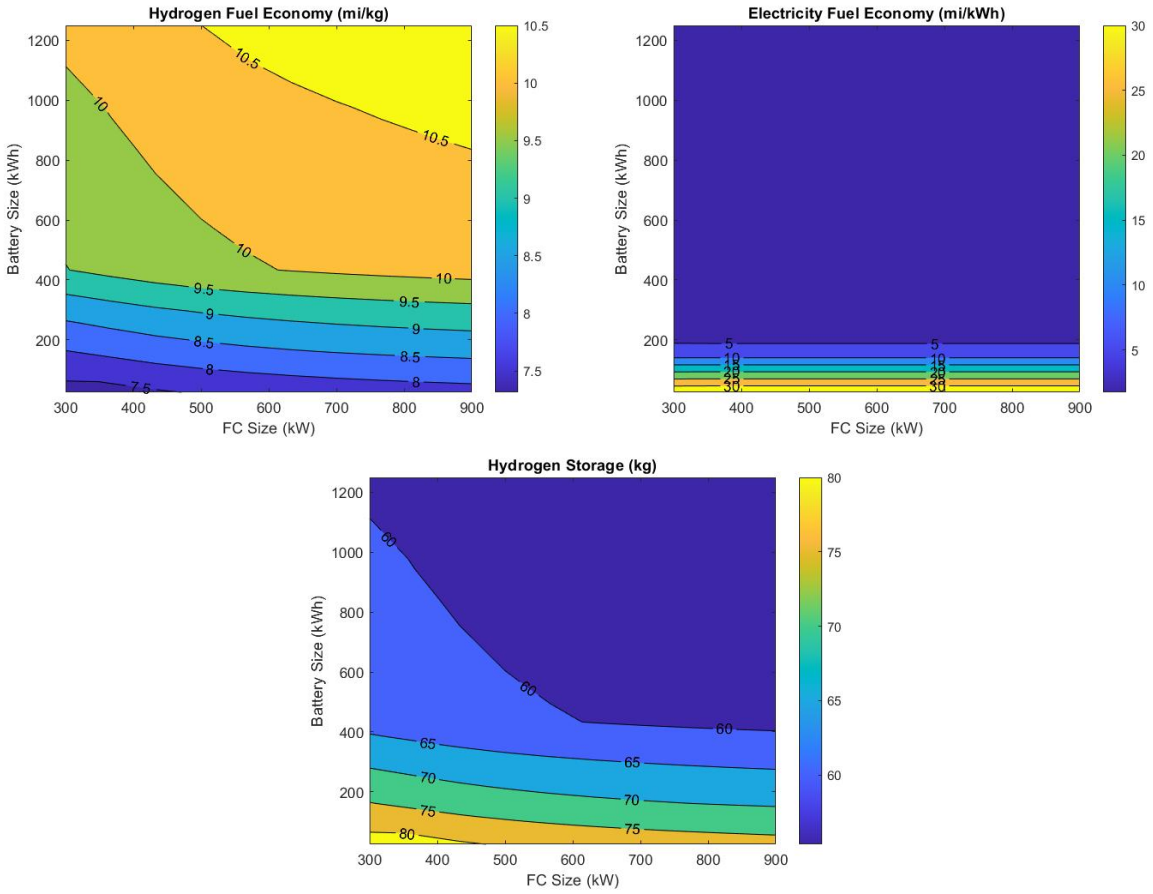

Figure 3.12. H-FCET Parallel PHEV fuel economies and required hydrogen storage considering various battery and fuel cell sizes

	Powertrain						
	H-ICET		H-FCETHEV		H-FCETPHEV		
Fuel Economies & H_2 storage	mi/kg	kg	mi/kg	kg	mi/kg	mi/kWh	kg
Present	6.74	89.0	7.56	79.4	9.46	2.03	63.4
Mid-term	7.48	79.4	8.11	74.0	10.41	2.03	57.6
Long-term	8.60	80.2	9.08	66.1	11.02	2.03	54.5

The final powertrain component sizes are selected based on a minimum TCS value while maintaining performance requirements over the USLHC8 cycle. The results of the battery and fuel cell sizing on TCS are given in figures 3.13 and 3.14. Starting with the present-day scenario, there is a minimum TCS corresponding to small fuel cell sizes and intermediate sized batteries. Larger fuel cell sizes result in higher total costs due to the tradeoff between fuel economy, payload penalty, and

capital cost. Increasing the fuel cell size increases the capital cost and payload penalty; however, fuel economy improves. By tripling the fuel cell size from 300 kW to 900 kW, the fuel economy improves only by roughly 8%, however the capital cost and weight penalty increase by 50-90% and 31-247% respectively. This led to a small fuel cell to be favored for the H-FCETPHEV architecture in present day scenario. The battery sizing experiences an optimum around 450 kWh in all time scenarios for the H-FCETPHEV. In the present scenario, electricity is significantly cheaper than hydrogen allowing for the presence of intermediate sized batteries. However, as the battery size passes the 450 kWh mark, the combination of the capital and weight penalty prevent further improvement in TCS. In addition, the excess energy stored by the battery is not needed and is not used during operation over the USLHC8 cycle. The optimal battery size for the H-FCETHEV occurs around 100 kWh for all time scenarios.

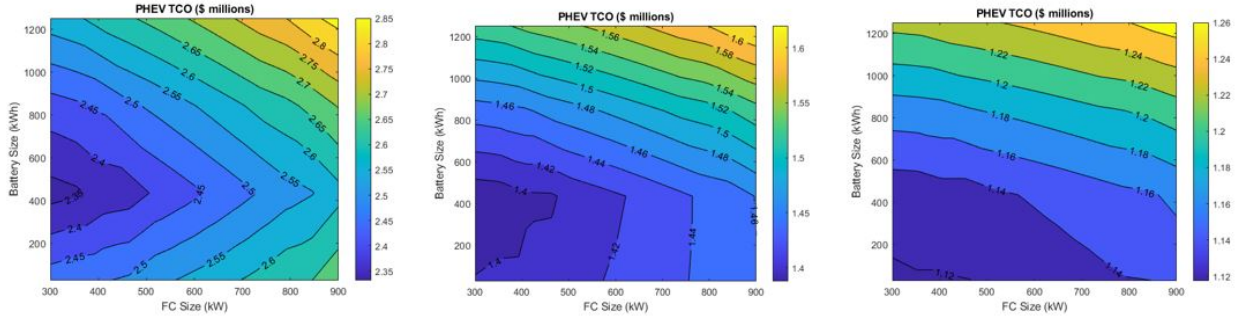

Figure 3.13. The influence of the fuel cell and battery size on the PHEV total cost of ownership. left - present; middle - mid term; right - long term

The trends of the present scenario continue for the mid-term and long-term scenarios. In the midterm and long-term scenarios, hydrogen costs much less which further biases smaller fuel cells. The optimal fuel cell sizes for both the midterm and long-term scenarios occurs at 300 kW. The optimal battery size tends to decrease in time. This again is due to the cost of hydrogen. The hydrogen cost drops enough that electricity consumption is not necessarily favored to hydrogen. In the long term, the smallest battery is favored for the lowest TCS. In the latter scenarios the increased capital costs of the larger battery and fuel cell out weight the reduced operating costs associated with smaller powertrain components.

The energy losses for the fuel cell and combustion hydrogen powertrains are given in Figure 3.15. The fuel cell powertrain utilizes one more energy conversion step than the hydrogen combustion when considering the direct path shown in Figure 3.15, however a small portion of energy flows to charge the battery and adds an additional energy conversion step. Additionally, the hydrogen fuel cell has a much higher auxiliary power load than the hydrogen combustion engine. The fuel cell cooling load is larger than the combustion engine's due to the smaller temperature gradient between the ambient environment and the fuel converter. The fuel cell operates at much lower temperatures, which

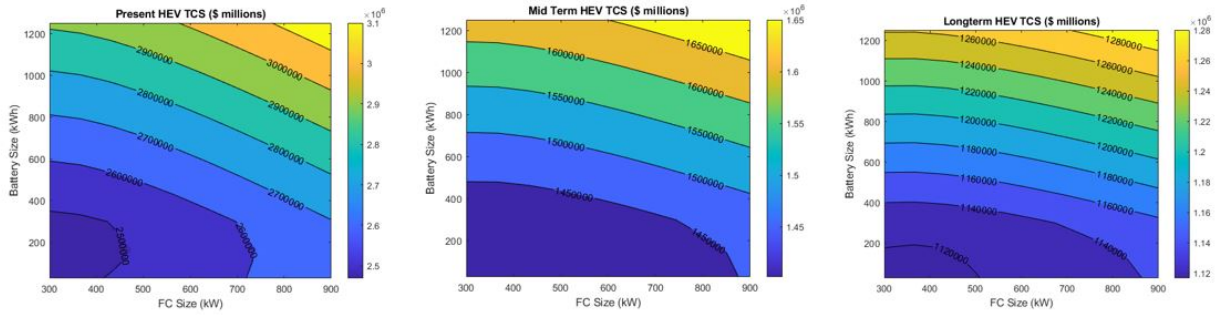

Figure 3.14. The influence of the fuel cell and battery size on the HEV total cost of ownership. left - present; middle - mid term; right - long term

requires a larger fan and coolant pump to satisfy the cooling duty. Additionally, the compressor that supplies air to the fuel cell requires a substantial amount of energy. The fuel cell has a slightly higher overall efficiency than the combustion engine even when considering the additional energy conversion steps and much higher auxiliary load. This is primarily due to the fuel conversion step. The single unit efficiency of the hydrogen fuel cell exceeds the combustion engine by 18%.

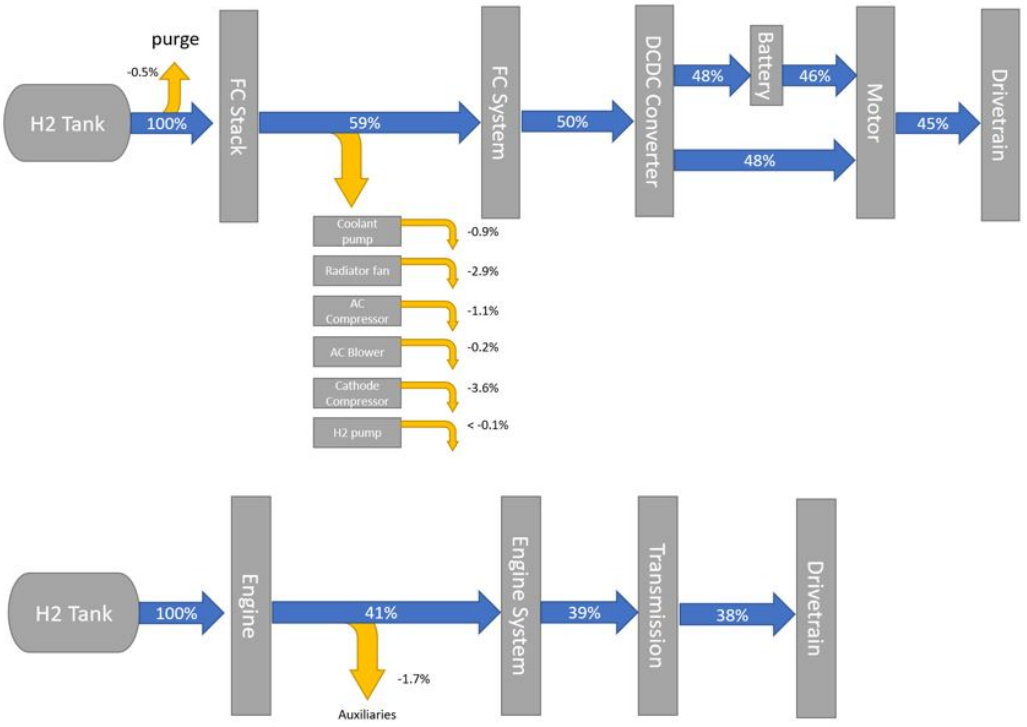

Figure 3.15. Diagram representing the energy losses for the fuel cell and combustion systems

3.3.4 Emissions analysis

The results for all the considered hydrogen pathways are given in Figure 3.16. The electrolysis pathways include the highest and lowest WTP emissions. The renewable pathways, electrolysis from wind or solar, have zero emissions. This is because all electricity is generated from either solar or wind power with no connection to the grid. There would likely be emissions associated with the photovoltaic or wind turbine manufacturing process, however the calculations presented are limited to a WTP scope. Electrolysis when utilizing grid electricity, is calculated to be the highest emitting pathway. This is due to the upstream grid's electricity being primarily produced from fossil fuel sources and the large amount of electricity needed to produce hydrogen by electrolysis. Hydrogen electrolysis pathways using nuclear or NSW demonstrate low emission potential. The emissions associated with these pathways are attributed mainly to the liquefaction step of delivery which uses grid electricity that has upstream emissions.

The SMR pathways exhibit an intermediate emission level for all scenario years. The SMR pathways have direct emissions from the production process and the carbon capture options are set to capture 90% of production emissions. A small amount of emissions for the coal and SMR pathways is due to upstream emissions from electrical utilities. The remainder of SMR emissions are due to delivery for the central based plants.

The scenario results in Figure S26 consider one production pathway per scenario year that is based on emission reduction goals and technology readiness. In the present term, central SMR without carbon capture is the selected technology because it accounts for nearly all present-day hydrogen generated in the United States. The midterm scenario uses central SMR with carbon capture because the carbon capture has been shown to add minor complexity and costs and an established technology, however it drastically reduces production emissions by 90%. The longterm scenario imagines a world with net zero emissions. To achieve this, only renewable electrolysis can be considered. Therefore, wind-based electrolysis is chosen as the preferred technology as it is the less expensive option of the renewables.

3.3.5 Total Cost of Ownership

The results from the capital cost modeling are given in Figure 3.17. The powertrain component sizes and cost values can be found in Tables S12, S13 and S14. The present-day diesel capital cost is $125,000 and represents the industry's current standard. The capital costs for the hydrogen powertrains are significantly more expensive than the diesel powertrain in the present, primarily due to the fuel tank and fuel cell costs. In the present day, the battery electric powertrains are 1.4 to 2.3 times more costly than diesel. In the longterm, the hydrogen powertrains are only 1.1 to 1.2 times more expensive. At low manufacturing volumes, the fuel cell dominates the capital costs of the H-FCET powertrains. However, The fuel cell capital cost decreases dramatically such that it

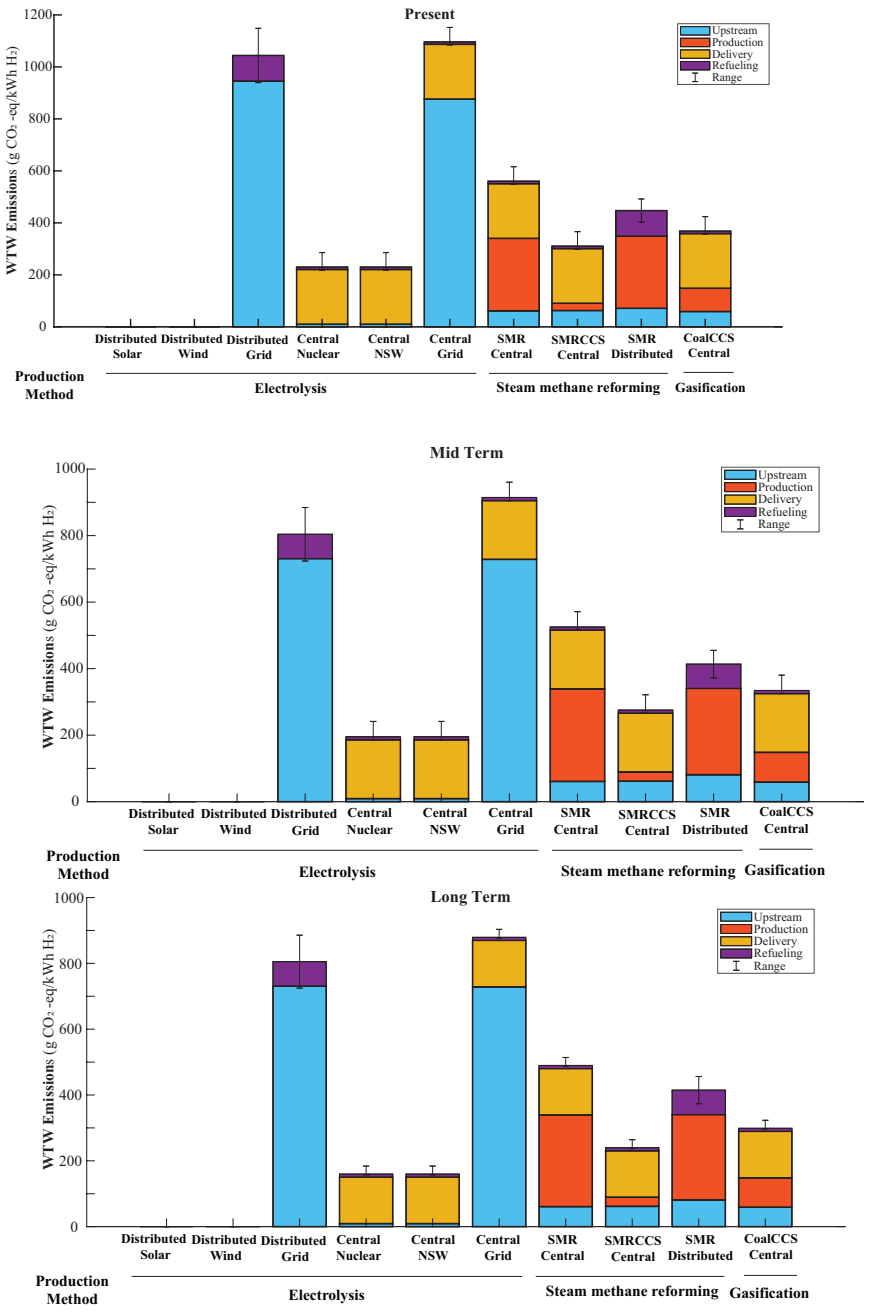

Figure 3.16. WTW emissions for the considered hydrogen pathways

becomes nearly on parity with the combustion engine in the long term.

The capital costs for all hydrogen powertrains decrease in time. The H-FCET capital cost decreases by only 4% in the longterm. This is because its powertrain components are nearly identical to the diesel powertrain which has already experienced high manufacturing volumes. The decrease for the H-ICET capital cost is attributed to the decrease in fuel tank cost, however this decrease is near offset by the addition of a waste heat recovery. The fuel cell powertrains experience much larger decreases with the H-FCETHEV and H-FCETPHEV decreasing by 36% and 45% respectively.

These large decreases are attributed to the economies of scale achieved by the fuel cell stack and battery. The hydrogen tank capital cost decreases in time primarily due to powertrain efficiency increases, which reduce the hydrogen needed for the long haul duty cycle. The hydrogen tank also experiences benefits from high manufacturing volumes, however carbon fiber raw material costs keep the tank relatively expensive.

Each time scenario tells a different story for the hydrogen powertrains' capital costs. In the present, the H-ICET is the lowest cost option by far. By the midterm, the H-FCET is the lowest cost option followed by the H-FCETHEV and H-FCETPHEV. In the longterm, both fuel cell powertrains become less expensive than the H-ICET. The largest cost component is the glider for all scenarios except the present where the fuel cell for the H-FCETHEV is slightly more expensive. The second largest cost component is the fuel cell in the present scenario, however by the midterm the fuel tank and battery within the PHEV surpass it. The combustion engine is consistently third for the H-ICET.

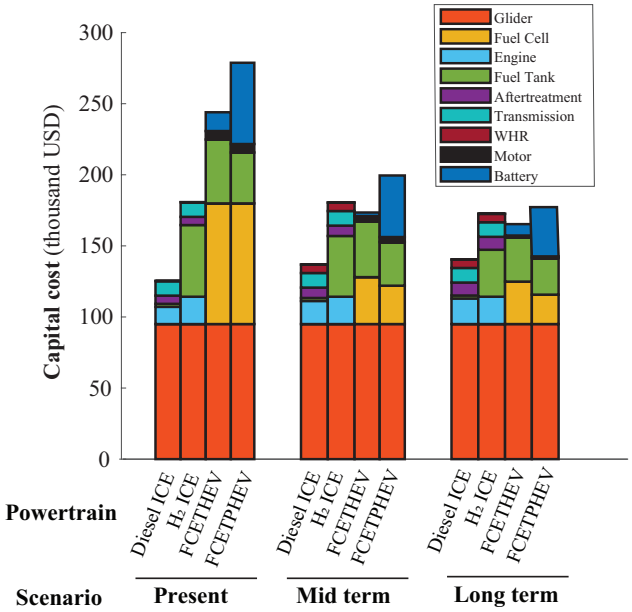

Figure 3.17. Capital cost breakdown for hydrogen powertrains

The results for the operating cost are shown in Figure 3.18. The present-day operating cost for the diesel powertrain is $842,000 and is less expensive that the hydrogen powertrain for all scenarios. In the present, H-ICET, H-FCETHEV, and H-FCETPHEV operating costs are 2.26, 2.02, and 2.15 times more costly than the diesel and in the long term, they are 1.30, 1.25, and 1.26 times more costly. The hydrogen costs for the hydrogen powertrains remains much higher than the cost of diesel due to the unit cost of hydrogen, despite the fuel cell powertrains being more efficient. The maintenance of the fuel cell powertrains is significantly less than the diesel powertrain by 40% in all scenarios, however the H-ICET is assumed to be the same.

Across all scenarios, the operating costs for all hydrogen powertrains declines. The H-ICET, H-H-FCETHEV, and H-FCETPHEV powertrains decrease in the midterm by 33%, 31%, and 31%, repectively, and in the longterm by 41%, 37%, and 40%. The largest cost component driving this decrease is the hydrogen cost. Not only does the unit price of hydrogen decrease by 52%, but the fuel economy also improves according to the values in Table 3.12. The labor generally makes up the second largest operating cost component and is assumed not to change in time. Autonomous driving could drastically change labor costs in the longterm scenario, however an analysis on autonomous driving is outside the scope of this study. There is a weight penalty in earlier years for the fuel cell powertrains, however as the battery's specific energy increases in time and smaller batteries are used in future scenarios, the weight penalty diminishes by the longterm. Early years have a slight operating cost regarding replacement, however as fuel cells become more durable in time, this value diminishes.

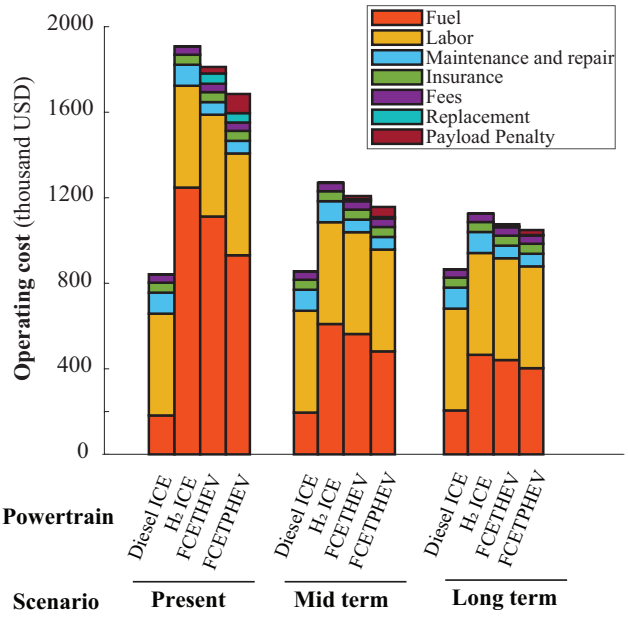

Figure 3.18. Operating cost breakdown for hydrogen powertrains

3.3.6 Total Cost to Society

The results for the TCS metric are presented in 3.19. All results are compared to the conventional diesel powertrain, which is presented in a previous study by the authors. The TCS decreases in time for all hydrogen powertrains as market penetration and therefore scale increases. The carbon cost for the hydrogen powertrains decreases in time. The social cost of carbon increases in time, however fuel economy increases and hydrogen pathway emissions decrease. This is due to the adoption of cleaner hydrogen production technologies being implemented. The capital cost decreases in time primarily due to the economies of scale associated with larger production volumes. Large reductions

in the capital cost are seen in fuel cell, fuel tank, and battery costs. The operating cost decline is largely attributed to decreasing fuel costs and more efficient powertrains.

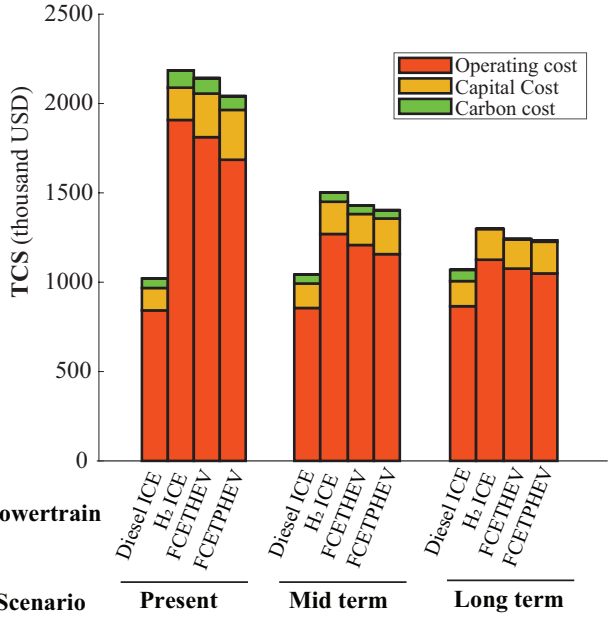

Figure 3.19. Total Cost to Society of powertrain options

At scale, hydrogen powertrains are more expensive that the diesel powertrain even when considering the carbon cost. This study used the social cost of carbon which leads to a small carbon cost that does not penalize the diesel powertrain much. A carbon tax could be useful to further penalize the diesel powertrain and make the hydrogen powertrain options more appealing.

3.4 Conclusion

In this work, benchmarks for hydrogen combustion and fuel cell powertrains were established for long-haul trucks operating in the US. The benchmarks include fuel consumption, costs, and emissions for present to long term scenarios. The analysis included a deep dive into powertrain design, hydrogen future demand, hydrogen upstream pathways, and powertrain manufacturing costs.

Across all scenario years, the hydrogen powertrains are more costly than diesel, even when considering carbon costs. In the present scenario, hydrogen powertrains cost 99-115% more than diesel. In the longterm, all alternative powertrains have nearly the same TCS with the hydrogen powertrains costing slightly more. Because of the large investment in early years, the government will need to play a large role providing support in the form of subsidies and incentives until scale is met. Banks will be needed to provide capital for the large upfront investments. In addition, legislation may be needed to increase the cost of carbon to disincentivize fossil fuel use.

The cost of delivered hydrogen dominated the total cost of ownership, which was estimated at

$12.24/kg for the today's deployment conditions here considered. By the longterm, the hydrogen powertrains become significantly more competitive as the cost of hydrogen drops to $5.83/kg. The cost of hydrogen would have to drop to USD$4/kg for the hydrogen powertrains to be on parity with diesel. This is challenging as the costs associated with liquefaction from delivery for central plants and compression from refueling for distributed plants poses as a large obstacle. Future efforts for lowering hydrogen delivery costs. The authors of this study are currently investigating liquid organic hydrogen carriers in the context of long haul trucking.

Fuel consumption for the various hydrogen powertrain were simulated through system level vehicle models. The hydrogen combustion engine model used engine map data for a hydrogen combustion engine previously developed and validated by the authors of this study. The fuel cell models used a hybrid physical based model in combination with Toyata Mirai polarization curve data. Hydrogen fuel economies for the combustion model were 6.74 mi/kg in the present and projected to be 8.6 mi/kg in the long-term. Hydrogen fuel economies for the HEV and PHEV fuel cell models range from 7.56-9.46 mi/kg in the present and 9.08-11.02 mi/kg in the long run. On-board storage requirements range from 54.5 to 89.0 kg depending on powertrain type and scenario year. This study used a parameter sweep of key energy management parameters to identify optimal fuel economies. Future work should seek to implement various energy management control strategies in the context of long-haul operation.

Hydrogen powertrains were shown to be very effective in reducing greenhouse gas emissions when using a well-to-whell analysis. Nearly all scenarios show a reduction in emissions. The long term scenario shows net zero emissions when using hydrogen produced from electrolysis using electricity from renewable sources such as solar or wind. However, renewable electricity using solar and wind might not be suitable for every geographical location. Nuclear power can be used to subsidize low carbon electricity generation.

As in Part 1, we hope this work can provide a more consistent baseline for comparing hydrogen powertrains to their diesel counterparts in terms of costs, fuel consumption and emissions.

3.5 Appendix

Scale of Hydrogen Demand

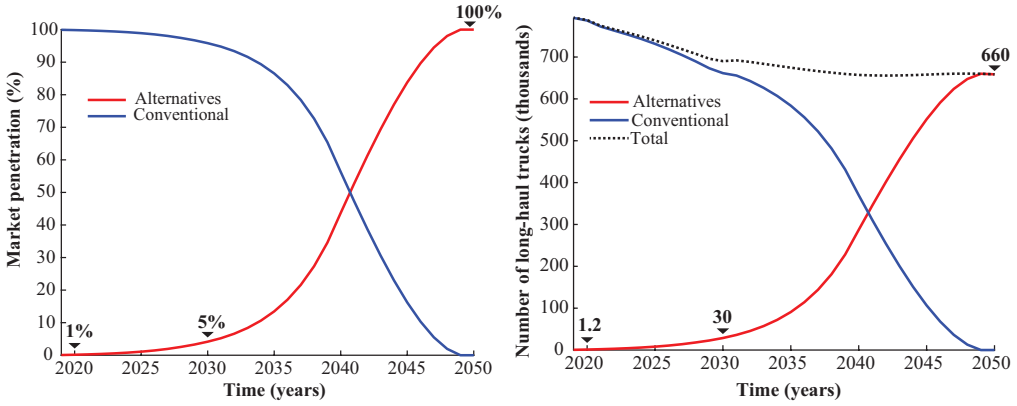

(a) Market penetration **(b)** Total number of trucks

Figure S1. Long-haul truck alternative deployment projections

Figure S2 shows the projections for alternative and conventional long haul production.

Cost of hydrogen

Cost of H_2 production

Steam-methane reforming

In a typical SMR plant, natural gas reacts with steam in a steam reformer to make carbon monoxide and hydrogen. The reformer products are further reacted in shift reactors to form more hydrogen and carbon dioxide. After the reactions, products are sent to an initial amine unit to capture the reaction product carbon dioxide. Hydrogen is separated from the other products using a pressure swing adsorber. The remaining fuel gas is used to heat the reformer, forming more carbon dioxide which is removed by a MEA treatment process. The version of this process that does not capture carbon excludes the amine and MEA based separation processes. A diagram of the process including carbon capture is given in S3. Parameters for SMR in present-day and future scenarios are available in S2.

The output spaces to the longterm SMR financial models are shown in Figure S5. The output space is generated by varying input parameters in table S1 between lower and upper bounds for a total of 27 values for each time -based scenario. Lower and upper bounds for the electricity and natural gas costs were generated by considering a 10% variation and 5% variation for the capacity factor bounds. The results of the parameter sweep are given in Figure S5. Central SMR has the lowest cost production method for all scenario years, followed by distributed SMR and SMRCCS.

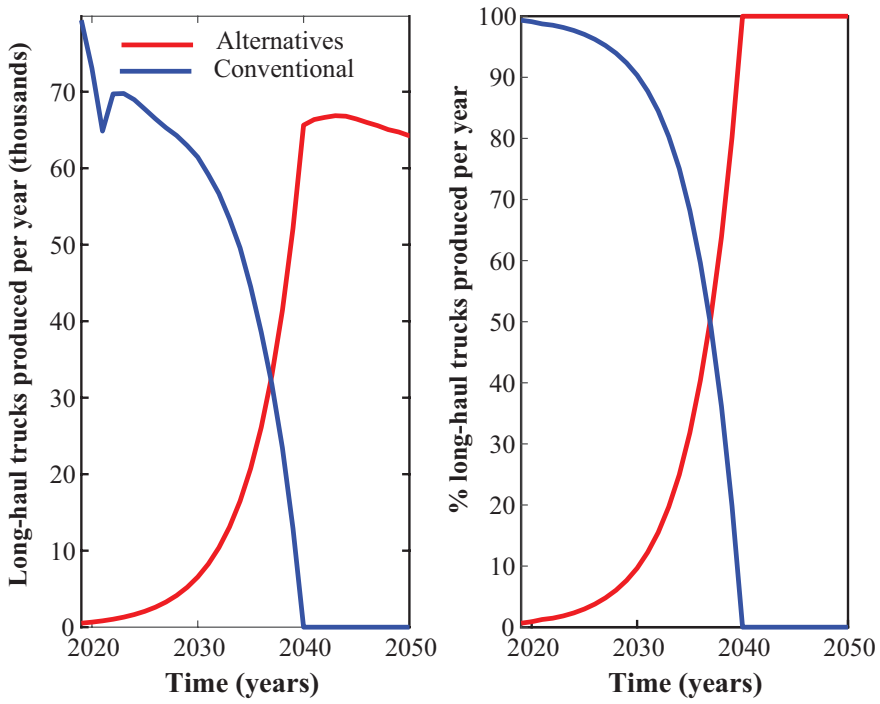

Figure S2. Production of long-haul trucks over time

This is expected as Central SMR benefits from the economies of scale associated with mass production. While the SMRCCS benefits from economies of scale, the carbon capture increases production costs, causing it to be more expensive than distributed SMR that has a much lower design capacity. A cost breakdown analysis is provided in Supplementary Information.

A production cost breakdown is given in Figure S4 for each SMR production method in the 2050 baseline scenario. Cost components are grouped into the cost categories capital, utilities, fixed operation and maintenance, and natural gas. Capital costs refer to all costs purchased prior to plant operation and include process equipment, engineering and design, construction, and land. In the case of a plant with carbon capture and sequestration, only the process equipment associated on the plant site are included in production capital costs. Yearly equipment replacements and debt interests are also included in capital cost. In the context of SMR, utilities include demineralized water, cooling water, and electricity with electricity counting for two thirds. Fixed operation and maintenance refers to costs associated with employees, licensing, permits, fees, property taxes, and repairs or maintenance. Natural gas considers natural gas used in the chemical reactions and as fuel to heat the process.

Natural gas is a primary material input to the process and the highest cost component, followed

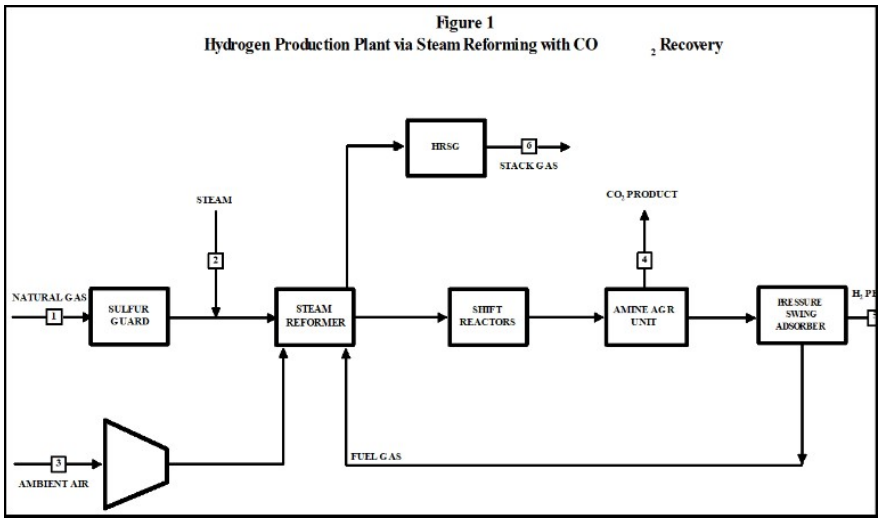

Figure S3. SMR with CC process flow diagram. Source: H2A [12]

Table S1. Base case parameters used for the SMR processes and cost results

		Present	Midterm	Longterm	Source
Parameters	Natural gas price ($/mmBtu)	3.99	4.59	5.74	[11]
	Electricity (cents/kWh)	6.8	6.8	6.9	[11]
	Capacity factor	90%/86%*	90%/86%	90%/86%	H2A
Production cost	SMR Central ($/kg)	0.95	1.00	1.19	This work
	SMRCCS Central ($/kg)	1.36	1.42	1.61	This work
	SMR Distributed ($/kg)	1.30	1.24	1.42	This work

* values are for central (left) and distributed (right) plants

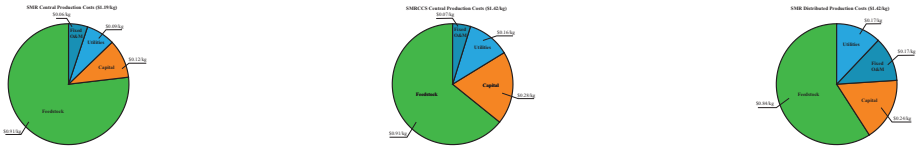

Figure S4. SMR cost component breakdown

by capital, Fixed O&M, and utilities with the remainder. This trend is true for all SMR production methods, however the proportions of each cost component differ up to 25% (in the case of natural gas costs). As expected, the capital cost is much more significant for central SMRCCS and distributed SMR due to the added cost of carbon capture process equipment in the case of central SMRCCS and the lack of economies of scale in the case of distributed SMR. The addition of carbon capture

Table S2. Parameters considered for SMR production

Parameters	SMR Central		SMR CCS Central		SMR Distributed	
	Present	Future	Present	Future	Present	Future
Operating capacity factor (%)	90	90	90	90	86	86
Plant design capacity (KTA)	125	125	125	125	0.47	0.47
Electricity usage (kWh/kgH_2)	0.57	0.57	0.60	0.60	1.11	2.27
Natural gas usage (mmBtu/kgH_2)	0.16	0.16	0.16	0.16	0.16	0.15
Carbon Sequestration (kgCO2/kgH_2)	0	0	8.3 (90%)	8.3 (90%)	0	0
Process Energy Efficiency (%)	72	72	72	72	65	68
Plant life (years)	40	40	40	40	20	20

process equipment more than doubles the capital costs of central SMR and increases production cost by 33%. Having production happen at or near the refueling station increseases production cost by 28%.

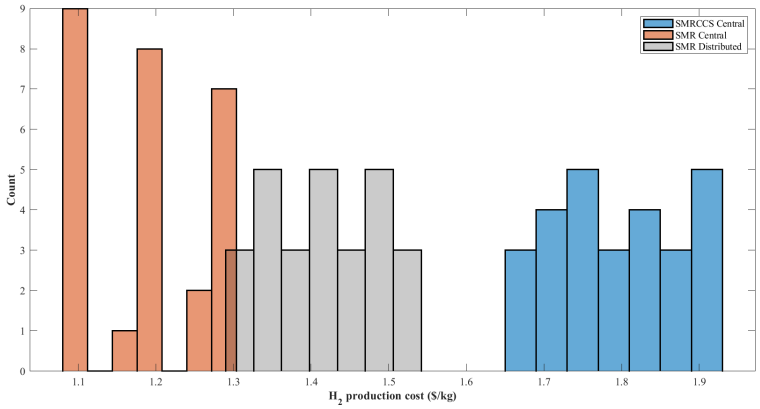

Figure S5. Output space from parameter sweep for the SMR long term scenario

Electrolysis

Electricity and water are the primary inputs to the process. Hydrogen and oxygen are the products and there are no direct GHG emissions associated with electrolysis. The technical model process flow diagram for distributed electrolysis uses PEM electrolyzers and is shown in Figure S6. The electrolyzer stack operates at 1.9V/cell, 80°C, 450 psi with a current density of 2A/cm^2. The 4

MW system is designed to produce 1500 kg/day and consumes 55.8 kWh/H_2 of electricity and 3.5 gal/kgH_2 of water.

Financial Models considering central electrolysis assume a 40 year plant life and a 20 year plant life for the distributed models. Central models are designed to produce 56,500 kg H_2/day while the distributed model produces 1,500 kg H_2/day. In present models, major replacement costs occur every 7 years while future scenarios assume 10 years. Replacement costs assume 15% of the electrolyzer system's initial capital costs.

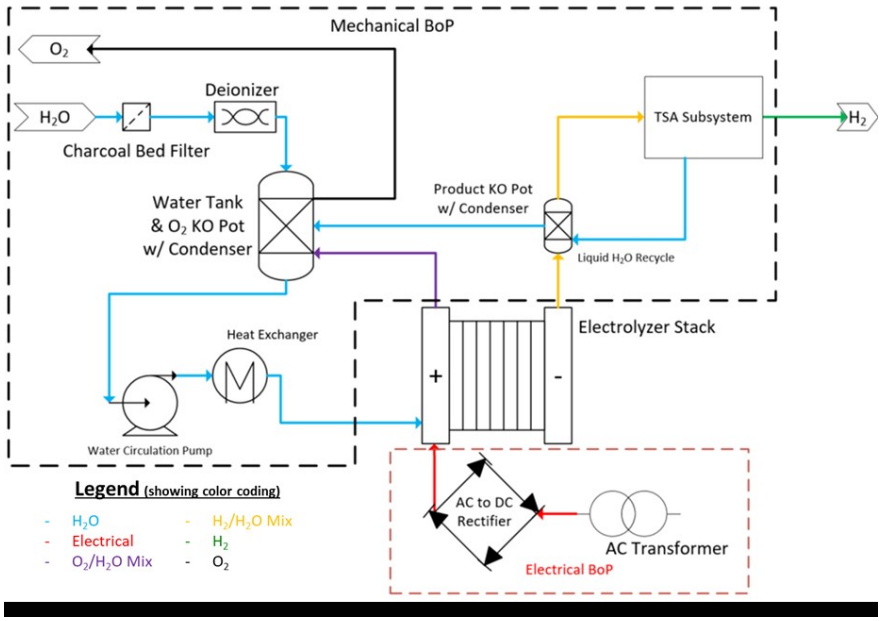

Figure S6. Process flow diagram for electrolysis. Source: H2A [12]

The capacity factor largely influences the hydrogen prices and varies significantly based on the electricity source. Central plants have the largest capacity factors, with nuclear and NSW having the largest, followed by the grid, nuclear, and renewable plants. The distributed plants have lower capacity factors with solar being the lowest, followed by wind, and grid. Plants with lower capacity factors must install larger electrolyzers and storage to meet daily hydrogen production requirements when only operating a fraction of the day. The central grid and the NSW capacity factors are set to H2A central defaults, while the central nuclear electrolysis plants are assumed to be operated solely by a nuclear power plant that determines the electrolysis plant's capacity factor. Solar and wind distributed capacity factors are also assumed to be limited by their production sources and distributed grid electrolysis is given default H2A values. Capacity factors and their ranges for electricity production sources are obtained from NRELATB database [37]. The capacity factor range for central nuclear is generated by assuming a 5% variation.

Table S3. Parameters for electrolysis

Parameters	Central Electrolysis		Distributed Electrolysis	
	Present	Future	Present	Future
Operating Capacity (%)	97	97	86	86
Electricity Usage (kWh/kgH_2)	55.5	51.3	55.8	
Plant Design Capacity	20 KTA	20 KTA	3000 kgH_2/day	3000 kgH_2/day
Process Energy Efficiency (%)	60	65	56	65
Plant life (years)	40	40	20	20

$$LCOE_{NSW} = \sum_{i}^{3} w_i LCOE_i \tag{S1}$$

$$w_i = \frac{CF_i}{\sum_i^3 CF_i} \tag{S2}$$

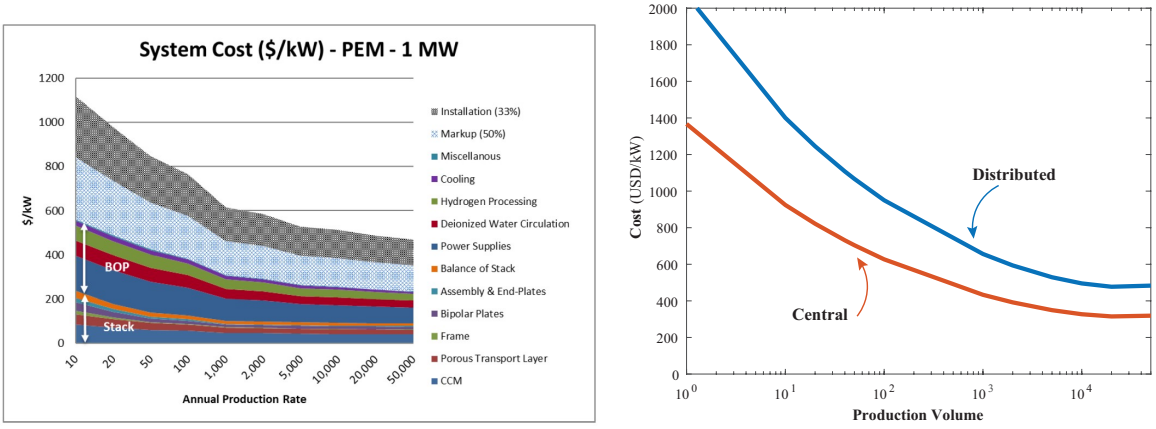

Figure S7. The HFTO's manufacturing analysis for PEM electrolyzers. Right - electrolyzer installed capital cost for distributed and central plants considering scale factors derived from H2A [12].

The results of the electrolyzer capital cost model are shown in Figure S8. The bar values represent base case scenarios with inputs parameters given in Table S1. Error bars represent EIA projections according to the 2019, "The Future of Hydrogen", report. As expected, the electrolyzer costs decrease in time as large production volumes are met. In the longterm, the electrolyzer installed capital cost asymptotes to around \$500/kW for all plants. Plants with lower capacity factors such as plants powered by renewables and distributed plants show \$/kW benefits in earlier years due to larger production volumes needed to supply the given year's hydrogen demand. However; it should be noted that more total national capacity would need to be installed potentially resulting in higher costs at the macro level. Large central plants gain benefit from the many cells or MW needed to

Table S4. Base case parameters used in the electrolysis production costs

Parameter		Distributed			Central		
		Solar	**Wind**	**Grid**	**Nuclear**	**NSW**	**Grid**
Electricity Cost ($/kWh)	**Present**	0.033	0.038	0.105	0.080	0.075	0.070
	Midterm	0.021	0.021	0.106	0.076	0.067	0.068
	Longterm	0.016	0.017	0.104	0.070	0.060	0.069
Capacity Factor	**Present**	0.242	0.430	0.86	0.93	0.97	0.97
	Midterm	0.282	0.471	0.86	0.93	0.97	0.97
	Longterm	0.303	0.482	0.86	0.93	0.97	0.97
Electrolyzer Capital Cost ($/kW)	**Present**	1115	1115	1115	1115	1115	1115
	Midterm	780	780	780	780	780	780
	Longterm	530	530	530	530	530	530

be produced per given plant as shown in equation 3.4, however they are ultimately more costly per kW due to producing more H_2 per kW installed, lowering their benefit from economies of scale.

Table S5. Electrolysis base case production costs

Technology		**Production cost (USD/kg)**		
		Present	**Midterm**	**Longterm**
Distributed	Solar	6.84	3.48	2.68
	Wind	5.32	2.60	2.00
	Grid	7.80	6.42	6.05
Central	Nuclear	5.72	4.63	4.08
	NSW	5.44	4.08	3.58
	Grid	5.13	4.16	4.03

The hydrogen production cost results are given in Table S5. In the present scenario, all electrolysis results in production costs over $5/kg. However in the longterm, production costs drop to as low as $2/kg, with the renewables showing the most promise due to their low levelized cost of energy (LCOE). A production cost breakdown is given in Figure S10.

The output spaces to the 2050 electrolysis financial models are shown in Figure S9. Input parameters explored include the discussed electricity costs, capacity factors, and electrolyzer capital costs. The output space is generated by varying input parameters between lower and upper bounds for a total of 27 scenarios. All distributions have about a dollar spread except for central nuclear and distributed grid. Nuclear has a large spread due to the lower bound on electricity being significantly less from the long-term operation. Distributed grid has a large spread due to the production price being sensitive to the electricity.

A production cost breakdown is given in Figure S10 for each electrolysis production method in

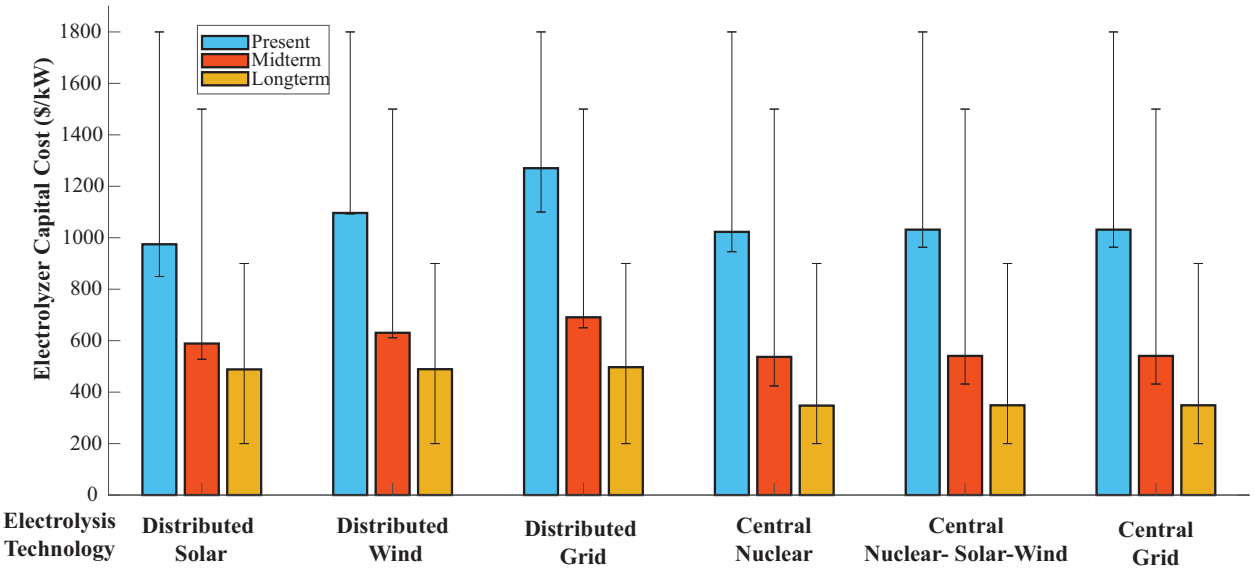

Figure S8. Electrolyzer capital cost considering scale for each scenario. Error bars show max and min projects according to EIA

the 2050 baseline scenario. Cost components are grouped into the cost categories capital, electricity & water, and fixed operation and maintenance. Capital costs refer to all costs purchased prior to plant operation and include process equipment, engineering and design, construction, and land costs. In the case of a distributed plant, capital associated with refueling infrastructure including storage, compression and other equipment is not included and delivery equipment is not included for central plants. Equipment replacements and debt interests are also included in capital cost. The electricity and water category is largely dominated by the cost of electricy with electricity contributing nearly all the cost. Fixed operation and maintenance refers to costs associated with employees, licensing, permits, fees, property taxes, and unplanned repairs or maintenance.

Generally speaking, the renewable distributed plant's results are quite different from the rest. The electricity costs dominates in all electrolysis cases except the plants powered by renewables. The lower electricity and higher capital portions in the case of the renewables are attributed to two factors. Renewables have much less capacity factors than all other plants. This leads to the plants sparsely producing hydrogen, making operating costs proportionately less significant and capital costs more significant. Renewables also are able to generate electricity much cheaper than other electricity sources, making the operating cost portions less significant. Fixed operation and maintenance relating to renewables is more expensive because it is directly related to operation time and capital cost. Because of renewables' low capacity, more electrolyzer MW capacity must be installed to meet the same daily demand, leading to higher capital and therefore maintenance costs. The assumptions for labor, licensing, permits, taxes and fees are constant, however maintenance is assume to be 5% of initial capital costs, which implies all plants degrade at the same rate. The maintenance and repair costs within the current model do not consider operation time. Plants that

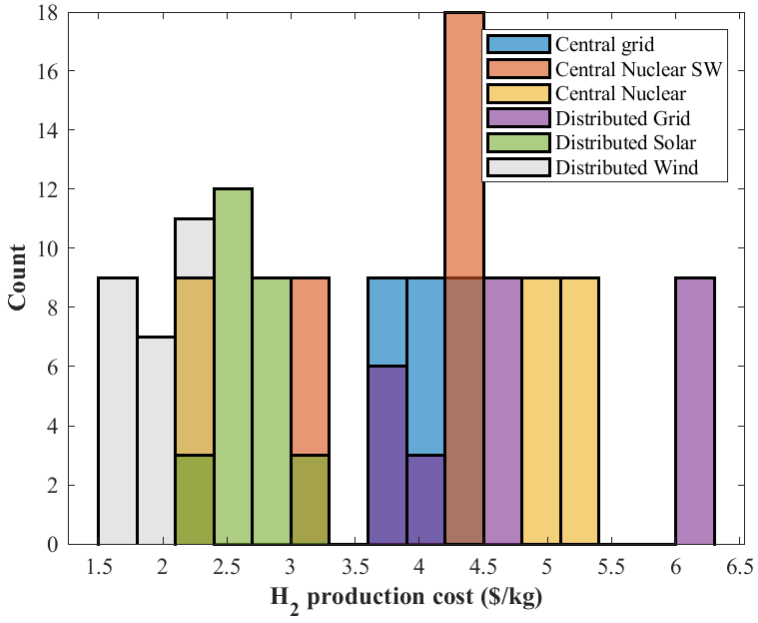

Figure S9. Parameter sweep for the electrolysis production methods

operate less should have lower repair and maintenance cost due to less stress placed on the system. Future models should incorporated a maintenance repair model based not only on calendar time, but hours of operation as well.

As expected, the primary difference between central and distributed production costs is the share of capital and electricity costs. In this analysis the distributed and central grid cases provide a good comparison to asses the impacts of plant location. Distributed plants proportionally exhibit much lower operation costs. While proportionately lower, the absolute cost of electricity used is nearly the same as can be seen by a comparison of the central and distributed grid plants. To account for any differences the distinguishing factor is the system level electricity used to produce a kg of hydrogen which is 51.3 kWh/kg for central and 51.4 for distributed. The slight difference is the 0.1 kWh/kg more used by the distributed BOP. The capital cost differs in both absolute and proportional costs. The distributed grid plant capital cost is over 1.5 times more expensive than the central grid plant. This is due to the distributed plants having higher BOP costs per MW of electrolyzer stack.

Total Production Cost

The results for hydrogen production costs for all production methods are given in Figure S11. Across all model years, electrolysis remains the most expensive production method, followed by

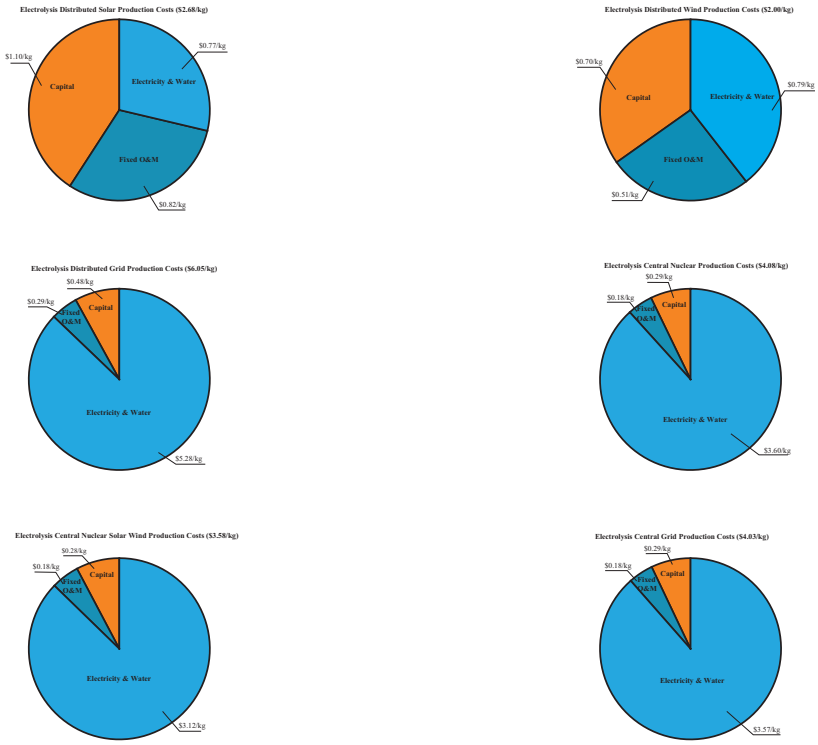

Figure S10. Cost breakdown for electrolysis

coal gasification and SMR. Electrolysis production ranges from $5.28-7.49/kg in the present-day scenario, $2.88-4.75/kg in the midterm, and $2.07-4.29/kg in the longterm. In the present, solar powered electrolysis has the highest production cost at $7.49/kg, however in the longterm, solar drops to the second lowest at $2.74/kg. This price drop in production is mainly attributed to the LCOE dropping to half it's present value in the longterm and a capacity factor increase of 6%. It should be noted that in the longterm, wind-based electrolysis becomes as competitive as the current industry standards, coal gasification and SMR. The centralized electrolysis plants start slightly cheaper in the present, however due to the higher electricity costs, centralized electrolysis results in more costly hydrogen, even with considering the benefits gained from lower capital costs and higher operating factors. SMR remains the cheapest production method with production costs ranging from $0.95-1.36/kg in the present, $1.00-1.42/kg in the midterm, and $1.19-1.61/kg in the longterm. Centralized SMR without **CCS!** (**CCS!**) remains the cheapest SMR production method, with centralized SMRCCS being the most expensive for all time scenarios. The hydrogen price steadily increases overtime due to the steady increase in natural gas and grid electricity costs over time. Because SMR is already a highly developed technology already at scale, the price variation is small over time with only the costs of process inputs significantly affecting hydrogen prices. Coal gasification with carbon capture is intermediately costly between electrolysis and SMR.

This production method has almost no variation with a present production cost of $1.99/kg and a longterm cost of $2.02/kg. Like SMR, coal gasification is a heavily developed technology, primarily used in China.

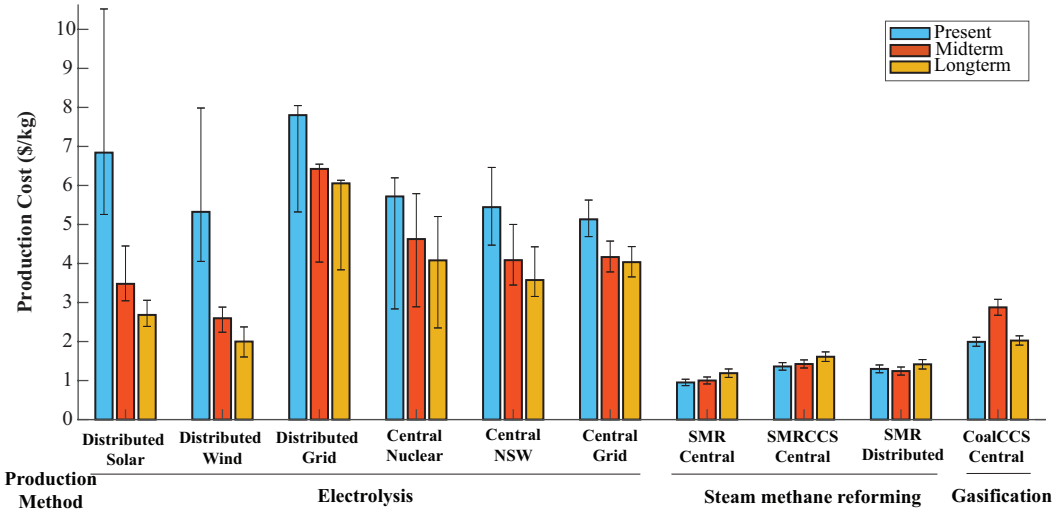

Figure S11. Cost for all production methods considered. Carbon capture and sequestration costs are included

Cost of H_2 delivery

The cost of liquid hydrogen delivery relies on hydrogen demand, geographical distribution, market dynamics and the state-of-the-art of the technologies used. The output space generated while sweeping over such parameters is given in Figure S14. The present-day scenario showed values ranging between $4.66/kg and greater than $15/kg. For the mid term scenario, these values were between $3.06-7.94/kg, while the long term ranged between $2.19-2.92/kg. The input parameter exhibiting the highest impact on the cost estimates was the number of interstate segments: the more interstate segments, the lower the cost. However, it is more common for two highways to intersect leading to four segments [13].

Given the selected input parameters for a base case with four interstate segments of 250 km-length, the resulting cost of hydrogen delivery is shown in Figure S12. The liquefier accounted for a very large share of the cost, ranging between 60 to 80 % of the total delivery cost across scenarios. In the long term, improvements in liquefaction will have the largest impact in making the liquid delivery pathway a more affordable option. The work by Liu et al.[38] in hydrogen infrastructure for long-haul applications showed contributions around $3.17/kg for liquefaction out of the $3.89/kg delivery cost in a 10% market penetration scenario. Mintz et al. [13] also used the HDSAM tool to

evaluate different delivery scenarios in urban and interstate markets under both gaseous and liquid pathways. They showed the high share of components such as liquefier and compressors, with costs over \$7/kg at 1% market penetration dropping to over \$1/kg in fully penetrated markets.

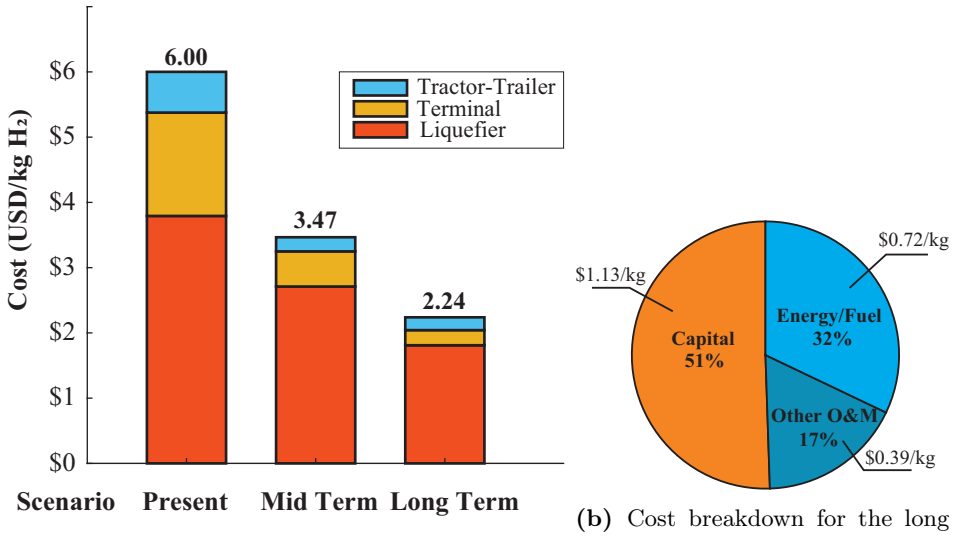

(a) Cost of liquid hydrogen delivery

(b) Cost breakdown for the long term scenario

Figure S12. Hydrogen delivery cost

Refueling station capacity: The average dispensing capacity was calculated using Equation S3

$$Ave.station\ capacity\ (ton/day) = \frac{N_{alt}\ \cdot\ D_{between\ refueling}}{FE_{HDT}\ \cdot\ N_{truck\ stops}\ \cdot\ MP} \tag{S3}$$

Where FE in $mi/kg\ H_2$ is the fuel economy of the hydrogen-powered long haul truck, MP (%) is the market penetration, N_{alt} is the number of alternative trucks in the US, and $N_{truck\ stops}$ is the total number of truck stops currently in rural interstate highways with the infrastructure to dispense sizable trucks. We assumed a distance between refueling to be 300 miles, which is half the daily range. This number of truck stop facilities in the U.S.A. was found in [39] based on the geographical information from U.S. DOT. Hence, the truck stops considered here correspond to around 8253 facilities by 2020.

Production volume: The hydrogen delivery system benefits from the economies of scales; this is quantified by the HDSAM model through cost reduction factors as a function of production volume (i.e., low, medium, high). We determined the cost reduction factors for the three technology groups with different maturity levels (Group 1, Group 2 and Group 3) through the approach found in [16]. They reported cost reductions for each doubling of refueling by 5%, 10% and 15%, allocated to each group, respectively. These factors are listed in Table S6

for low ($\sim$ 80 stations), medium ($\sim$ 4000 stations) and high ($\sim$ 8000 stations) production volumes.

Table S6. Cost reduction factors for different production volumes

Technology group	Low volume	Medium volume	High volume
Group 1	1	0.80	0.76
Group 2	1	0.64	0.57
Group 3	1	0.50	0.42

Rural interstate parameters: Delivery scenarios for rural interstate are defined in the HDSAM model from a set of parameters including road segment length, average distance of hydrogen refueling station from interstate, number of interstate segments and average miles travelled per day. While these parameters depend on geographical location and infrastructure network developments of the refueling stations, we assumed four interstate segments based on [13]. A distance of 1 mi from the interstate was considered here according to a preliminary survey about trucks driver preferences ($\leq$2 mi [40]) and the work from [39].

As shown in Figure S13a, the cost of small stations in early markets was 4.35 USD/kg, in which the cryogenic pump and the storage vessels most contributed. The mid and long term scenario benefit from the economy of scales since the average station capacity increases 5 and 6 folds compared to today, respectively. Also, more mature markets enable cost reductions particularly in a futuristic horizon with high volume manufacturing of station components and more technical innovations.

These values were compared with those available in the literature. A recent study with focus on fuel cell electric long-haul trucks also used the HDRSAM tool to determine parameters correlating the station capacity with the refueling cost. Authors derived the distribution of station capacities across United States based on the demand data from the freight analysis framework (FAF) model for trips between different origin-destination pairs. They calculated the average cost of the stations at \$1.23/kg for a 10% market penetration scenario and most station capacities with small and mid size. As stated by the authors, smaller and larger stations could lead to refueling station costs above \$5/kg and below \$1/kg, respectively.

The U.S. Department of Energy has also published studies on the levelized cost of dispensing hydrogen. The report by Koleva and Rustagi [41] considered liquid supply of hydrogen in an urban market and under assumptions characteristic of stations currently in operation in California. Authors used the HDSAM tool for light duty vehicles and determined the cost of delivery and dispensing of \$ 11.35/kg for an average station capacity of 450 kg/day. This station capacity suggested by authors is suitable for early markets. Their work resulted in a

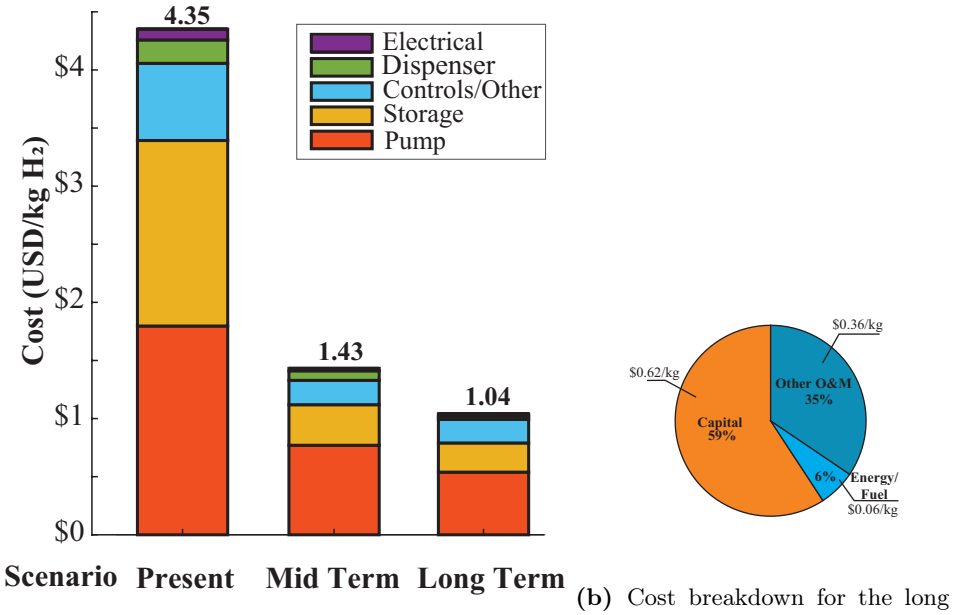

(a) Cost of liquid hydrogen refueling

(b) Cost breakdown for the long term scenario

Figure S13. hydrogen refueling station costs

delivery and dispensing cost of $ 10.35/kg in the present day scenario with an average capacity of 500 kg/day and rural interstate market.

Li et al. [42] also employed the HDRSAM tool to determine the cost of refueling stations for buses in the US and China. The input parameters relied on an average station capacity of 3000 kg/day. Since the maximum fill mass for buses is lower than for long-haul trucks, the stations were able to supply a larger fleet size, and consequently requiring more hoses. For a four-hose dispensing station, they reported cost estimate of $ 0.94/kg, which is slightly lower than the value here reported for the long term.

Figure S13b shows the cost breakdown of refueling stations when a mature market is assumed. The capital cost accounted for a large share of the station cost. It was reduced from $2.79/kg to $0.62/kg in the transition from a very early market to the long term scenario. The energy/fuel component remained the same across scenarios at $0.06/kg. Other operating and maintenance costs also exhibited significant reductions from $1.50/kg in the present to $0.36/kg in the longterm. A similar cost breakdown was observed by Reddi et al. [16] for a liquid refueling station with an average capacity of 1200 kg/day under high-volume manufacturing of station components. They found that cryogenic pumps contributed the most, followed by controls and storage system. However, the state-of-the art of the technology and the manufacturing volumes significantly bring down the cost of these equipment in future scenarios.

Output space of liquid hydrogen cost: The output space was generated by sweeping between parameters values over a range of 1-4 for the number of interstate segments, 100-450 km for the segment length, and over ± 10% average dispensing capacity and ± 10% HDVs miles traveled per rural interstate highway mile (i.e. 3870, 4300 and 4730 mi per mi-highway). The output space is given in Figure S14.

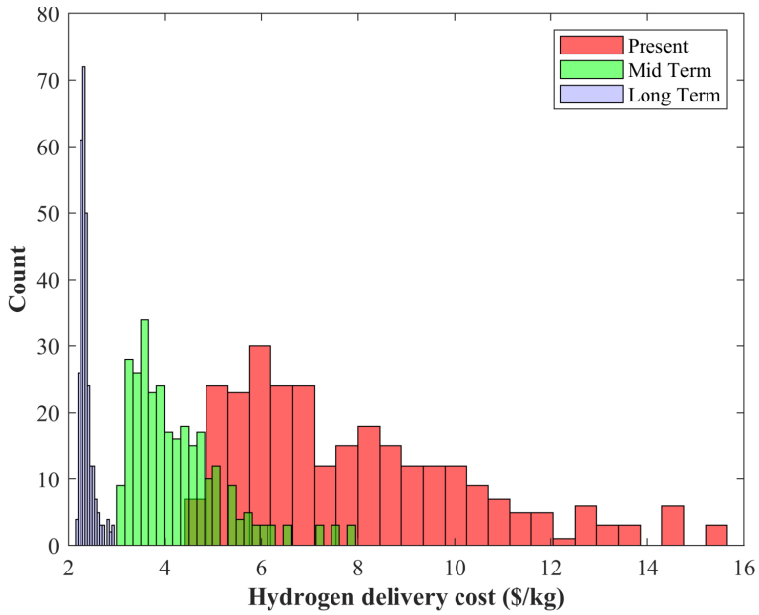

Figure S14. Output space of H_2 delivery costs

Cost of H_2 refueling

Dispensing profile: Figure S15 depicts the profile of fleets being refueled per hour and matching the dispensing profile from Chevron [19, 20].

Station type and dispensing option: Liquid refueling station was set consistently with the estimates from HDSAM tool. The dispensing option for this type of station was 700 bars via cryogenic pump because it reached lower costs than the compressor counterpart for larger station sizes. Reddi et al. [16] also reports the suitability of 700-bar compression as dispensing option for early markets with low utilization of the refueling station.

Production volume: The cost reduction factors for each production volume remains the same from the HDSAM tool.

Maximum dispensed amount per vehicle (kg): The amount of hydrogen demand per fill for each vehicle was specified at 80 kg, following the work from [43].

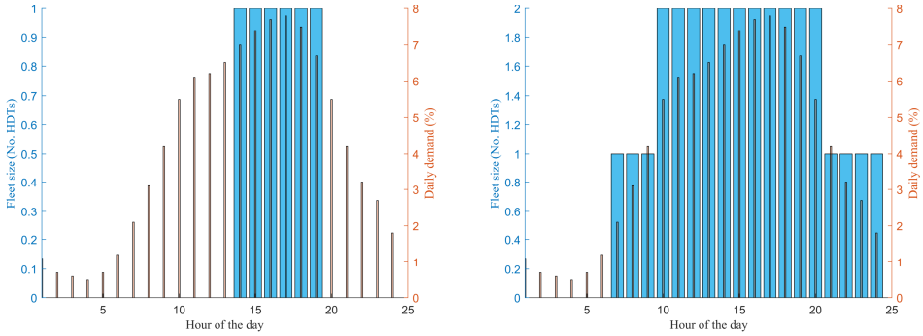

(a) Fleet size for the short term scenario **(b)** Fleet size for the mid term scenario

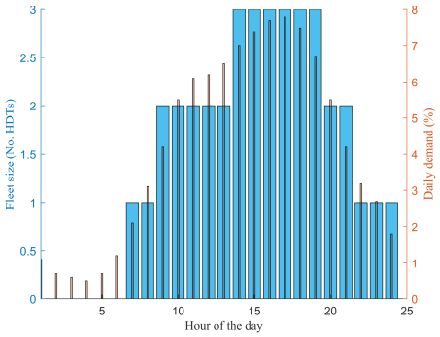

(c) Fleet size for the long term scenario

Figure S15. Hourly fleet distribution. Daily demand from [19, 20]

Fueling Rate (kg/min): The dispensing rate and time of 7.2 kg/min and 11 min, respectively, were within the range of 10-15 min reported by [44] for 60-100 kg dispensed at 700 bar.

Onboard storage tank: The type of tank used was IV, able to handle maximum pressures around 700 bars [45].

Economic assumptions: Analysis period over 15 years, real after-tax discount rate of 7%, and debt interest (nominal) of 6% over a period of 10 years. These assumptions were consistent with HDSAM tool.

On-site production at refueling stations

The storage requirements for the refueling stations with on-site production depended on the daily production profiles from on-shore wind and solar shown in Figure S16. These profiles derived from the hourly breakdown of electricity production from renewables in the US. Regions with high solar and wind intensity were considered. For solar, data from the California Independent System Operator (CAISO) was used and is available in [46]. For on-shore wind, data from central region (CENT) was found in [47].

Results are shown in Figure S17a for the base case, while Table S7 reports all the cases covered.

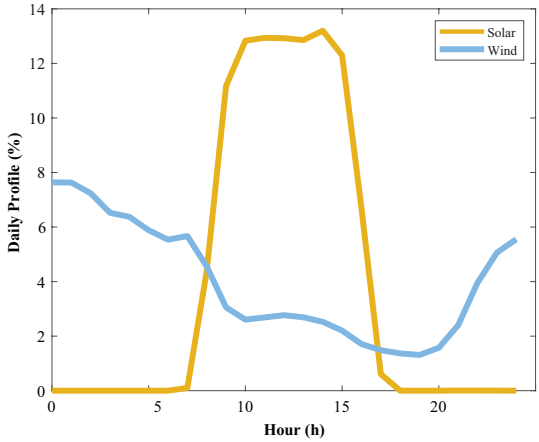

Figure S16. Solar and wind profiles used to calculate storage requirements

Table S7. Refueling cost for on-site production facilities

Cases	No reserve for outage			2-day reserve			10-day reserve		
Renewable	Solar	wind	Grid	Solar	wind	Grid	Solar	wind	Grid
2020	8.18	8.18	8.18	9.70	9.70	9.70	15.77	15.96	15.77
2030	3.44	3.52	3.33	5.01	5.09	4.90	11.37	11.45	11.25
2050	2.62	2.72	2.55	3.75	3.84	3.70	8.30	8.39	8.25

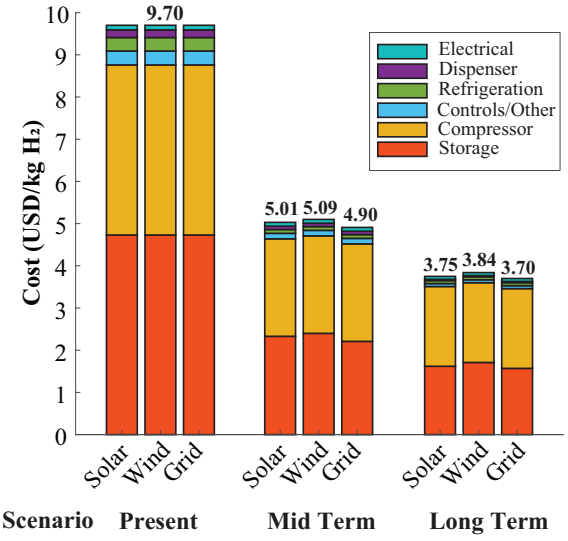

(a) Cost of gaseous refueling with two-day reserve

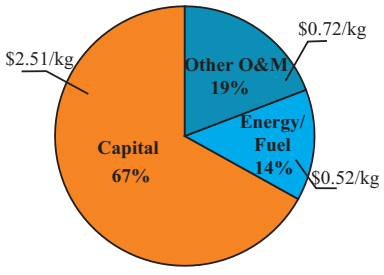

(b) Cost breakdown for the long term scenario

Figure S17. Cost of gaseous hydrogen refueling

Fuel consumption model

H_2-ICE powertrain: Figure S18 presents an overview of the hydrogen engine maps in steady-state condition. Accordingly, the hydrogen engine is capable of delivering 2000 Nm in brake torque in a range between 1000 and 1600 RPM. The rated power amounts to 335 kW. The brake thermal efficiency stays above 40% for the majority of the engine map – above ca. 600 Nm, where wide open throttle operation is applied. The efficiency reaches values up to 43 % at around 1400 RPM. The engine-out NO_x values remain very low and are less than 2 g/kWh for most of the map, where high lambda can be applied. However, at full load operation at low (at ca. 1000 RPM) and high engine speeds, the turbocharger system is not capable of delivering enough boost pressure to maintain the lambda value of lower loads. As a result, the NO_x emissions increase. Nevertheless, prior investigations by the authors have shown that using the developed hydrogen engine in combination with an SCR aftertreatment system is capable of reaching very high conversion efficiencies and, thus, keeping the tailpipe emissions on a very low level.

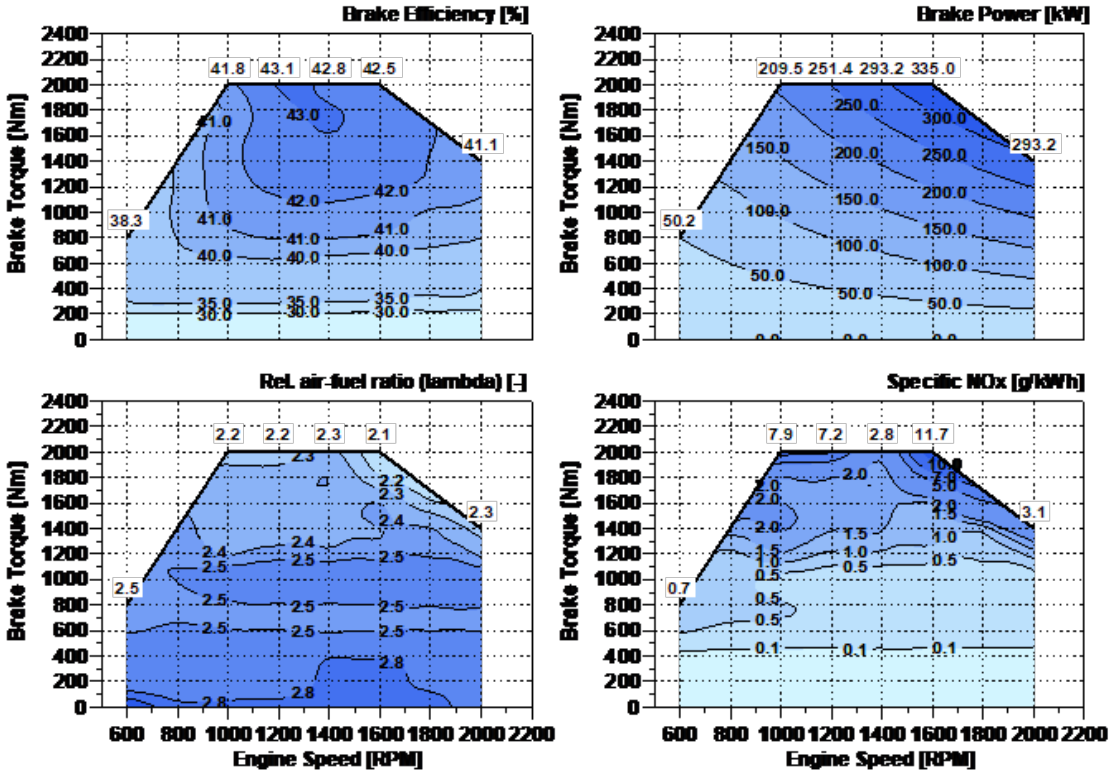

Figure S18. Overview of H_2 engine maps

The fuel economies from gear ratio sweep for the H-ICET is shown in Table S8.

Table S8. minimum and maximum gear ratios swept over in fuel economy optimization for the H-ICET

Variable	Minimum	Maximum	Optimized
Final drive ratio	2.75	4.0	3.04
16th gear	0.8	1.1	0.82
17th gear	0.65	0.9	0.75
18th gear	0.55	0.8	0.71

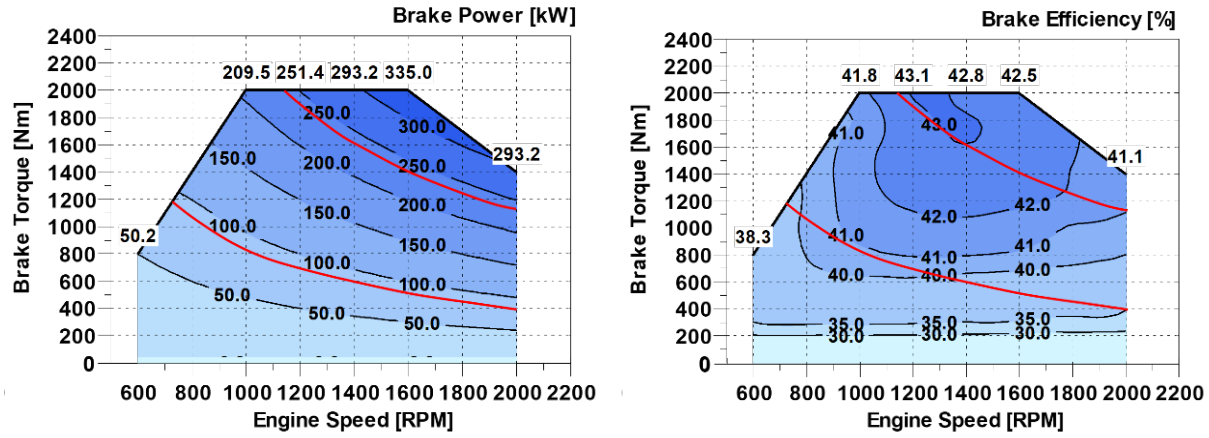

Figure S19. isopower curves (red) representing a one standard deviation envelope of the engine power demand profile. The lower bound is 90 kW and the upper bound is 240 kW

H_2 **FC electric hybrid powertrain:** The equations to model voltage losses in the fuel cell hybrid powertrain are shown below. The initial and maximum state of charge (SOC) assumed for the hybrid and plug-in architecture are listed in Table S9.

Table S9. Parameters associated with transitions

Parameters	Parallel HEV	Parallel PHEV
$SOC_{initial}$	0.3	0.9
SOC_{max}	0.9	0.9
SOC_{min}	0.3	0.3
$SOC_{supermin}$	0.1	0.1
$DeltaSOC$	0.1	0.1

$$V_{cell} = V_{OV} - V_{Loss} \tag{S4}$$

$$V_{Loss} = V_{act} + V_{mt} + V_{ohm} + V_{\Delta OC} \tag{S5}$$

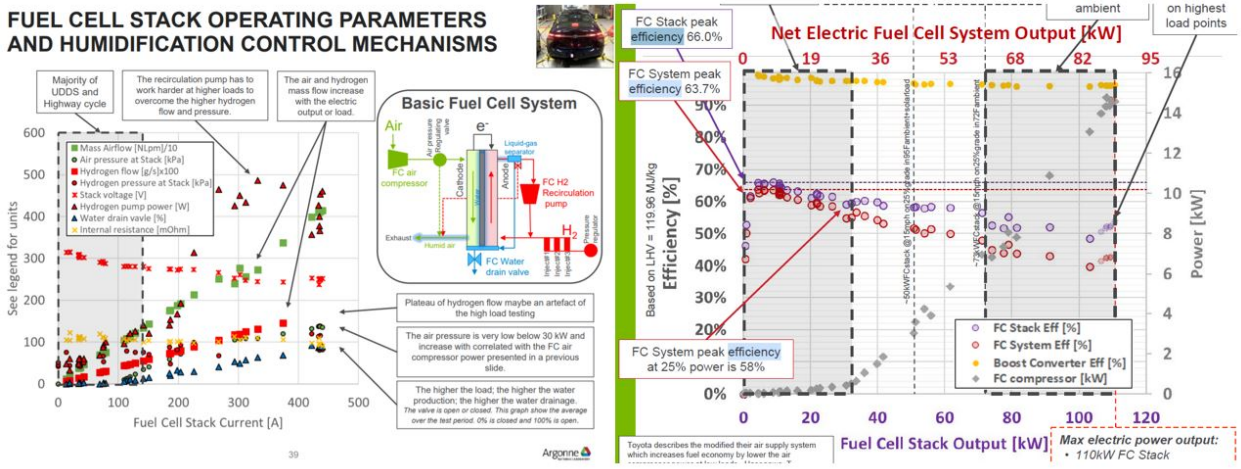

Figure S20. Data representing a 2017 Toyota Mirai Fuel Cell. The data is provided by Argonne National Lab

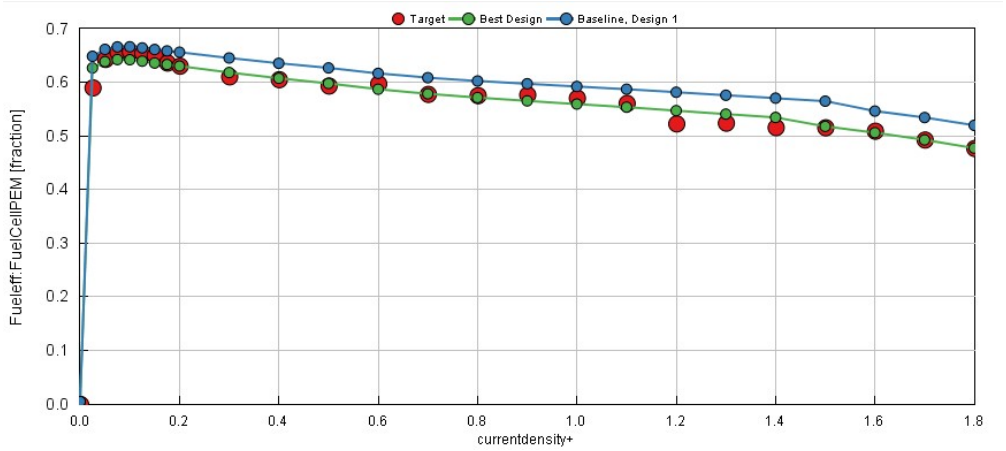

Figure S21. Hydrogen fuel cell stack efficiency based on Toyota Mirai data. The red curve represent the Mirai's efficiency. The green curve is the matched efficiency used in this study

Table S10. Attributes for cooling system components

Cooling Component	Attribute	Source
Radiator	1100mm x 1000mm x 77mm	[48]
Fuel Cell Jacket	$\frac{6804cm^3}{400cells} \times (\#stack\ cells)$	[26]
Grill	4.5 kg/s	[49]
Radiator Fan	7 kW	this work & [49]
Coolant Pump	2 kW	this work
Battery Cooling Plate	1 m^2, Aluminum	[50]
Power Electronic Cooler	Aluminum	[51]
WCAC	60mm x 300mm x 0.1mm	GT default

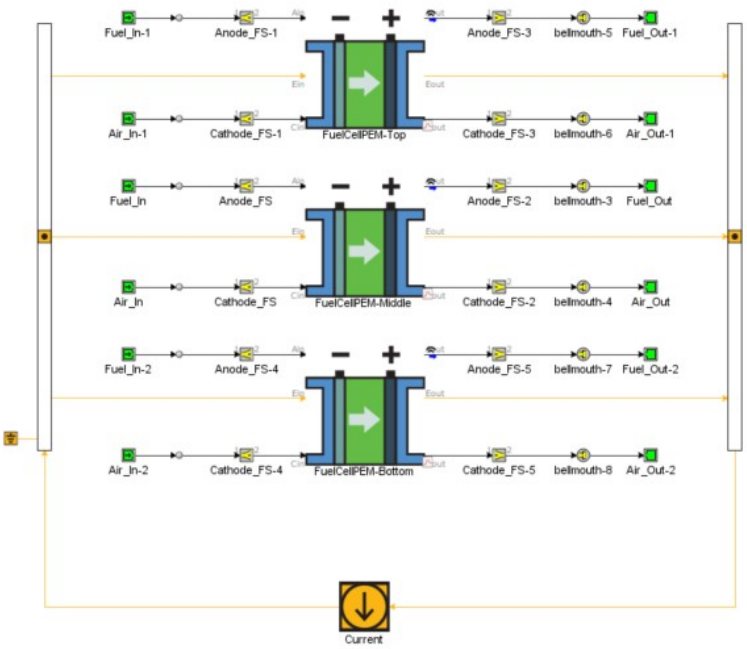

Figure S22. GT-Suite fuel cell model used to tune parameters to match Toyota Mirai data.

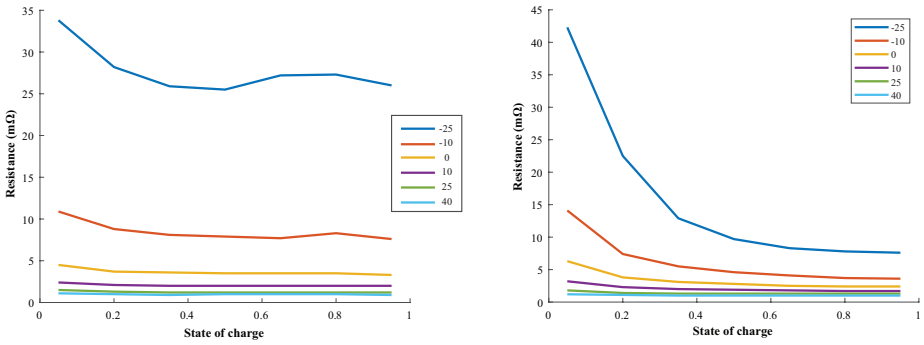

Figure S23. The resistance of a battery cell used to model the battery pack when charging (left) and discharging (right)

Table S11. Specifications of battery pack

Parameter	Value	Sources
Cell capacity	37 Ah	
Cells in series	90	
Max C-rate	9	
Cells in parallel	2-100	This work
SOC	0.1-0.9	
Depth of Discharge	0.8	
Cell open circuit voltage	3.3-4.2 V	
Minimum Discharging Voltage Limit	3.3 N_{series}	
Maximum Charging Voltage Limit	4.2 N_{series}	
Maximum Charging Current Limit	$= [C - RATEmax] * [Cell_{Capacity}] * [NParallel]$	
Maximum Discharging Current Limit	$= [C - RATEmax] * [Cell_{Capacity}] * [NParallel]$	

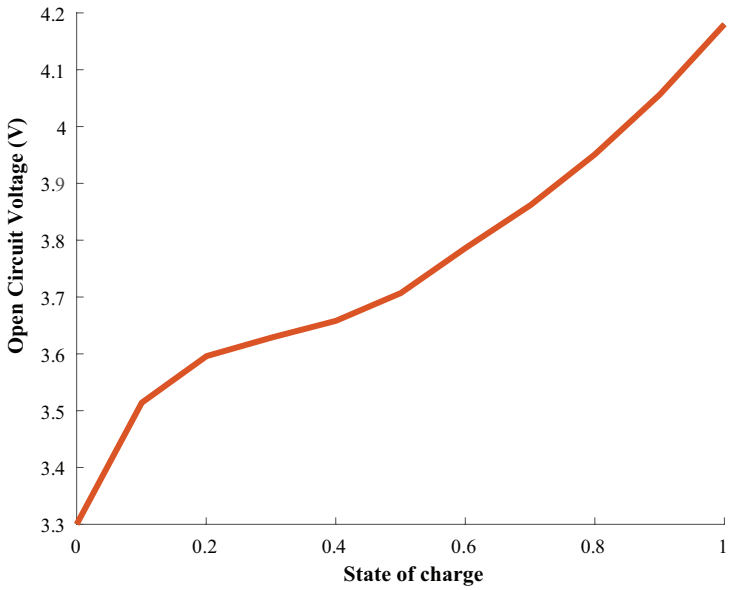

Figure S24. The open circuit voltage of a cell used to model the battery pack

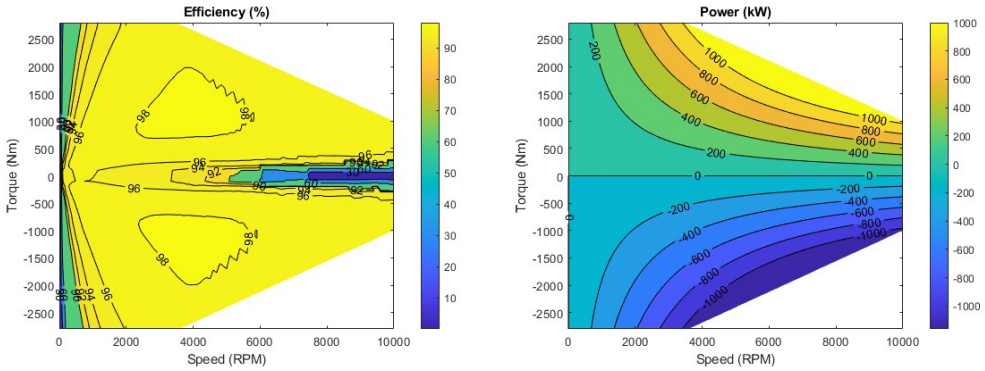

Figure S25. motor efficiency (left) and power (right) for the H-FCET

Total cost of Ownership

Tables S12, S13 and S14 reports the cost of powertrain components in each year scenario.

Table S12. Capital cost for each powertrain component for the present scenario

$×1000	D-ICET	H-ICET	H-FCET-HEV	H-FCET-PHEV
Glider	95.0	95.0	95.0	95.0
Fuel Cell System	0	0	99.1	84.9
Engine	12.1	19.3	0	0
Fuel Tank	2.1	50.4	41.0	41.0
Aftertreatment	5.8	5.8	0	0
Transmission	10.3	10.3	0	0
WHR	0	0	0	0
Motor	0	0	6.0	6.0
Battery	0.1	0.1	3.3	57.2

Table S13. Capital cost for each powertrain component for the midterm scenario

$×1000	D-ICET	H-ICET	H-FCET-HEV	H-FCET-PHEV
Glider	95.0	95.0	95.0	95.0
Fuel Cell System	0	0	31.5	27.0
Engine	16.2	19.3	0	0
Fuel Tank	2.1	42.7	37.2	37.2
Aftertreatment	7.3	7.3	0	0
Transmission	10.3	10.3	0	0
WHR	5.9	5.9	0	0
Motor	0	0	3.5	3.5
Battery	0.1	0.1	2.5	43.3

Table S14. Capital cost for each powertrain component for the longterm scenario

$×1000	D-ICET	H-ICET	H-FCET-HEV	H-FCET-PHEV
Glider	95.0	95.0	95.0	95.0
Fuel Cell System	0	0	24.2	20.7
Engine	18.0	19.3	0	0
Fuel Tank	2.1	33.0	32.3	32.3
Aftertreatment	9.1	9.1	0	0
Transmission	10.3	10.3	0	0
WHR	5.9	5.9	0	0
Motor	0	0	1.2	1.2
Battery	0.1	0.1	2.0	8.0

WTW emissions

Figure S26 shows the total emissions for all the hydrogen powertrain architectures considering hydrogen production from SMR for present day, SMR with CC for mid term, and renewable electrolysis in the long term.

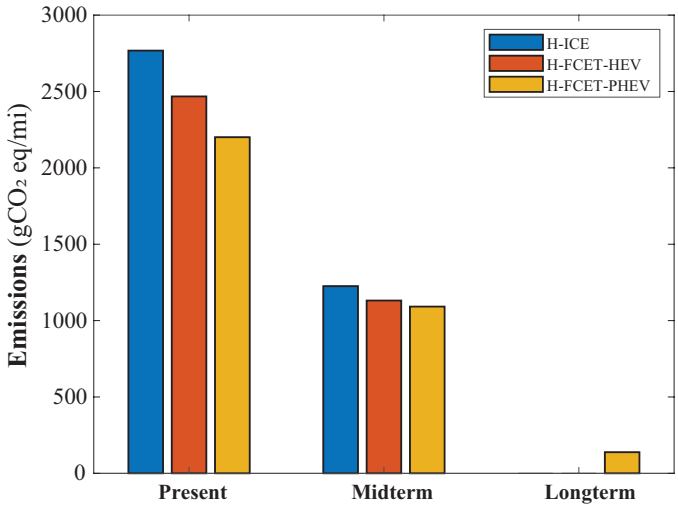

Figure S26. The well-to-wheel emissions for the powertrains considered in this study.

3.6 references

(1) Li, L.; Feng, L.; Manier, H.; Manier, M.-A. Life cycle optimization for hydrogen supply chain network design. *International Journal of Hydrogen Energy* **2022**, DOI: 10.1016/j.ijhydene.2022.03.219.

(2) Kast, J.; Vijayagopal, R.; Gangloff, J. J.; Marcinkoski, J. Clean commercial transportation: Medium and heavy duty fuel cell electric trucks. *International Journal of Hydrogen Energy* **2017**, *42*, 4508–4517.

(3) Kast, J.; Morrison, G.; Gangloff, J. J.; Vijayagopal, R.; Marcinkoski, J. Designing hydrogen fuel cell electric trucks in a diverse medium and heavy duty market. *Research in Transportation Economics* **2018**, *70*, 139–147.

(4) Mauler, L.; Dahrendorf, L.; Duffner, F.; Winter, M.; Leker, J. Cost-effective technology choice in a decarbonized and diversified long-haul truck transportation sector: A U.S. case study. *Journal of Energy Storage* **2022**, *46*, DOI: 10.1016/j.est.2021.103891.

(5) Lee, D. Y.; Elgowainy, A.; Kotz, A.; Vijayagopal, R.; Marcinkoski, J. Life-cycle implications of hydrogen fuel cell electric vehicle technology for medium- and heavy-duty trucks. *Journal of Power Sources* **2018**, *393*, 217–229.

(6) Forrest, K.; Kinnon, M. M.; Tarroja, B.; Samuelsen, S. Estimating the technical feasibility of fuel cell and battery electric vehicles for the medium and heavy duty sectors in California. *Applied Energy* **2020**, *276*, DOI: 10.1016/j.apenergy.2020.115439.

(7) Lajevardi, S. M.; Axsen, J.; Crawford, C. Simulating competition among heavy-duty zero-emissions vehicles under different infrastructure conditions. *Transportation Research Part D: Transport and Environment* **2022**, *106*, 103254.

(8) IEA. The Future of Hydrogen for G20. Seizing today's opportunities. *Report prepared by the IEA for the G20, Japan* **2019**.

(9) Wickham, D.; Hawkes, A.; Jalil-Vega, F. Hydrogen supply chain optimisation for the transport sector – Focus on hydrogen purity and purification requirements. *Applied Energy* **2022**, *305*, DOI: 10.1016/j.apenergy.2021.117740.

(10) Frank, E. D.; Elgowainy, A.; Reddi, K.; Bafana, A. Life-cycle analysis of greenhouse gas emissions from hydrogen delivery: A cost-guided analysis. *International Journal of Hydrogen Energy* **2021**, *46*, 22670–22683.

(11) EIA. *International Energy Outlook 2019*; US. Energy Information Administration, 2019.

(12) NREL. H2A: Hydrogen Analysis Production Models, 2018.

(13) Mintz, M.; Gillette, J.; Elgowainy, A.; Paster, M.; Ringer, M.; Brown, D.; Li, J. In. National Research Council: 2006, pp 114–120.

(14) NREL. Annual Technology Baseline, 2021.

(15) Lazard. Levelized Cost Of Energy, Levelized Cost Of Storage, and Levelized Cost Of Hydrogen, 2021.

(16) Reddi, K.; Elgowainy, A.; Rustagi, N.; Gupta, E. Impact of hydrogen refueling configurations and market parameters on the refueling cost of hydrogen. *International Journal of Hydrogen Energy* **2017**, *42*, 21855–21865.

(17) Lee, Y.; Lee, U.; Kim, K. A comparative techno-economic and quantitative risk analysis of hydrogen delivery infrastructure options. *International Journal of Hydrogen Energy* **2021**, *46*, 14857–14870.

(18) FHWA. Annual Vehicle Distance Traveled in Miles and Related Data by highway category and vehicle type 2020, 2021.

(19) Chen, T.-P. *The Power of Experience Final Report Hydrogen Delivery Infrastructure Options Analysis*; Nexant Inc, 2008.

(20) Reddi, K.; Elgowainy, A.; Sutherland, E. Hydrogen refueling station compression and storage optimization with tube-trailer deliveries. *International Journal of Hydrogen Energy* **2014**, *39*, 19169–19181.

(21) Papadias, D. D.; Peng, J. K.; Ahluwalia, R. K. Hydrogen carriers: Production, transmission, decomposition, and storage. *International Journal of Hydrogen Energy* **2021**, *46*, 24169–24189.

(22) Rezaei, R.; Kovacs, D.; Hayduk, C.; Mennig, M.; Delebinski, T. In. 2021; Vol. 4, pp 559–569.

(23) Sens, M.; Danzer, C.; Essen, C. V.; Brauer, M.; Wascheck, R.; Seebode, J.; Kratzsch, M. *Hydrogen Powertrains in Competition to Fossil Fuel based Internal Combustion Engines and Battery Electric Powertrains*; 2021.

(24) Rezaei, R.; Hayduk, C.; Fandakov, A.; Rieß, M.; Sens, M.; Delebinski, T. O. In. SAE International: 2021.

(25) R., R.; M., S.; M., R.; Bertram, C. In. Ed. by Christian; Johannes, M. W. L.; Beidl, Springer Fachmedien Wiesbaden: 2021, pp 99–114.

(26) Toyota. *Toyota Mirai Technical Specifications*.

(27) Partnership, 2. C. T. *Research blueprint*; 2019, pp 1–19.

(28) Marcinkoski, J.; Vijayagopal, R.; Adams, J.; James, B.; Kopasz, J.; Ahluwalia, R. DOE Advanced Truck Technologies: Technical Targets for Hydrogen-Fueled Long-Haul Tractor-Trailer Trucks. *Electrified Powertrain Roadmap* **2019**.

(29) CommercialTruckTrader. Heavy Duty, 2022.

(30) Frith, J. Battery Price Declines Slow Down in Latest Pricing Survey, 2021.

(31) Lajevardi, S. M.; Axsen, J.; Crawford, C.; Lajevardi, S. M.; Axsen, J.; Crawford, C.; Lajevardi, S. M.; Axsen, J.; Crawford, C.; Lajevardi, S. M.; Axsen, J.; Crawford, C.; Lajevardi, S. M.; Axsen, J.; Crawford, C. Comparing alternative heavy-duty drivetrains based on GHG emissions, ownership and abatement costs: Simulations of freight routes in British Columbia. *Transportation Research Part D: Transport and Environment* **2019**, *76*, DOI: 10.1016/j.trd.2019.08.031.

(32) James, B. 2021 DOE Hydrogen and Fuel Cells Program Review Presentation, 2021.

(33) Houchins, C.; James, B. 2020 DOE Hydrogen and Fuel Cells Program Review, 2020.

(34) Norris, J.; Escher, G. *Heavy Duty Vehicles Technology Potential and Cost Study*; Ricardo Energy & Environment, 2017.

(35) eia. Energy Prices: Electricity, 2021.

(36) Burnham, A.; Gohlke, D.; Rush, L.; Stephens, T.; Zhou, Y.; Delucchi, M. A.; Birky, A.; Hunter, C.; Lin, Z.; Ou, S.; Xie, F.; Proctor, C.; Wiryadinata, S.; Liu, N.; Boloor, M. Comprehensive Total Cost of Ownership Quantification for Vehicles with Different Size Classes and Powertrains. *U.S. Department of Energy, Argonne National Laboratory* **2021**.

(37) Laboratory, N. R. E. Diesel Fuel. https://atb.nrel.gov/transportation/2020/diesel_fuel.

(38) Liu, N.; Xie, F.; Lin, Z.; Jin, M. Evaluating national hydrogen refueling infrastructure requirement and economic competitiveness of fuel cell electric long-haul trucks, 2020.

(39) Hurtado, A.; Rilett, L. R.; Nam, Y. Driving coverage of charging stations for battery electric trucks located at truck stop facilities. *Transportation Research Record* **2021**, *2675*, 850–866.

(40) Garber, N. J.; Wang, H.; Charoenphol, D. *Estimating the supply and demand for commercial heavy truck parking on interstate highways: A case study of I-81 in Virginia*; Virginia, 2002, pp 1–61.

(41) Koleva, M.; Rustagi, N. *DOE Hydrogen and Fuel Cells Program Record Title: Hydrogen Delivery and Dispensing Cost*; Department of Energy, 2020, pp 1–4.

(42) Li, X. J.; Allen, J. D.; Stager, J. A.; Ku, A. Y. Paths to low-cost hydrogen energy at a scale for transportation applications in the USA and China via liquid-hydrogen distribution networks, 2020.

(43) Acharya, T.; Jenn, A.; Miller, M.; Fulton, L. *Spatial Modeling of Future Light-and Heavy-Duty Vehicle Travel and Refueling Patterns in California*; Institute of Transportation Studies, 2021.

(44) Bouwkamp. In. 2019.

(45) Aydin, M. I.; Dincer, I.; Ha, H. Development of Oshawa hydrogen hub in Canada: A case study. *International Journal of Hydrogen Energy* **2021**, *46*, 23997–24010.

(46) CAISO. Hourly Breakdown of Renewable Sources, 2021.

(47) eia. Hourly Electric Grid, 2022.

(48) Parts, B. M. Freightliner Cascadia Radiator 42-10293, 2022.

(49) Slone, L. M.; Birkel, J. F.; Nine, R. D.; Slezak, L. A. *Advanced Electric Systems and Aerodynamics for Efficiency Improvements in Heavy Duty Trucks*; 2007, pp 1–20.

(50) DANA. Battery Cold Plate, 2022.

(51) DANA. Power Electronics Cooler, 2022.

Chapter 4

Battery electric: Does the momentum from the light-duty vehicle market encourage electrification of long-haul heavy-duty trucks?

This work is currently underway and will be continued by Kariana Moreno-Sader in preparation for publication. Future improvements will include high fidelity battery performance modeling for the lithium-ion batteries discussed. In addition, a cooling system will be implemented to assess its impact on fuel economy.

4.1 Introduction

While climate change poses an ever-increasing challenge for the world, the transportation sector brings additional barriers to reducing carbon dioxide emissions, particularly for heavy-duty trucking [1]. Heavy-duty freight trucks are responsible for approximately 30% of the highway transportation emissions even though they only represent about 5.5 % of vehicles on the road [2]. Heavy-duty trucks are also the backbone of US freight, as they account for 71 % of freight deliveries [3]. The corresponding on-road freight energy consumption has been consistently increasing over the last decades and is expected to grow even further in the future [4, 5].

Different alternative powertrains are being explored to answer the crucial question: how can road freight emissions be cut to net-zero carbon by 2050 while at the same time facing a growing transportation demand? The complexity of this question presents a challenging dilemma for the transportation sector: neither the scientific community nor large auto manufacturers have reached a consensus on which powertrain will be the best solution for the future of the long-haul sector. This lack of consensus has impacted decision-making among stakeholders. For example, policymakers are hesitant on large-scale incentives because an excessive bias towards one technology option could hinder the market penetration of competing technologies. However, these competing technologies might turn out to be a significantly better solution in the long run. Moreover, investors typically avoid substantial uncertainty, which makes it even more difficult for manufacturers to carry the burden of research and development costs for a multitude of different possible future powertrain solutions. Lastly, truck operators are uncertain which powertrains to purchase for their fleet to comply with future regulations and customer sustainability demands.

Zero emitting vehicles may provide a solution in decarbonizing the long-haul heavy-duty truck market. In particular, the battery electric powertrain has no tail pipe emissions and there is potential for future electricity to be generated carbon free such that the well to wheel (WTW) emissions lead to the net zero targets established by the Conference of the Parties [6]. The battery electric has seen significant market penetration in recent years within the light duty vehicle market. This has allowed battery prices to decrease rapidly over the past few decades as battery production reaches scale. Since their commercial introduction in 1991, lithium-ion batteries have seen a 97 % decrease in price per energy capacity with a 13 % decline per year [7]. This cost decline has allowed the battery electric powertrain to be considered for long-haul duty cycles where large batteries were once prohibitively expensive.

Considering the potential of the battery electric powertrain leads to this study's aims. Its aims are to

1. Develop an advanced technoeconomic model that establishes fuel economy, costs, and emis-

sions for the present and future scenarios for long-haul heavy-duty trucking.

2. Assess the viability of the battery electric powertrain in heavy-duty long-haul trucking duty cycles and compare the results to the conventional diesel powertrain.

4.2 Background

4.3 Methods

This study establishes the fuel economy, costs, and emissions for the battery electric powertrain in the context of long-haul trucking. Time scenarios consider the present, midterm, and longterm. Future scenarios predict the market adoption of the battery electric powertrain to allow economies of scale to be met. This allows for a fair comparison between the conventional diesel and battery electric powertrains. The total cost to society is used as the metric of comparison by incorporating emissions and costs into one single metric. The battery chemistries considered in this study are the nickel manganese cobalt (NMC) and the lithium iron phosphate (LFP) lithium-ion batteries. Technical modeling is performed in the automotive engineering software GT-Suite. Economic modeling uses literature manufacturing analysis values with an in-house discounted cash flow model. Emissions are modeled using data obtained from The Greenhouse Gases, Regulated Emissions, and Energy Use in Technologies Model (GREET).

4.3.1 Fuel Consumption Model

A battery electric truck model was developed to assess the viability of replacing the diesel internal combustion engine. The models use the USLHC8 drive cycle (Figure 2.4) as input to calculate the fuel economy in a long-haul operation scenario. The models are developed in GT-Suite and are discussed in the following sections. An overview of the BET fuel consumption model is given in Figure 4.1 and specifications for major powertrain components are given in Table 4.1. Due to thesis time constraints, the battery electric model is much simpler than the fuel cell model. The modeled powertrain consists of a motor, inverter, tractive battery, auxiliary battery, DC-DC converter, and an auxiliary load. The motor converts electrical energy to mechanical energy and is a map-based model identical to the motor used in the fuel cell from chapter 3. The inverter converts DC power to AC power used by the motor. The inverter can change the speed at which the motor rotates by adjusting the frequency of the alternating current and can adjust the torque by modifying the amplitude of the current. The inverter is modeled with a constant efficiency of 98.5% and follows technical targets outline by the DOE [8]. The tractive battery stores electrical energy to propel the vehicle. The battery is a generic GT-Suite default lithium-ion map-based model considering open circuit voltage and internal resistance and has an average efficiency of about 98% over the USLHC8.

The battery is assumed to have a depth of discharge of 80% and operates between a SOC of 10% and 90%. More information on the battery can be found in the fuel cell chapter. The DC-DC balances the voltages of the powertrain's various electrical systems. In the model it reduces the high voltage output of the tractive battery to the voltage required by the auxiliary units. It is modeled with a constant efficiency of 95%. The auxiliary load is implemented to model electronics such as the air conditioning system, vehicle lights, etc and is set to 10 kW [9].

Table 4.1. Specifications for the major powertrain components in the battery electric truck model

Component	Specifications	
Battery	LFP: 870 kWh, 3000 cycles, 98% efficiency	NMC: 870 kWh, 1000 cycles, 98% efficiency
Motor	1100 kW, 96 % efficiency	
DC-DC Converter	95% efficiency, 10 kW	
Inverter	98.5% efficiency	
Auxiliary Load	10 kW	

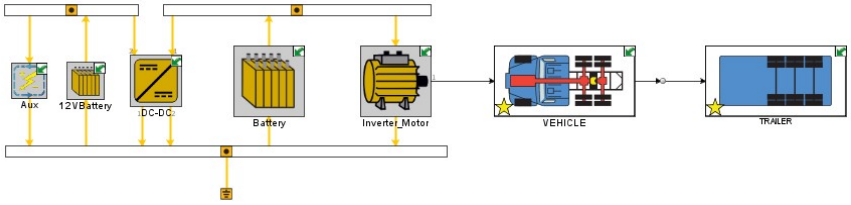

Figure 4.1. Overview of the battery electric fuel consumption model represented by GT-Suite blocks

The specific or gravimetric energy plays an important role in an industry whose purpose is to haul mass. In this study, the mass of the battery is the source of the payload penalty discussed in section 4.3.2. Of the two battery chemistries covered in this study, the NMC chemistry has a superior specific energy than the LFP chemistry. Both batteries' specific energies are projected to decrease in future scenarios from technological advances are based on targets set by the department of energy through various projects. The present-day NMC's value is based on Tesla Model 3's battery pack and is 260 Wh/kg [10]. Future values for the NMC's specific energy are from DOE's Batter500Consortium. The present-day LFP's value is based on the commercially available heavy-duty battery from Proterra [11]. Future values for LFP are modeled to proportionately follow the NMC's decreasing trend.

Wh/kg	Present	Midterm	Long term	Source
NMC	260	350	500	[10]
LFP	170	230	330	[11]

4.3.2 Economic Model

This study uses a Total Cost to Society (TCS) analysis to combine operating cost, capital cost and the social cost of GHG emissions over a 10-year lifespan. A conservative discount rate of 7% is used and based on recommendations by the White House's Office of Management and Budget. Assumptions for each cost consideration vary by year and are included in the present, midterm and long term.

Capital Cost

The capital cost for the battery electric truck considers the battery, motor, DC-DC converter, and tractor body. The capital cost is calculated by summing the manufacturing cost of each component according to 4.1.

$$Capital\ Cost = \$_{Battery} + \$_{Motor} + \$_{DCDC} + \$_{Inverter} + \$_{Tractor} \tag{4.1}$$

Special attention was given to costs of the battery due to its large influence on overall costs. A combination of literature and simulation methods were used to determine the battery cost for the given time scenarios (Figure 4.2). Literature values were obtained for the present-day battery manufacturing costs and the software BatPac was used for the midterm and longterm scenarios. BatPac is a manufacturing model that estimates the cost of lithium-ion batteries after they have reached a mature state of development and are being manufactured at high volumes [12]. This study's battery pack cost values are given in table 4.2. The present-day battery pack cost, \$132/kWh, is based on BloombergNEF's annual battery price survey for 2021 [13]. Bloomberg does not specify the battery chemistry; therefore, it is assumed NMC represents their quoted cost due to the NMC's prevalence in the light duty market. A value of \$110/kWh is used for the present day LFP cost, however costs as low as \$80/kWh have been reported [13]. The longterm cost value for LFP, \$72/kWh, is based on a BatPac simulation value considering a production value of 100,000 units per year. the NMC's long term value of \$80/kWh is aligned with the DOE's ultimately target for light duty vehicles [**EnergyGov2022**]. Some sources predict battery pack costs dropping to around \$50/kWh in the long run. However, while costs for batteries have continuously been plummeting, one cannot neglect considering the spike in raw material costs if the entire vehicle market transitions to battery electric vehicles. It is possible battery prices increase in time due to supply limitations of raw materials, however more in-depth analysis is needed.

Battery durability heavily influences the total cost to society, as the battery is one of the largest cost components. Battery durability is often defined by either cycle count or calendar life. The United States Council for Automotive Research's subdivision, United States Advanced Battery Consortium has defined calendar and cycle life goals of 1000 cycles and 15 years, respectively, for NMC batteries [16]. In the context of heavy-duty trucking, the 1000 cycle life come well before

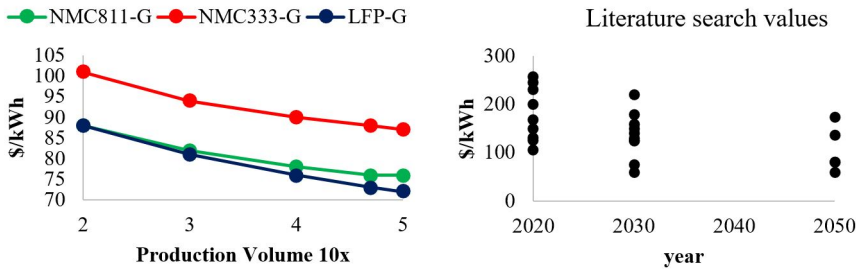

Figure 4.2. Battery costs from BatPac (left) and a literature search (right)

Table 4.2. Capital cost parameters

Powertrain Component	Present	Midterm	Longterm	Source
NMC Battery Cost	\$132/kWh	\$100/kWh	\$80/kWh	[**EnergyGov2022**, 13]
LFP Battery Cost	\$110/kWh	\$88/kWh	\$72/kWh	[12]
Motor	\$17/kW	\$10/kW	\$3.3/kW	[14]
DC-DC Converter	\$50/kW	\$30/kW	\$30/kW	[9]
Inverter	\$3.3/kW	\$2.7/kW	\$2.7/kW	[9]
Tractor	\$95,000	\$95,000	\$95,000	[15]
On board charger	\$2,797	\$2,517	\$2,266	source

the 15-year calendar life and is used as the battery durability metric in this study. The LFP battery chemistry is significantly more durable than the NMC battery chemistry. Proterra utilizes LFP chemistry for their line of heavy-duty trucking batteries and boasts a cycle life of 4,000 [11]. Because of their high cycle life, LFP batteries are attractive for the heavy-duty truck market even with lower specific energy and energy density. In this study, batteries are replaced when they meet their cycle life count. Time of replacements is considered to account for the discount factor. Batteries with remaining cycles at the end of the truck's life are sold at a price proportional to their remaining cycles. The total cost of a truck's lifetime of battery is given by the following equations.

$$Battery\ Cost = N_{Batteries} * \ Battery\ Capital\ Cost - Resale\ value \tag{4.2}$$

$$Resale\ value = \frac{Remaining\ Cycles}{Cycle\ life} * Battery\ Capital\ Cost \tag{4.3}$$

$$N_{Batteries} = \frac{VMT}{Cycle\ life * Battery\ Range} \tag{4.4}$$

The power electronics modeled consist of an inverter, on-board charger, and DC-DC converter. An inverter is needed to convert the DC energy from a battery to AC power to drive the motor. The DC-DC converter is used to increase or decrease battery voltages to accommodate the voltage needs of motors and other vehicle systems. Onboard vehicle chargers convert AC energy from the

electrical grid to DC energy required to recharge batteries. On-board chargers are typically only needed for direct grid connection. Charging stations specifically designed to charge electric vehicle batteries provide DC power and eliminate the need for an onboard charger. Capital cost values for these components are obtained from Roush's Medium and Heavy-Duty Electrification report [17]. The motor converts the electrical energy in mechanical energy and cost values are obtained from Lajevardi et al. [18].

Operating Cost

The general model for the operating cost is discussed the diesel paper (chapter 2). For the battery electric powertrain, special attention was given to the electricity cost, payload penalty, and charging penalty. This chapter covers these topics and for the full model the reader is referred to chapter 2.

Charging penalty:

A charging penalty is calculated to account for the monetary loss of charging during a working shift. The monetary loss is determined by accounting for the time spent leaving the route and finding a charger, charging, and leaving the charger to get back to the route. The value of this lost time is calculated from the hourly wages paid to the truck driver. The number times the truck needs to charge in a working shift is dependent on the battery's range. The working shift mileage requirement or daily range is assumed not to change from the diesel case and is 600mi. The charger power for the present-day scenario is 500 kW and is discussed further in section 4.3.2. The charging penalty is calculated according to Eq. 4.5

$$\$_{Charging\ Penalty} = (\frac{Battery\ Capacity}{Charger\ Power} + t_{find}) * \$_{labor} * No.\ Changes \tag{4.5}$$

Where $\$_{labor}$ is the labor rate, $t_{find} = 10 minutes$, $No. Changes during shift = \frac{Daily\ range}{Battery\ range} - 1$. t_{find} is defined as time to find and leave charger from highway.

Payload penalty:

A monetary payload penalty is calculated to account for the reduced payload capacity of the battery electric truck. The payload penalty assumes the reduced payload is compensated by proportionately purchasing more trucks. For example, a ten percent decrease in payload would results in a fleet purchasing ten percent more trucks to carry the same weight of goods. The payload penalty is only applied to the fraction of long-haul trucks that are weight constrained. The portion of trucks that would be penalized include the trucks weighing between 80,000lbs and the battery electric / diesel weight powertrain weight difference. The powertrain weight difference is assumed to be the

weight of the battery. The weight distribution of class 8 long haul trucks is derived from the VIUS data set and is given by Figure 4.3.

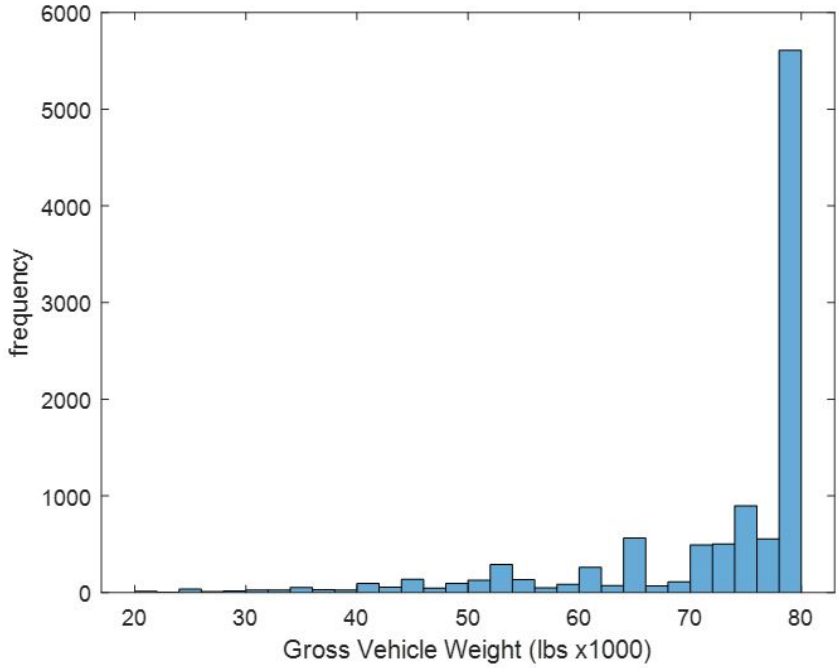

Figure 4.3. gross vehicle weight from the VIUS survey for class 8 trucks

The payload penalty is calculated by the following

$$\$_{Payload\,loss} = \int_{G-\Delta}^{G} P(w)(w - 80000lbs + \Delta)dw \tag{4.6}$$

$$\$_{Payload\,penalty} = 1 + \frac{payload\,loss}{max\,payload} * TCO \tag{4.7}$$

Where w is the truck weight, Δ is the weight difference between the diesel and battery electric powertrains, and P(w) is the weight probability distribution from Figure 4.3. For the NMC and LFP present scenario, the weight difference between the diesel and battery electric powertrain was 8,000 and 14,100 lbs, respectively, and the average payload loss was calculated to be 5,900lbs and 9,100 lbs. This payload loss resulted in a payload decrease of 11.7% and a payload penalty of $123,000 over the lifetime of the truck.

Electricity Cost (slow vs fast charging):

The cost of electricity has little uncertainty with respect to generation, transmission, and distribution, however electric vehicles have brought new challenges to electricity costs by requiring new

charging infrastructure to be built. Delivered electricity cost data exists for the current blossoming light duty vehicle market, however long-haul heavy duty charging infrastructure has yet to be built. The long-haul sector has unique challenges that the current light duty charging infrastructure fails to meet. The electricity cost for the long-haul heavy-duty truck market is split between fast and slow charging. A brief review is presented on the costs for heavy duty long haul electric charging stations considering slow and fast charging.

Slow charging in the context of the long-haul heavy-duty truck market refers to the chargers commonly used to satisfy the light duty charging demand. These charges are typically on the scale of 50kW. A battery capable of a long-haul duty cycle would require more than 1 MWh of stored energy. Using a slow charger, this would take on the order of 20 hours, rendering the truck inoperable for nearly a day while it charged. In the most ideal scenario, this charger could only be used for 13 hours since a typical long-haul shift can last up to 11 hours. To overcome this issue, the heavy-duty trucking community has raised the need for fast charging. Roughly speaking, the heavy duty trucking literature has defined fast charging as charging between 350-1000kW [19, 20]. This study uses a fast-charging value of 500 kW.

Authors responsible for modeling heavy duty charging infrastructure typically design a station to include a combination of fast and slow chargers. The stations usually contain a large number of slow chargers for overnight charging and a small number of fast chargers for shift charging. Authors from the ICCT estimate the needs for slow and fast chargers to be about 1.2-0.8 and 0.4-0.2 per truck, respectively. This is denoted by the red and yellow lines depicted in Figure 4.4. Their estimates are based on the number of trucks for slow chargers. For fast chargers, they accounted for the remaining energy demand not met by the slow chargers while minimizing charging time to maximize the time available for driving. Authors from [19] assume the ratio of slow to fast chargers to be 0.21 when considering the need for a 45-minute fast charge during the middle of the daily shift and rest stop charging at night.

Charging infrastructure costs consists of hardware cost for each charger as well as the installation and grid connection costs per site. The ICCT has performed estimates for these costs in terms of \$/kW and is given in Figure 4.5. From the blue and orange lines the hardware costs to not vary with charging site size, however the installation costs decline as the total charging power per station increases. The ICCT claims that, for a given number of stations, it is generally less costly to build more chargers at a few sites, rather than distributing chargers across many stations. The ICCT assumed slow charging as 50kW chargers and ultra-fast charging as 350 kW+. Their present-day delivery electricity cost resulted in \$0.14/kWh for slow charging and \$0.23/kWh for fast charging. Authors from [19] considered a specific charging station with six 880 kW fast chargers and twenty-

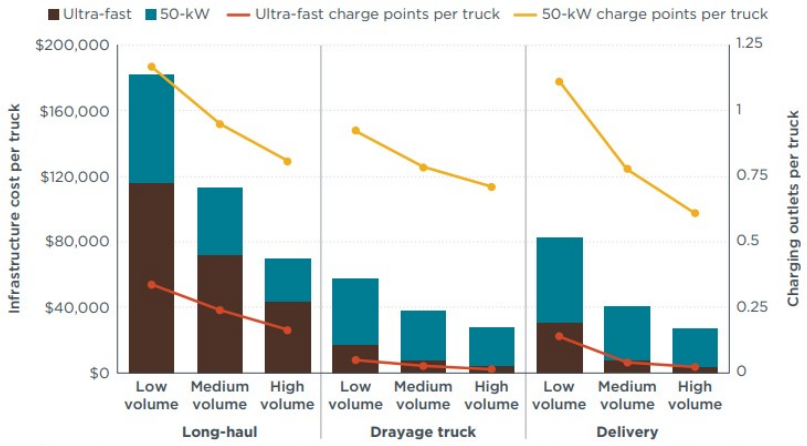

Figure 4.4. Charging infrastructure and associated capital costs required for battery electric trucks.Source:[21]

eight 50kW chargers for a total of 6,680 kW charging power. The results from their analysis are given in Figure 4.6 and their delivered cost of electricity is 0.139 €/kWh.

In the context of this thesis, delivered electricity cost values for slow charging are based on the eia's 2019 Annual Energy Outlook projections for transportation end use electricity. For fast charging, or shift charging, the ICCT's projections for ultra-fast charging are used and extrapolated to this thesis's longterm scenario. The values used are given in Table 4.3.

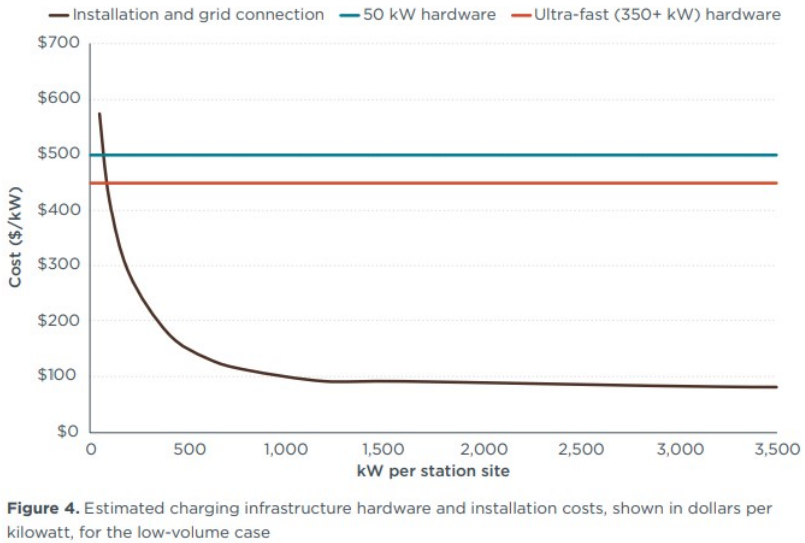

Figure 4.5. Estimated charging infrastructure hardware and installation costs, shown in dollars per kilowatt. Source:[21]

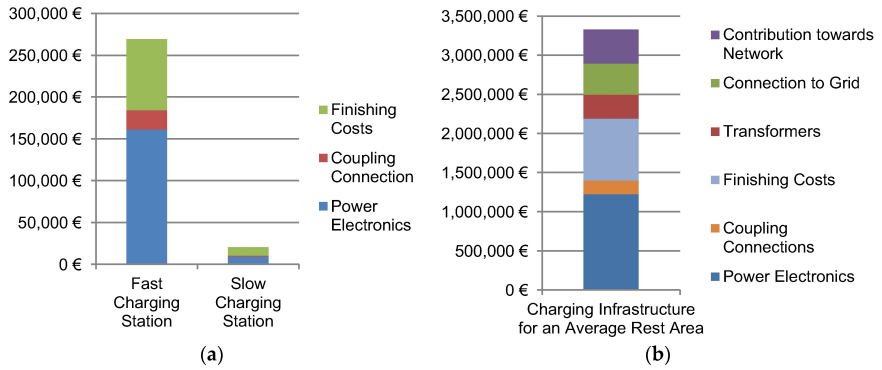

Figure 4.6. (a) Costs composition for a particular charging station; (b) Composition of total construction costs for an average charging station equipped with 6 fast and 28 slow charging stations. Source: [19]

Table 4.3. Operating cost values used in this study

Parameters	Present	Midterm	Longterm	Units	source
Slow charging electricity	0.13	0.13	0.12	$/kWh	[22]
Fast charging electricity	0.23	0.22	0.21	$/kWh	[21]
Maintenance and Repair	0.09	0.09	0.09	USD/mi	[23]
Labor	0.69	0.69	0.69	USD/mi	ATRI
Tolls	0.03	0.03	0.03	USD/mi	ATRI
Permits & Licenses	0.02	0.02	0.02	USD/mi	ATRI
Insurance	0.07	0.07	0.07	USD/mi	ATRI
NMC Cycle Life	1,000	1,000	1,000	Cycles	[16]
LFP Cycle Life	4,000	4,000	4,000	Cycles	[11]

Emissions

This study considers greenhouse gas emissions produced during the fuel production process, well to pump (WTP), and emissions as the vehicle operates, pump to wheel (PTW). The entire process consisting of fuel production and vehicle operation is known as well to wheel (WTW), and is a primary output of this study. The Greenhouse Gases, Regulated Emissions, and Energy Use in Technologies Model was used to obtain the well to pump emissions associated with electricity production, transmission, and distribution. The WTP emission data for delivered electricity produced from wind, solar, hydro, nuclear, natural gas, coal, and biomass were extracted from GREET and are given in Table 4.4. All scenario years assume electricity is obtained from the grid. The production composition for the grid is assumed to change in future years and follows the projections from the eia's AEO [24]. A summary of grid composition is given in Table 4.4. By weighting the different electricity production methods and summing them based upon grid composition, the WTP emissions for this study are derived and given in Table 4.5.

The battery electric powertrain has no direct emissions associated with the PTW component

Table 4.4. Intensities for electricity production and grid composition based on scenario year. Values are from the eia's AEO

	Emission Intensity (gCO2Eq/kWh)	Present	Midterm	Longterm
Wind/Solar/Hydro	0	0.17	0.23	0.42
Nuclear	6	0.2	0.16	0.12
Natural Gas	509	0.33	0.38	0.34
Coal	1058	0.29	0.22	0.1
Biomass	51	0.01	0.01	0.02

Table 4.5. Well to pump emission intensities for grid-based electricity

Scenario	Present	Midterm	Longterm
WTP emission intensity (gCO2eq/kWh)	477	428	281

of the WTW emissions. As such, the WTW emissions come directly from the WTP portion. The WTP emissions are converted to WTW emissions by the fuel economy according to Eq. 4.8

$$WTW = \frac{WTP}{Fuel\ economy} \tag{4.8}$$

4.4 Results and Discussion

4.4.1 Fuel economy

The resulting fuel economies used in this study are given in Table [**table:fuel_economy**]. The resulting base case present-day fuel economy for the battery electric powertrain is 2.5 kWh/mi over the USLHC8 drive cycle. This fuel economy is nearly identical with results from University of California researcher who studied long-haul trucking energy consumption and charging load profiles in the United States [25]. A Sankey diagram showing the energy flow and losses is shown in Figure 4.7. Relative to the hydrogen and diesel powertrains, the battery electric is by far the most energy efficient. The battery electric is so efficiency that the small amount of auxiliaries on board account for a large portion of the powertrain's energy loss. The auxiliary load for the battery electric is assumed to be 10 kW which is nearly one third of the hydrogen fuel cell's larger auxiliary load. The average power to propel the battery electric powertrain is only 124kW whereas the least efficient powertrain studied, the hydrogen combustion engine, requires an average fuel power of 274 kW. Unlike conventional powertrains that have higher highway than city fuel economy, the battery electric is opposite due to regenerative break. The USLHC8 and other long-haul duty cycles have very minimal breaking that the battery electric can recover energy from. Because of this and the long-range requirements, the batteries designed for long haul tend to require much more energy storage than regional or drayage duty cycles.

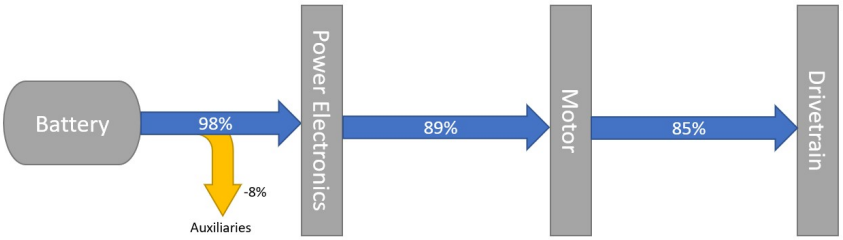

Figure 4.7. Energy losses associated with the battery electric powertrain.

Various studies have been developed to evaluate the fuel economy of the battery electric powertrain; however, few have modeled heavy-duty long-haul duty cycles. Researchers at Argonne National Laboratory developed simulation software called Autonomie to model conventional and alternative powertrains that the national labs consistently use for their simulations. Vijayagopal et al. [26] simulated six conventional and alternative powertrains over various duty cycles. For highway driving the battery electric fuel economy resulted in around 3.5 kWh/mi. The highway cycles they used are the EPA 65 cycle, EPA 55, and the CARB transient. The first two cycles consist of steady driving at 55 and 65 mph and the transient includes accelerating and decelerating with speeds up to 40 mph. These cycles are less energy consuming than the USLHC8 duty cycle which consists of sustained transient high speeds. The fuel economy results from this study would strongly prohibit battery electric from long-haul trucking. The resulting full range battery would be 2.1 MWh, 27,000 lb battery, and cost $231,000 for LFP chemistry. The battery weight alone is over half the maximum payload carried by conventional powertrains.

Table 4.6. The battery electric's fuel economies used in this study resulting from GT-Suite modeling and projected into the future.

kWh/mi	Present	Midterm	Longterm
Fuel Economy	2.5	2.4	2.3

Some studies claim much more optimistic projections of battery electric fuel economy and are mainly electric truck manufacturers and review papers (source1, source2, source3). The freightliner ECascadia boasts an impressive 1.4 kWh/mi, however with a maximum range of 230 miles, this truck is ill suited for long-haul. It is likely optimistic fuel economies utilize low speed drive cycles incorporating significant amounts of regenerative breaking.

4.4.2 Emissions

The results for the WTW emissions are given in Figure 4.8. Because the battery electric powertrains are zero emitting vehicles, there are no PTW emissions, unlike diesel. The emissions decrease in time as the grid relies less on fossil fuel electricity generation and more on renewable sources. By

the longterm scenario, more than 40% of electricity is generated by renewable sources. The WTW emissions are directly related to the social cost of carbon which is discussed in detail in chapter 1 (diesel chapter).

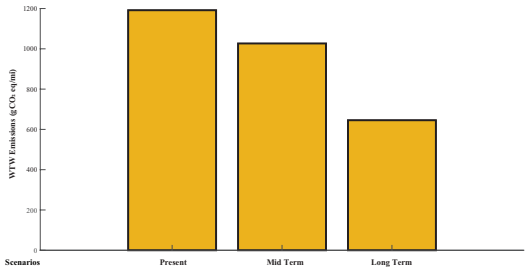

Figure 4.8. WTW emissions for the battery electric powertrains

4.4.3 Total Cost to Society

The results for the total cost to society is presented in this section and is the main output of this study. All results are compared to the conventional diesel powertrain, which is presented by the black column in all plots. The results are presented as stacked bar columns where each colored stack represents a cost component. Time-based scenarios represent the present-day, midterm, and longterm. For a full analysis of diesel baseline costs, the reader is referred to chapter 1.

The results from the capital cost modeling are given in Figure 4.9. The powertrain component sizes and cost values can be found in Table 4.7 and Table 4.8. The present-day diesel capital cost is $125,000 and represents the industry's current standard. The capital costs for the LFP and NMC battery electric powertrains is significantly more expensive than the diesel powertrain across all scenarios. In the present day, the battery electric powertrains are 4.0 and 2.6 times more costly than diesel for NMC and LFP respectively. In the longterm, the NMC and LFP are 2.3 and 1.8 times more expensive, respectively, than the diesel capital cost. While the battery for the LFP is cheaper than the NMC and does not require replacements, the battery alone is more expensive than the diesel's entire capital cost.

The capital costs for both battery electric powertrains decrease in time. The NMC capital cost decreases the most by 42% followed by the LFP at 30%. In every time scenario, the LFP capital cost is significantly lower the NMC's. The battery $/kWh cost decline is the primary driver of cost decreases. The battery is the most significant capital cost component for both battery electric powertrains. The battery represented in the final model is a full range (600 miles) battery with a total energy storage requirement of 1865 kWh for the present-day scenario and 1725 kWh for the longterm. The battery for the NMC chemistry is more costly and requires replacement in

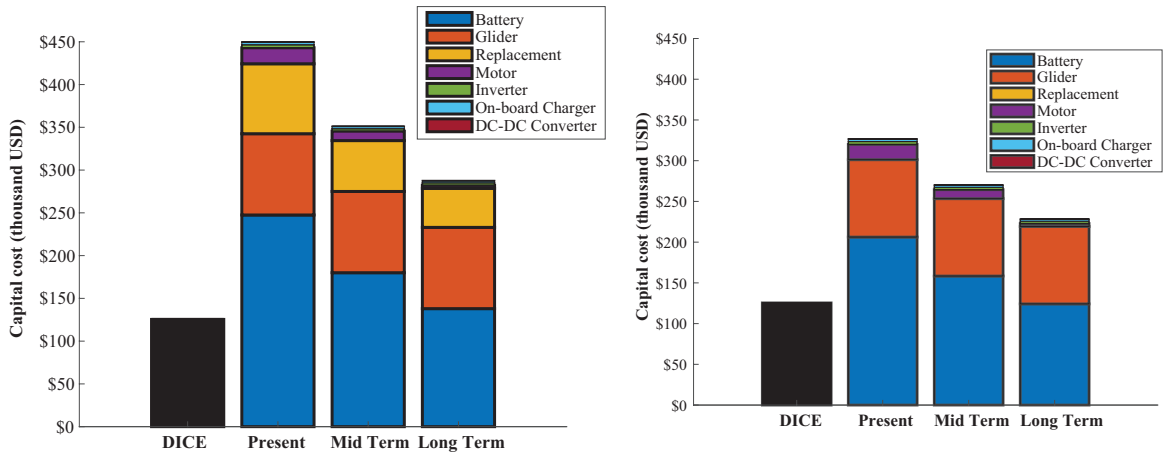

Figure 4.9. Capital cost for the NMC (left) and LFP (right) battery electric powertrains

future years. Every powertrain component capital cost either remains constant or decreases in time as large production volumes are met due to the adoption of alternative powertrains. The second largest cost component is the glider and represents all components of the tractor that are not a part of the powertrain. The glider cost is assumed constant for all powertrains and scenario years. The remaining capital cost components, including the inverter, on-board charger, motor, and DC-DC converter only constitute 4.0-5.1% and 4.0-7.8% for the NMC and LFP respectively.

4.4.4 Diesel Comparison

The results for the operating cost are shown in Figure 4.10. The powertrain component sizes and cost values can be found in Table 4.9. The present-day operating cost for the diesel powertrain is $842,000. In the present, the NMC and LFP operating costs are 1.33 and 1.51 times more costly than the diesel and in the long term, they are 1.07 and 1.13 times more costly. The electricity costs for the battery electric powertrains remains lower than the cost of diesel due to the battery electric powertrains being significantly more energy efficient. In addition, the maintenance of the battery electric powertrains is significant less than the diesel powertrain by 36%. However, the operating costs for the battery electric powertrains remain higher than the diesel for all scenarios. This is primarily due to the significant payload penalty associated with heavy battery electric power trains.

Across all scenarios, the operating costs for both battery electric powertrains declines. The LFP powertrain decreases by 24.8% in the longterm and the NMC by 20.1%. The only operating cost variations between the two battery electric powertrains is the payload penalty and accounts for the NMC having a lower operating cost relative to LFP in every scenario. The LFP's payload penalty is significantly large than the NMC's and is 1.52 times larger and is reflective of the dif-

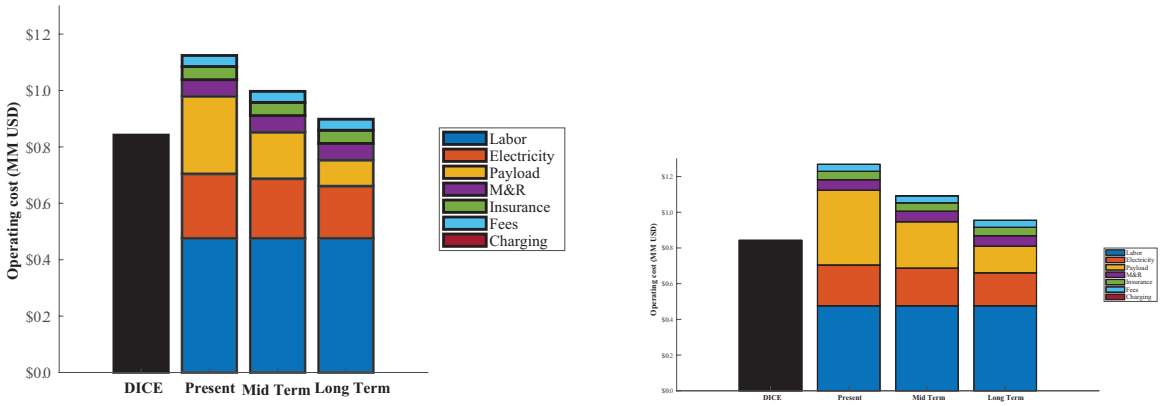

Figure 4.10. Operating costs for the NMC (left) and LFP (right) battery electric powertrains

ference in the battery's specific energy. The labor cost remains the largest cost component in all scenarios and accounts for 42.3-53.0% and 37.5-50.0% for NMC and LFP. The payload is the second largest operating cost component in early scenarios, but is out passed by electricity costs in the longterm. The remaining costs, including maintenance and repair, insurance, fees and charging, make up between 11.4-12.9% in the present scenario and 15.2-16.1% in the longterm. A charging penalty is not incorporated into the baseline scenarios because the battery is sized to provide energy for an entire daily long-haul duty cycle. The charging penalty with battery range in section 4.5.

The total cost to society represents a combination of capital, operating, and carbon costs and the results are shown in Figure 4.11. The present-day NMC TCS is 58.8% higher than diesel and LFP is 60.8% higher. In the best-case scenario, the longterm, both the NMC and LFP powertrains' TCS are about the same and is 19.6% higher than diesel. The carbon cost makes up only a negligible contribution to the overall TCS and is roughly 3% for all scenario years. Surprisingly, the NMC and LFP have TCSs nearly identical for all scenario years. This is indicative that the payload penalty associated with the LFP is balanced by the increased capital cost associated with the NMC powertrain. The two powertrains become more distinguishable when battery range is considered and is discussed in section .

4.4.5 Battery range considerations on TCS

Manufacturers for long-haul heavy-duty trucks are faced with a challenging dilemma when considering a battery size suitable for the long-haul duty cycle. The batter size is synonymous with the range of the vehicle and is associated with many trade-offs including weight, charging times, charger sizing, capital costs, and replacements costs. An analysis was performed to determine the optimal battery size (Figure 4.15). In the context of this study, optimal battery sizing refers

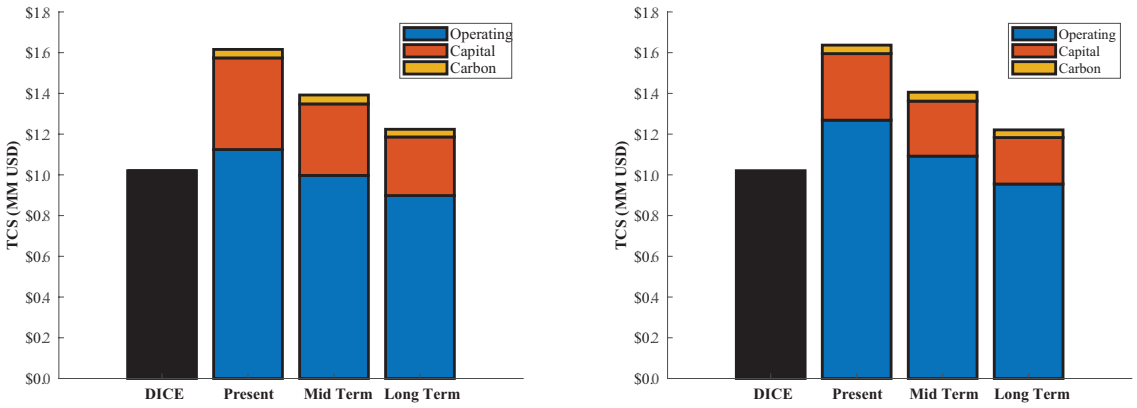

Figure 4.11. Total cost to society for the NMC (left) and LFP (right) battery electric powertrains

to the battery size with the lowest TCS. Other factors besides emissions and costs such as practicality are important, however they can be difficult to quantify and are not included in the analysis.

The analysis calculates the TCS for batteries sizes to last 100 to 600 miles on one full charge. The upper limit corresponds to the daily distance driven in a long-haul shift and represents the case where no charging is required during the trucker's shift. The lower limit of 100 miles represents a case where many charges per day becomes necessary and impractical. A list of electric truck models in or planned for production is given in Figure 4.16. The battery ranges in this list span 50 to 550 miles with only the Tesla semi reaching ranges near the length of a long-haul duty cycle.

The impact of battery size on the charging penalty is shown in Figure 4.12.The charging penalty decreases with increasing battery size. As the battery size decreases, the time required to charge increases and therefore the charging penalty increases. In addition to battery size, the number of times the battery must be charged contributes to extra time exiting and getting back onto the highway. The total time required to charge spans from 1hr28min to no charging for the smallest and largest battery sizes respectively. The charging penalty trend is identical for both the LFP and NMC battery chemistries. This is because across chemistries, the same amount of energy is needed to charge the battery and therefore the charging time is the same. Across scenario years the charging penalty slightly decreases due to smaller batteries needed from improved fuel economy. The slope of the charging penalty is much steeper at lower battery sizes. At small battery sizes, the driving time spent between the highway and charging station begins to make a significant contribution due to the large number of charging occurrences. At the lower range limit, this transit time accounts for one third of the charging time and at the upper range limit, none because no charging occurs. Not included in the charging penalty, but directly related to charging is the cost of electricity. Electricity purchased during a shift is assumed to come directly from a fast charger at a

higher rate (refer to electricity cost section). Large batteries benefit from lower electricity costs due to the ability to solely charging overnight using a slow charger. The NMC and LFP chemistry do not appear different because they use the same technical model and have the same fuel economy. Future scenario curves are shift down and have slightly different slopes due to lower electricity costs and improved fuel economies.

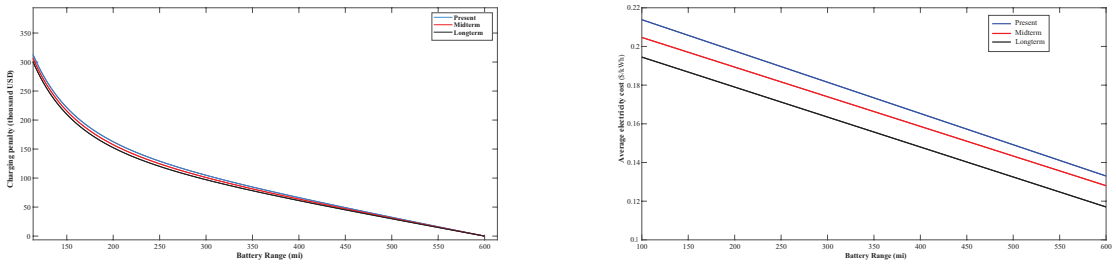

Figure 4.12. The impact of battery size on the charging penalty (left) and average electricity cost (right). The colors correspond to the scenario year

The impact of battery size on payload penalty is shown in Figure 4.13.The payload penalty increases with increasing battery size because increased battery weight decreases payload capacity. The result is the need to purchase more trucks to deliver the same amount of goods. The LFP battery chemistry has a higher payload penalty than the NMC chemistry because it has a lower specific energy. This causes the LFP batteries to be heavier for the same energy requirement. The payload penalty decreases in future scenarios due to technological advances that increase battery specific energy. The highest payload reduction for a full range battery is over 19,100 lbs (38% of diesel payload) and occurs in the present scenario for the LFP battery. The lowest occurs in future scenarios for the NMC chemistry and is over 4,200 lbs (8.4% of diesel payload).

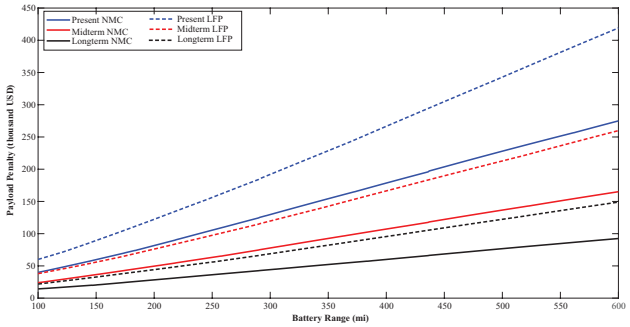

Figure 4.13. The impact of battery size on the payload penalty for NMC and LFP battery chemistries. Dash lines correspond to the LFP battery chemistry and solid lines to the NMC chemistry. The colors correspond to the scenario year

The impact of battery size on battery cost and battery replacement number is shown in Figure 4.14. The battery cost increases with battery range, however unintuitively, this is not due to the capital costs associated with purchasing a large battery. The same amount of battery cells will be purchased over the lifetime of the truck because the lifetime energy requirement does not vary with battery size. Instead, battery cells purchased later are discounted due to the discounted cash flow model. There are step changes in battery costs where there is a change in the number of battery replacements. This is because trucks with more batteries and therefore lower range benefit from purchasing batteries in the future. There is a steeper slope for the LFP battery because there are less replacements, and this affects resale. The resale is proportional to the remaining cycles left on the battery. The most ideal case would be to completely use the last battery because the resale has the largest discount applied at the end of the truck's life. The battery replacement graph only shows the longterm scenario because the present and midterm step curves are equivalent and overlap. This is because even though battery capacity changes in time, the batteries are designed based on required range rather than energy capacity.

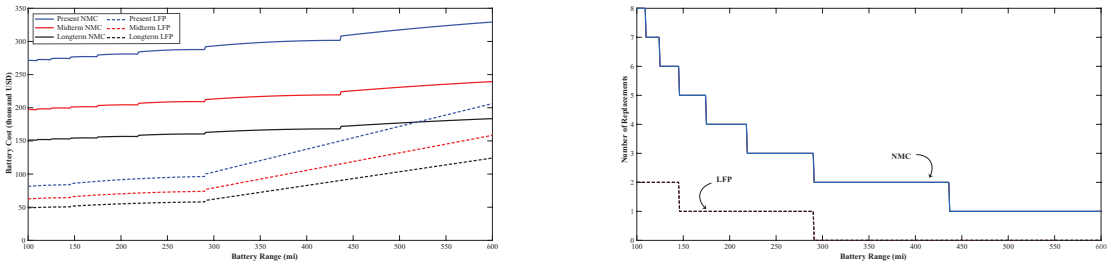

Figure 4.14. The impact of battery size on the battery cost (left) and battery replacement number (right) considering purchase and resale for NMC and LFP battery chemistries. Dash lines correspond to the LFP battery chemistry and solid lines to the NMC chemistry. The colors correspond to the scenario year. In the battery replacement graph, all scenario year overlap each other

Considering all the mechanisms associated with battery size, the TCS is calculated and shown in Figure 4.15. With respect to battery size, the TCS decreases in all cases except for the present and midterm scenarios for the LFP chemistry. The tradeoffs amongst all mechanisms discussed result in a TCS minimum with a battery range of 290 miles in the present term and midterm. The other cases decrease rapidly until a battery size of 150 miles before slowly decaying with increasing battery size. The magnitude of decay with increasing battery size is more prevalent in the NMC case because of the smaller payload penalty and battery cost slopes. Under all time scenarios, the LFP chemistry has a lower TCS than the NMC except for cases near full range. This indicates the significance of the payload penalty and resale values. Future scenarios have lower TCSs due to technological improvements and declining unit costs as market penetration increases.

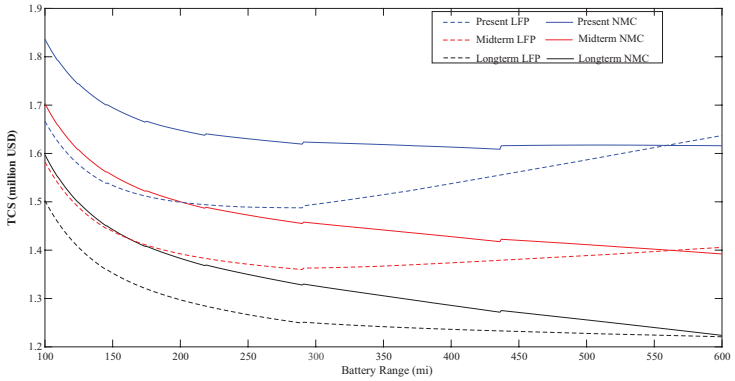

Figure 4.15. The impact of battery size on the TCS for NMC and LFP battery chemistries. Dash lines correspond to the LFP battery chemistry and solid lines to the NMC chemistry. The colors correspond to the scenario year

4.5 Conclusions

The results of this study inform the long-haul trucking community of the battery electric powertrain's potential to replace the conventional diesel powertrain on the basis of costs and emissions. This study's results do not apply to the heavy-duty trucking market in general as regional haul, drayage, and specialty trucking have different duty cycles that would significantly alter the potential of battery electric trucking. For example, duty cycles associated with city driving usually require less daily range and more braking. These duty cycles give more favor to the battery electric powertrain as regenerative breaking and less range can improve fuel economy and require smaller batteries. The resulting fuel economy of this study is 2.5 kWh/mi. While this value falls within previously published literature values, it should be noted as a preliminary value. The powertrain model developed in GT-Suite does not include the presence of a cooling system. The cooling system can significantly affect the fuel economy when adding auxiliary loads such as the radiator fan and cause it to decrease. This affect is particularly important for the battery electric powertrain because of its low power demand relative to other powertrains due to its high efficiency. An increase of 10 kW to include the radiator fan can significantly affect the fuel economy for a powertrain with an average power require of 100 kW versus a powertrain with an average power requirement of 200 kW. Based on the results presented, there is no advantage or disadvantage between using an LFP or NMC battery when considering full range batteries. The TCS for all time scenarios was nearly equivalent with the largest percent difference being 1.6% in the present with the LFP battery having the advantage. The increased payload penalty of the LFP was generally matched by the lower durability and higher capital cost of the NMC. When the range of the battery is considered, The LFP generally outperforms the NMC, except for at very high ranges where they are nearly equal. This is because the payload penalty affects the LFP more than the NMC and reducing battery size

reduces the payload penalty. Due to the significance of the payload penalty, future modeling efforts should be devoted to the specific energy of the battery. In addition, the technical difference in fuel economies between the LFP and NMC was not modeled. As the chemistry is different between the two batteries, one would expect a difference in performance, durability, and efficiencies. Including this analysis will separate their fuel economies and therefore sizing, allowing for more differentiation between their TCSs. Future work will center around using the software GT-AutoLion to model these technical differences.

Not fully developed in this study is the cost of electricity, especially for lower carbon electricity production methods. The electricity cost is the second largest cost component next to labor. The electricity cost difference between slow and fast charging is nearly 100%. Fast charging is significantly more expensive, however the payload penalty for large batteries is shown to have a larger effect on the TCS in section 4.4. A constant charger size of 500 kW was used in this study and the electricity cost was limited to literature charging station values. The size of the charger can have a significant effect on the cost of fast charging and the charging penalty and was not explored in this study. Future efforts should explore the feasibility of larger chargers up to and over 1MW. Chargers over 1 MW could allow truckers to charge full range batteries enough during their breaks such that they can finish their shifts before using a slow charger.

Relative to the conventional diesel powertrain, the battery electric powertrain is more costly, even when accounting for emissions. In the longterm this difference 20%. The metric used to evaluate emissions is the social cost of carbon. While the social cost of carbon evaluates damages done to society, the use of a larger carbon tax may be more appropriate. Politicians are face with the challenge of developing the carbon tax's price. The social cost of carbon could be used to pass on societal damages to the emitters or a higher value could be used to put battery electric on par with diesel or cheaper than diesel. The higher carbon tax would cause truckers to switch to the lower cost option and allow the ambition carbon targets to be met. In any scenario it is likely that in order to reach low carbon or net zero carbon targets, consumers will have to pay more for the shipping of their goods.

4.6 Appendix

Table 4.7. Battery electric powertrain component sizes. Results apply to both LFP and NMC chemistries

Powertrain Component Sizes (kWh/kW)	**Present**	**Midterm**	**Longterm**
Battery	1875	1800	1725
Motor / inverter	1100	1100	1100
On-board charger	50	50	50
DC-DC converter	10	10	10

Table 4.8. Battery electric powertrain component capital costs

Capital Costs (x$1,000)	**LFP**			**NMC**		
	Present	**Midterm**	**Longterm**	**Present**	**Midterm**	**Longterm**
Battery capital	206	158	124	248	180	138
Battery replacement	0	0	0	81.8	59.5	45.6
Glider	95	95	95	95	95	95
Motor	18.7	11.0	3.6	18.7	11.0	3.6
Inverter	3.6	3.0	3.0	3.6	3.0	3.0
On-board charger	2.8	2.5	2.3	2.8	2.5	2.3
DC-DC converter	0.5	0.3	0.3	0.5	0.3	0.3
Total	327	270	228	500	351	288

Table 4.9. Battery electric powertrain component operating costs

Operating Costs (x$1,000)	LFP			NMC		
	Present	Midterm	Longterm	Present	Midterm	Longterm
Labor	476	476	476	476	476	476
Electricity	228	211	185	228	211	185
Payload Penalty	419	260	149	275	165	92
Maintenance & Repair	58.9	58.9	58.9	58.9	58.9	58.9
Insurance	46.7	46.7	46.7	46.7	46.7	46.7
Tolls, Permits, & Licenses (Fees)	39.2	39.2	39.2	39.2	39.2	39.2
Charging Penalty	0	0	0	0	0	0
Total	1,270	1,092	955	1,124	997	898

Table 4.10. Battery electric powertrain total cost to society cost components.

TCS (x$1,000)	LFP			NMC		
	Present	Midterm	Longterm	Present	Midterm	Longterm
Operating	1,270	1,092	955	1,124	997	898
Capital	327	270	228	500	351	288
Carbon	41.7	43.7	38.0	41.7	43.7	38.0
Total	1639	1406	1221	1666	1392	1224

DETAILS ON ANNOUNCED AND PRODUCTION ZERO-EMISSION TRUCKS

Table A1. Announced or in-production battery electric medium- and heavy-duty trucks

Make	Model	Range (miles)	Battery capacity (kWh)	Vehicle class	First demonstration	Start of regular production
Eforce	EF18 SZM	310	630	8 (Tractor-trailer)	2016	2017
Eforce	EV26	310	630	8 (Straight truck)	2016	2017
Thor	ET-One	300	800	8 (Tractor-trailer)		2019
Volvo	FL Electric	186	300	7		2019
BYD	Day Cab	167	435	8 (Tractor-trailer)		2018
emoss	EMS 18 Series	155	240	8 (Straight truck)	2017	2018
emoss	EMS 16 Series	130	200	8	2015	2018
emoss	EMS 12 Series	124	200	7	2013	2018
BYD	Class 6 Truck	124	221	6		2018
Cummins	AEOS	100	140	7	2018	2019
emoss	EMS 10 Series	93	120	6	2014	2018
Mitsubishi FUSO	eCanter	62	83	4	2017	2019
Tevva	eTruck	93	75	4-6		2018
Tesla	Semi	550	1000	8 (Tractor-trailer)	2018	2020
Nikola	Two	400	1000	8 (Tractor-trailer)	2019	
Freightliner	eCascadia	250	550	8 (Tractor-trailer)	2018	2021
Lion	Lion8	250	480	8	2018	2020
Freightliner	eM2 106	230	325	5	2018	2021
Mercedes-Benz	eActros	125	240	7-8 (Straight truck)	2018	2021
MAN	eTGM	124	150	7-8 (Straight truck)	2018	
Volvo	VNR	124	300	8	2019	2020
Volkswagen	e-Delivery	124	200	4	2018	2020
Peterbilt	e220	100	148	6	2019	
Xos	MDV	50	60	6	2018	2020
Eforce	EF18 SZM	310	630	8 (Tractor-trailer)	2016	2017
Eforce	EV26	310	630	8 (Straight truck)	2016	2017
Thor	ET-One	300	800	8 (Tractor-trailer)		2019
Volvo	FL Electric	186	300	7		2019
Volkswagen	e-Delivery	124	200	4	2018	2020
Peterbilt	e220	100	148	6	2019	
Xos	MDV	50	60	6	2018	2020

Figure 4.16. WTW emissions for the battery electric powertrains

4.7 References

(1) Agency, U. E. P. Sources of Greenhouse Gas Emissions, 2018.

(2) Davis, S. C.; Boundy, R. G., *Transportation Energy Data Book: Edition 37.2*, 2019.

(3) Of Transportation. Bureau of Transportation Statistics, U. D. 2017 CFS Preliminary Data. U.S. Department of Transportation, 2018.

(4) Framework, F. A. FAF Trend - Over Time (1997 - 2045), 2012.

(5) Of Transportation Statistics, B. National Transportation Statistics 9/4/19 Update, Shares of U.S. Energy Consumption and other categories, 2019.

(6) UN. *Framework Convention on Climate Change*; United Nations, 2021, pp 1–26.

(7) Ziegler, M. S.; Trancik, J. E. Re-examining rates of lithium-ion battery technology improvement and cost decline. *Energy and Environmental Science* **2021**, *14*, 1635–1651.

(8) Rohrer, E.; Marquart, B. *2020 Vehicle Technologies Office Annual Merit Review High Efficiency Powertrain for Heavy Duty Trucks using Silicon Carbide (SiC) Inverter*; Ricardo, 2020.

(9) Smith, D.; Graves, R.; Ozpineci, B.; Jones, P. T.; Lustbader, J.; Kelly, K.; Walkowicz, K.; Birky, A.; Payne, G.; Sigler, C.; Mosbacher, J. *Medium-and Heavy-Duty Vehicle Electrification An Assessment of Technology and Knowledge Gaps*; 2019.

(10) Yao, A. Tesla Battery Day, 2020.

(11) Proterra. *Proterra*; 2022.

(12) Laboratory, A. N. ANL-MDHD Vehicle Simulation. https://www.autonomie.net/pdfs/ANL-MDHD%20Vehicle%20Simulation%20Report.pdf.

(13) BloombergNEF. Battery Pack Prices Fall to an Average of $132/kWh, But Rising Commodity Prices Start to Bite, 2021.

(14) ANL. *Fuel Economy and Cost Estimates for Medium and Heavy Duty Trucks*; Argonne National Laboratory, 2019, pp 1–41.

(15) CommercialTruckTrader. Heavy Duty, 2022.

(16) USABC. United States Advanced Battery Consortium LLC (USABC), 2022.

(17) Nair, V.; Stone, S.; Rogers, G.; Pillai, S. *Medium and Heavy-Duty Electrification Costs for MY 2027-2030 Final Report*; 2022.

(18) Lajevardi, S. M.; Axsen, J.; Crawford, C. Examining the role of natural gas and advanced vehicle technologies in mitigating CO2 emissions of heavy-duty trucks: Modeling prototypical British Columbia routes with road grades. *Transportation Research Part D: Transport and Environment* **2018**, *62*, 186–211.

(19) Mareev, I.; Becker, J.; Sauer, D. U. Battery dimensioning and life cycle costs analysis for a heavy-duty truck considering the requirements of long-haul transportation. *Energies* **2018**, *11*, DOI: 10.3390/en11010055.

(20) Electrek. Tesla is deploying the first Megacharger to charge its Tesla Semi electric truck, 2021.

(21) Hall, D.; Lutsey, N. *Estimating the infrastructure needs and costs for the launch of zero-emissions trucks*; The International Council On Clean Transportation, 2019.

(22) EIA. *International Energy Outlook 2019*; US. Energy Information Administration, 2019.

(23) ANL. *Comprehensive Total Cost of Ownership Quantification for Vehicles with Different Size Classes and Powertrains Energy Systems Division*; Argonne National Laboratory, 2021, pp 1–227.

(24) Administration, U. E. I. Annual Energy Outlook 2021 with projections to 2050. https://www.eia.gov/outlooks/aeo/data/browser/#/?id=12-AEO2021%5C&region=0-0%5C&cases=ref2021%5C&start=2019%5C&end=2050%5C&f=A%5C&linechart=~ref2021-d113020a.32-12-AEO2021%5C&map=%5C&ctype=linechart%5C&sourcekey=0.

(25) Tong, F.; Jenn, A.; Wolfson, D.; Scown, C. D.; Auffhammer, M. Health and Climate Impacts from Long-Haul Truck Electrification. *Environmental Science and Technology* **2021**, *55*, 8514–8523.

(26) Vijayagopal, R.; Prada, D. N.; Rousseau, A.; Suarez, L. Y. T. Fuel Economy and Cost Estimates for Medium- and Heavy-Duty Trucks. *U.S. Department of Energy, Argonne National Laboratory* **2019**.

Chapter 5

Overall Conclusions and Future Directions

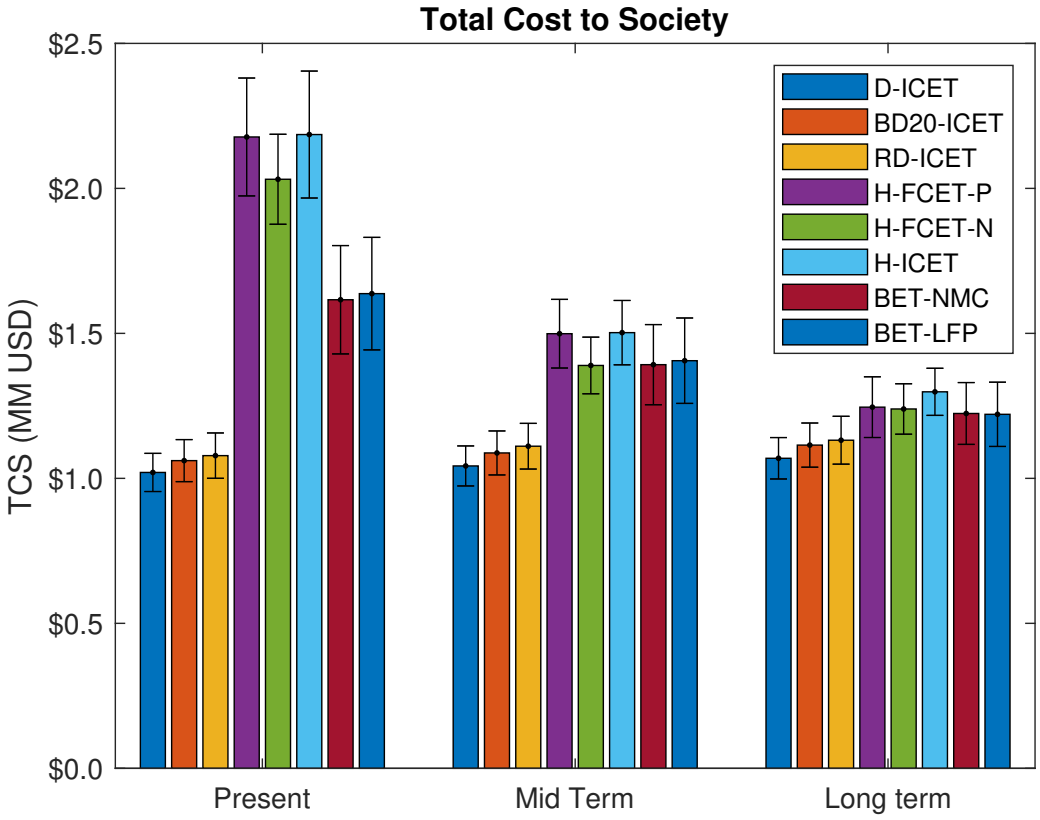

Figure 5.1. The total cost to society across all powertrains considered in this thesis. Error bars correspond to a Monte Carlo simulation considering input parameters with uniform distributions corresponding to ±10%.

The purpose of this study was to assess the viability of alternative powertrains to replace the conventional fossil-fuel based diesel powertrain. The long term scenario considers an apples to apples comparison and assumes all powertrains have reached their full potential and are produced at full scale. The final TCS results for this assessment are provided in figure 5.1.

Table 5.1. TCS factors for each powertrain relative to diesel.

Parameters	Present	Midterm	Longterm
D-ICET	1.00	1.00	1.00
BD20-ICET	1.04	1.05	1.04
RD-ICET	1.06	1.07	1.06
H-FCET-P	2.14	1.47	1.17
H-FCET-N	1.99	1.34	1.16
H-ICET	2.15	1.47	1.21
BET-NMC	1.59	1.34	1.14
BET-LFP	1.61	1.36	1.14

Across all scenarios, every alternative powertrain is more costly than diesel. In the present scenario, hydrogen powertrains cost 99-115 % more than diesel and 59-61 % for battery electric powertrains. In the midterm, the TCSs for hydrogen and battery electric powertrains decreases and the diesel powertrains stay approximately constant, however the hydrogen and battery electric powertrains are 34-47 % and 34-36 % more expensive. In the longterm scenario, the alternative powertrains' TCSs continue to decline, however are still 14-21 % more costly. In the longterm, all alternative powertrains have nearly the same TCS with the hydrogen powertrains costing slightly more than the battery electric powertrains. In all scenarios, the H-ICET is the most costly powertrains. The The battery electric is the lowest cost alternative in all scenarios with NMC being the lowest in the present day and LFP in the longterm.

In the present-day scenario, the hydrogen powertrains are significantly more expensive than the battery electric and diesel powertrains. This is largely due to the expensive cost of hydrogen at \$12.24/kg. By the longterm, the hydrogen powertrains become significantly more competitive as the cost of hydrogen drops to \$5.83/kg. As discussed in section ?, the cost of hydrogen would have to drop to ?/kg for the hydrogen powertrains to be on parity with diesel. This is challenging as the costs associated with liquefaction from delivery for central plants and compression from refueling for distributed plants poses as a large obstacle. From a powertrain perspective, the fuel cell electric truck has significant energy losses due to its numerous power auxiliaries and future work should strive to reduce this load.

In the present scenario, the battery electric powertrains have an advantage over the fuel cell powertrains due to the economies of scale achieved in the light-duty market. When this thesis was started and batteries were over \$200/kWh, the battery electric powertrain was significantly inferior. However, with decreasing battery costs and projected low future costs, the battery electric was calculated to be the lowest cost option, however still more expensive than the conventional diesel. For the battery electric to have parity with diesel, the battery cost needs to drop to \$/kWh in the longterm. In addition to the high battery cost, each battery electric powertrain is hindered uniquely.

In the case of the LFP chemistry, the low specific energy leads to a very large payload penalty. Reducing the battery range helps this option, however this may introduce longer unfavorable shifts for trucker due to the need for charging time. For the NMC chemistry, durability is the largest obstacle, and this powertrain suffers from costly battery replacements. Studies to increase the LFP's specific energy and NMC's durability are needed to better the viability of the battery electric powertrain. In addtion, cost projections for lithium-ion battery cost needs to incorporate the future supply and demand effects of an entire electric-based vehicle market.

The final conclusions of this work are

1. The diesel powertrain is not suitable for net zero emissions. The renewable diesel option has significantly less emissions for a slightly higher cost, however producing renewable diesel at scale seems unlikely. Therefore, zero emitting powertrains must be considered to align with net zero goals agreed upon by the Conference of the Parties.

2. Zero emitting powertrains such as the battery electric and hydrogen fuel cell are likely to be more costly than the conventional diesel powertrain, even under ideal circumstances. It is likely consumers must pay slightly more for shipped goods to limit global warming.

3. There are many challenges when transiting to either battery electric or hydrogen fuel cell powertrains for long-haul trucking. Most obvious, the need for new recharging or hydrogen refueling infrastructure, and also massive increases in production of low-GHG electricity of hydrogen. The new cleaner trucking system will be significantly more expensive in the short-term and there are likely to be operational difficulties. Will society make a massive investment to build the infrastructure for a system than is more expensive and less convenient than the incumbent technology?

Chapter 6

Capstone: Farm to Fuel

This study evaluates the feasibility of implementing small-scale methanol production facilities on farms, utilizing crop residues as a sustainable alternative to diesel fuel. Focused on technical feasibility, economic viability, and environmental impacts, the research uses a comprehensive methodological approach including a discounted cash flow analysis, which projects a positive net present value (NPV) of $238,323 over a 20-year operational period. This setup suggests substantial economic returns, particularly when surplus methanol is marketed to neighboring industries. The installation of a methanol plant is estimated to produce methanol at $0.75 per gallon, significantly undercutting the regional contract price of $1.94 per gallon for methanol, reflecting a 159% cost reduction and represent a diesel gallon equivalent (DGE) savings of $2.36 per gallon. Environmentally, the shift to methanol could lower greenhouse gas emissions, with the plant operations designed to achieve a net-zero emissions footprint. Technically, the adaptation of existing biomass conversion technologies is deemed feasible for on-farm methanol production. The study predicts that this initiative could transform energy practices in rural agriculture, making farms more energy-independent and reducing their environmental impact.

6.1 Introduction

In the face of escalating fuel prices and growing environmental concerns, farms worldwide are compelled to explore sustainable and cost-effective alternatives to conventional diesel fuel. Methanol, a versatile and less environmentally damaging biofuel, emerges as a promising substitute. This paper examines the feasibility of installing a small-scale methanol production facility on a farm, specifically designed to utilize farm-based resources for methanol synthesis, which could potentially replace diesel fuel used in agricultural operations.

The motivation for this study is twofold: firstly, the economic benefits of producing methanol in situ could significantly reduce operational costs associated with the purchase of diesel. Secondly, utilizing methanol as a cleaner fuel alternative could decrease the farm's carbon footprint, aligning agricultural practices with global sustainability goals. The objective of this research is to evaluate the technical feasibility, economic viability, and environmental impacts of installing and operating a small chemical plant for methanol production on a farm.

This paper will outline the methodological approach for assessing these three critical areas. It will consider the availability of raw materials, the technological requirements of small-scale methanol production facilities, and the integration of such a system within existing farm infrastructure. Additionally, it will explore the economic thresholds that make this investment viable, including initial capital costs, operational expenses, and potential savings on diesel. Finally, the environmental analysis will focus on the reduction of greenhouse gas emissions and the potential for achieving a net-zero energy balance.

By providing a comprehensive evaluation of these factors, this study aims to contribute valuable insights into the feasibility of farms becoming more energy self-sufficient through the adoption of innovative technologies. This could not only reshape the energy landscape of rural agriculture but also set a precedent for the broader adoption of sustainable practices in the sector.

6.2 Methods

A discounted cash flow was performed to assess the feasibility of producing methanol fuel on site at a farm using left over crop residues from farm operation. The discounted savings of not using diesel fuel were weighed against the capital and operating costs of producing methanol over the 20-year lifetime of the plant according to equation 6.1. The plant was assumed to be purchased and installed in the first year of operation. A positive net present value (NPV) indicates an economically feasible project while a negative net present value (NPV) indicates a poor investment.

$$\sum_{yr}^{lifetime} \frac{DieselFuelSavings - CapX - OpX}{(1+r)^n} \tag{6.1}$$

A small-scale methanol plant using crop residue as feedstock was modeled with the intention to use renewable methanol as a replacement for diesel fuel in farm operation equipment. The plant's methanol production was scaled down from 295,000 gallons per day to 172. This number represents the daily fuel requirement (70 diesel gallons) for a typical 750 acre corn farm. The energy conversion factor used in this work to convert the energy in a gallon of methanol to a gallon of diesel is 0.45. An overview of the process is given by the process flow diagram in figure 6.1. The process consists of three major steps. (1) indirect gasification of biomass, (2) syn gas cleanup and conditioning, and (3) catalytic conversion of syn gas to methanol. Detailed process design information for the conversion of biomass to clean syngas is available from previous Bioenergy Technologies Office (BETO) reports (Tan et al. 2015 [1]; [2]; [3]; Dutta et al. 2011 [4]). Syngas to methanol (step 3) is based on commercially operated processes.

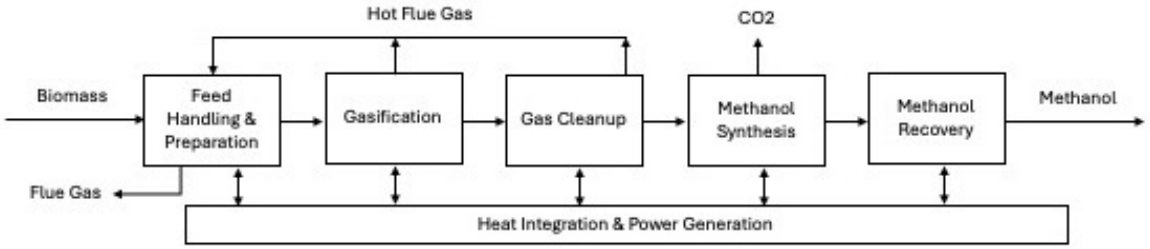

Figure 6.1. The process flow diagram for the conversion of biomass to methanol. This process is modified from NREL's HOG study.

This process is derived from the NREL study, *High-Octane Gasoline From Lignocellulosic Biomass via Syngas and Methanol/Dimethyl Ether Intermediates* [2]. Edits to this process include removing methanol dehydration to dimethyl ether (DME), and DME homologation to branched hydrocarbons.

The capital cost (CapX) of the plant was accounted for by scaling the capital costs from the NREL study for relevant unit operations. The CapX for this process includes feed handling and drying, gasification, gas cleanup, methanol synthesis, and methanol conditioning unit operations (table 6.1). Scaling down the large plant's CapX considers two scale factors (equation **??**). The first is a linear scaling factor based on the plant's input of dry biomass. The second is a scaling factor that considers the intrinsic costs of being at a smaller scale, such as being on the lower side of economies of scale. The second scaling factor is derived by considering the effects of gasifiers and their economies of scale in CHP plants from [5]. This ratio is found by finding the cost per feed rate for the small system in [5] and [2], and then taking he ratio of the two. The ratio was derived for gasifiers; however, this ratio was used for all CapX of plant equipment. Land purchase costs were left out because farmers are assumed to have ample land for the small production plant.

$$CapX_{small} = CapX_{large} \times \frac{(FeedRate)_{small}}{(FeedRate)_{large}} \times \frac{(\$/FeedRate)_{small}}{(\$/FeedRate)_{large}} \tag{6.2}$$

Table 6.1. Capital costs for the described process that converts biomass to methanol.

Unit Operation	CapX ($)	Source
Feed Handling & Drying	735	[2]/ [5]
Gasification	163,990	[2]/ [5]
Gas Cleanup	194,140	[2]/ [5]
Methanol Synthesis	123,912	[2]/ [5]
Methanol Conditioning	8,457	[2]/ [5]
Steam System and Power Generation	127,588	[2]/ [5]
Cooling Water	26,474	[2]/ [5]
Other Direct Costs	19,649	[2]
Total	664,945	

Operating costs for the plant include feedstock, catalyst replacement, olivine, waste disposal, maintenance and repair, insurance, and labor. Material operating costs were taken from the NREL HOG study [2] and linearly scaled, while feedstock and fixed costs are taken from NREL's distributed CHP study. Operating costs can be found in table 6.2. The process is self-sustaining, so no outside utilities are needed to run the process.

The feedstock for a small plant that is distributedly located at the source of the feedstock should be much less than feedstock that is purchased at retail for a large plant. Costs should consider the absence of retail mark up, feedstock preparation, feedstock packaging, and transportation costs. The feedstock costs should only include the labor and fuel costs required to bring crop residues to the hopper. As such the value of $10 per dry metric ton was used from a small scale NREL CHP study ([6]).

Table 6.2. Operating costs for the described process that converts biomass to methanol.

OpX Parameter	OpX ($/yr)	Source
Feedstock	3,819	[6]
Catalyst	6,801	[2]
Olivine	349	[2]
Other Raw Matrl	872	[2]
Waste Disposal	930	[2]
Maintenance & Repair	4,200	[6]
Insurance	500	[6]
Labor	4,928	[6]
Total	22,398	

A financing scheme was chosen that gave the farmer the highest NPV over the lifetime of the

operation. This financing scheme resulted in a loan that was amortized over the lifetime of the plant. The plant was financed with 100% of debt. With this financing scheme, all cash flows starting with year-one are positive. Other debt financing schemes considered shorter loan lives and paying off different parts of the capital off at different times.

The plant life was reduced from the assumption of 30 years in the NREL study ([2]) to 20 years based on the distributed CHP plant referenced earlier ([6]). A smaller plant life is attributed to the farmer's periodic use of the plant. Rather than running a large plant consistently with downtime scheduled for maintenance, the farmer is assumed to run the plant periodically when needed based on operational needs. This periodic nature leads to a decrease in durability.

Multiple scenarios are considered to give the farmer the most optimal solution for his or her situation. The crop types considered are corn, soybeans, rice, wheat, and sorghum. For a fuel production plant to be useful, it must be able to produce the minimum amount of fuel needed for farm operations. The total amount of yearly fuel needed is based on row crop production such as corn or soybeans. Farm operations that require fuel include field operations, crop residue drying, and fertilizer and pesticide production. The crop types have varying levels of crop residue available for used and are given in figure 6.3.

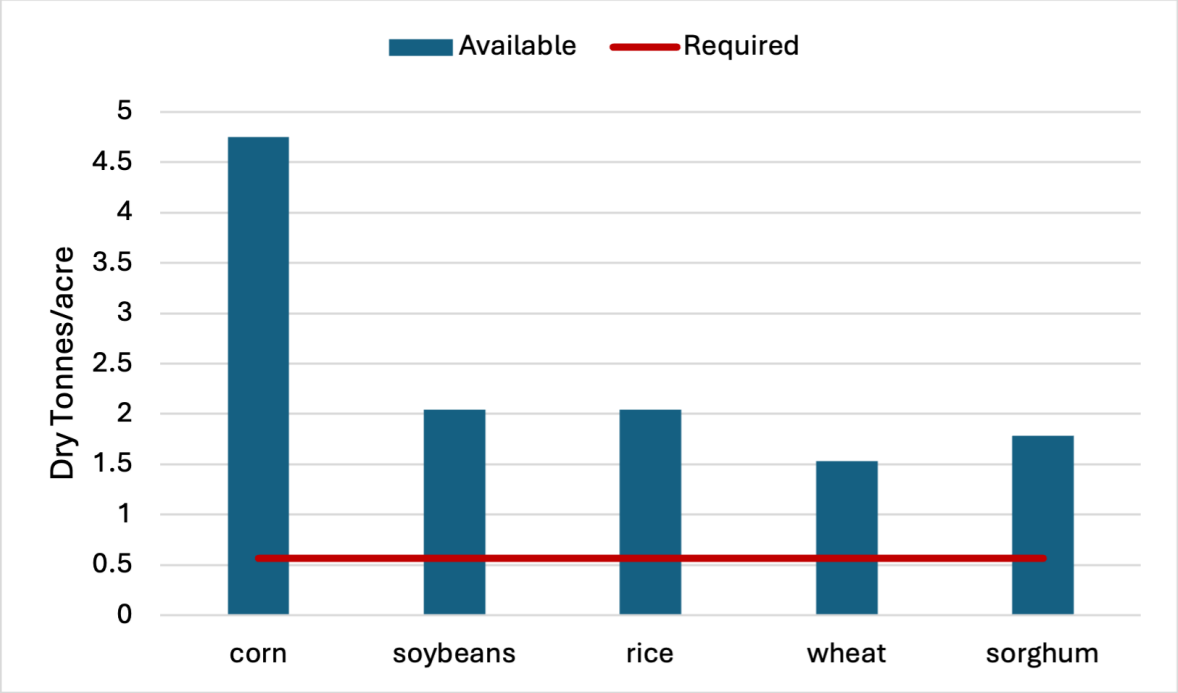

Figure 6.2. The available crop residue from harvest and the fuel requirement needed for farm operations shown in red.

The base case scenario considers using the farm's crop residues to fuel the farm's operations. Fuel production plant capacity is designed only to feed the farmers operational fuel demand. The extended scenario considers selling excess crop residue to neighboring farms for their fuel needs. This

scenario scales up production plants to equal total harvested crop residue rates and competitively sells the methanol at the price of diesel.

An additional scenario was assessed that considers buying electricity from the grid rather than generate electricity on site. The pros of this scenario is lower capital costs due to the absence of the turbine equipment and less consumption of feedstock. The cons are higher operating costs from purchasing electricity. The discounted cash flow previously describe was used to assess the trade offs. The electricity consumption for each sub process was taken from [1] and scaled down, and is given in table 6.3. Considering the operating factor, the total electricity consumed in a year is 150 MWh. An electricity rate of $0.10/kWh was used.

Table 6.3. The electricity consumed in the process.

Sub Process	kW
Gasification	4.97
Syn Gas Cleanup & Compression	15.26
Methanol Synthesis	4.43
Total	24.65

6.3 Results

The base case scenario resulted in a NPV of $238,323 over the 20-year lifetime of the plant and produces 172 gallons of methanol per day. This equates to a discounted return on investment of 36%. Because the loan of the discounted cash flow was designed to have no negative cash flows, there is no internal rate of return to report. The cash flows are constant during the life of the plant and are $22,496 per year. Considering costs alone, the discounted lifetime cost comes to $851,451, leading to a methanol cost of $1.67/DGE or $0.75/gal. This is split between a capital and operating costs of $614,166 and $237,285 respectively. The lifetime savings from not using diesel is $1,089,774.

The case for purchasing electricity from the grid resulted in a NPV of $212,475. This case is 10.8% lower than the base case that produced electricity on site. This plant produces the same amount of methanol per day, however without the need to produce electricity on site, the feedstock rate was reduced from 1.17 metric tonnes per day to 0.84. The feedstock reduction led to a savings of $11,282 over the plant life. The electricity costs over the plant life was $153,557. Taking into consideration the $127,878 CapX (with interest spread over 20 years) of generating equipment, overall trade off is -$25,865. It should be noted that this comparison is very sensitive to the price for feedstock, the electricity price, and interest rate.

The regional contract price for methanol in North America is $645 per metric tonne or $1.94 per gallon [7]. This is 159% higher than the cost calculated in this work. The national average price of diesel is $4.03 per gallon [8]. On an diesel gallon equivalent basis (DGE), methanol saves a farmer

$2.36 per DGE. Producing methanol on site eliminates the needs for transportation costs and resale markup. This work shows that methanol produced at the farm from renewable sources is not only cleaner, but also more economically favorable.

A sensitivity analysis was performed to see the impact on the base case of key parameters on the NPV and is shown in figure 6.3. Baseline parameters were varied by 10%. The price of diesel was found to have the largest impact on the model. As shown, a 10% variation on the diesel price can have a nearly 50% impact on the NPV, however it takes a diesel price of $3.15 to make the NPV zero. The second largest consideration in the model is the EOS factor which stands for the economies of scale factor and is the second factor in equation 6.2. This factor heavily influences the capital cost of the system.

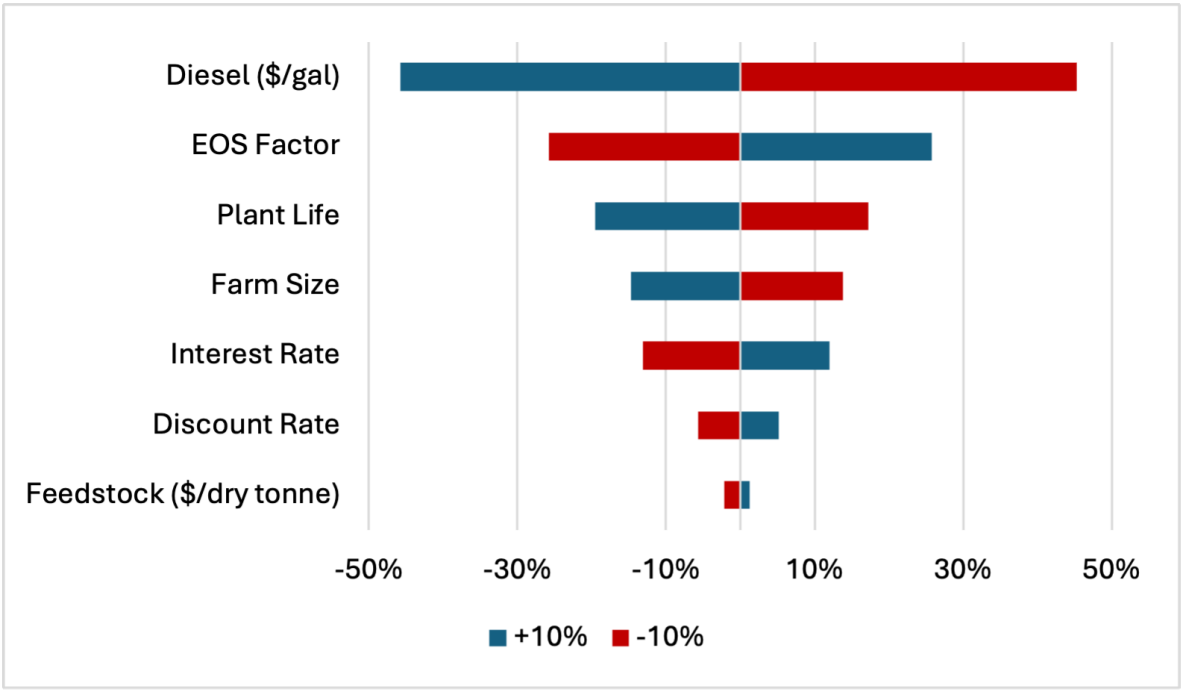

Figure 6.3. The available crop residue from harvest and the fuel requirement needed for farm operations shown in red.

Table 6.4. Parameters used in the sensistibity analysis and their values

Parameter	Base Case	-10%	+10%
Diesel ($/gal)	4.03	3.63	4.44
EOS Ratio	6.33	5.69	6.96
Plant Life	20	18	22
Farm Size	750	675	825
Interest Rate	6%	5.4%	6.6%
Discount Rate	7%	6.3%	7.7%
Feedstock ($/tonne)	10	9	11

The capital cost of the system and the price of diesel are the two most important parameters for a farmer to consider when choosing to purchase the methanol plant. Therefore, an analysis was performed to determine what the capital cost of the plant must be for the farmer to break even on his or her investment. Because the price of diesel is volatile, a plot of capital cost vs diesel price is constructed for a breakeven NPV (figure 6.4). Any cost lower than the curve, would result in a positive NPV and therefore is a good investment for the farmer. In the case of high diesel prices, such as California where the price can reach upwards of $6/gal, the breakeven cost of the system is around $1.5M. For the national average diesel price of $4.03/gal, a system capital cost of $923k is required to breakeven on the investment. The national average case is given by the red triangle in figure 6.4. The diesel price where the system has zero costs results in $0.88/gal. This is the price of diesel required to offset operating costs.

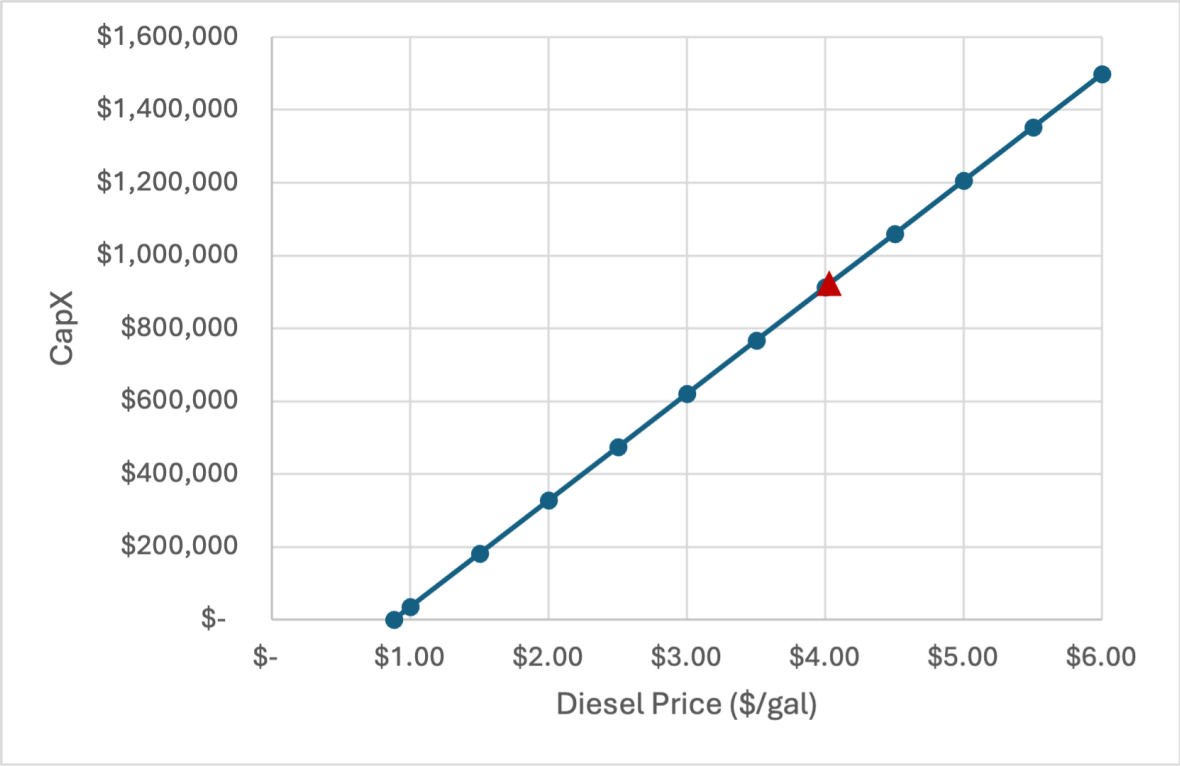

Figure 6.4. The break even capital cost for a system for a given diesel price.

The final scenario considered is the case where farmers utilize all their crop residues and sell the excess methanol fuel to neighboring farms. This case considers purchasing a larger system to take on the risk of selling fuel. The results for the considered crops are shown in figure 6.5. All crops show a large gain in NPV when considering selling excess fuel. The most dramatic case is that of corn due the large amount of crop residue provided per acre (figure 6.3). Selling methanol fuel results in an operation with nearly ten times the NPV of the base case for corn farms. This scenario assumes that all crop residue was not utilized, and therefore no opportunity cost was considered. In

addition, all excess fuel is assumed to be sold, which may not be realistic unless neighboring farm also use methanol powertrains.

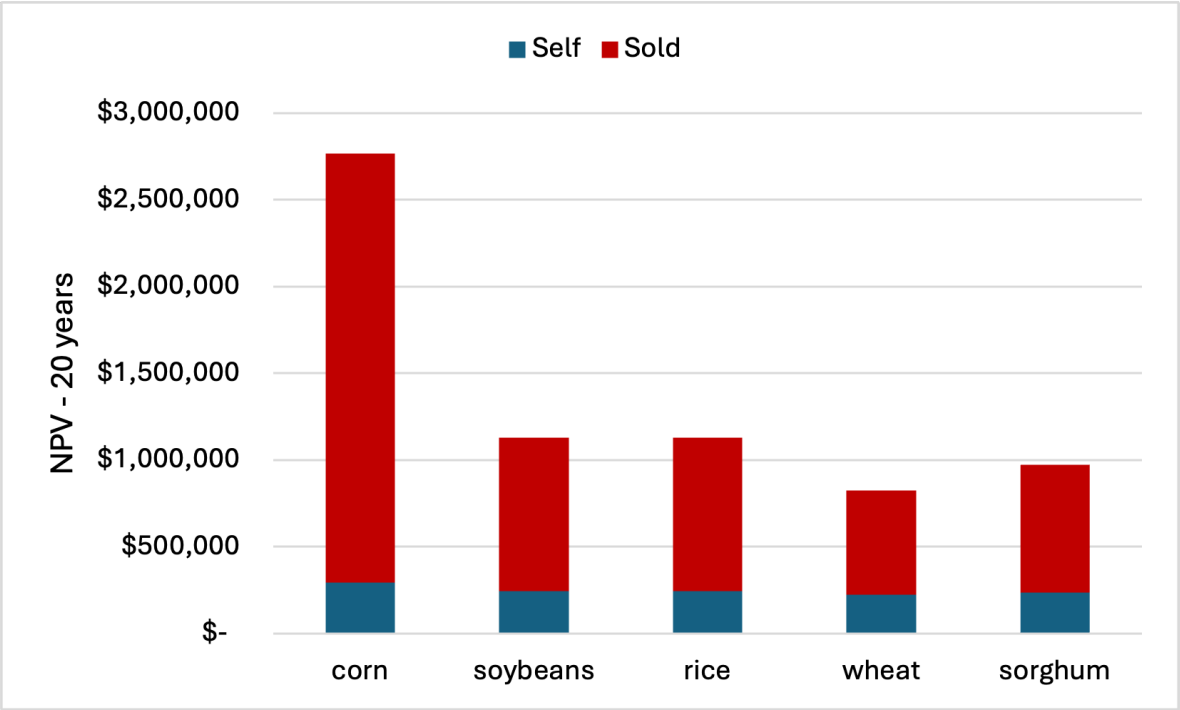

Figure 6.5. The break even capital cost for a system for a given diesel price.

The process described in this work has overall net zero emissions with the potential to have negative emissions. This process is completely self-contained with biomass being the only major material input stream. Generated syn gas from the gasifier is combusted to heat the process, which eliminates the need for external electricity or heat sources. The two direct sources of carbon dioxide being released into the atmosphere are the carbon dioxide in the flue gas stream leaving the gasifier and the carbon dioxide stream leaving the acid-gas removal system. The carbon dioxide from both these streams has a biogenic credit because it was produced from the biomass feedstock. Because of the biogenic credit, these streams can be considered carbon neutral. There is the possibility of the process having negative overall emissions. The high purity CO2 stream off the acid gas removal currently is directly emitted to the atmosphere, however it is possible to sequester this stream and claim the 45Q tax credit.

6.4 Conclusion

This study has thoroughly examined the viability of integrating small-scale methanol production facilities on farms using crop residues as feedstock. Our analysis spans technical, economic, and environmental perspectives, providing a holistic assessment of the potential impacts and benefits of

substituting diesel with renewable methanol in agricultural operations.

Economically, the establishment of a methanol production plant on a farm shows promising returns under specific conditions. The discounted cash flow analysis reveals a positive net present value (NPV) across various scenarios, particularly when excess methanol is sold to neighboring farms. This suggests that the investment can be financially sustainable, especially in regions with higher diesel prices. However, the capital cost and economies of scale are critical factors; the plant's financial viability is sensitive to these initial expenditures and operational efficiencies. It is crucial for farmers to secure adequate funding and manage production costs effectively to ensure the plant's economic success.

Environmentally, the adoption of methanol production from biomass represents a significant stride towards sustainable agricultural practices. By utilizing crop residues, this approach not only reduces waste but also contributes to a reduction in greenhouse gas emissions compared to conventional diesel usage. The process is designed to be self-sustaining with net-zero emissions, aligning with global efforts to mitigate climate change.

From a technical standpoint, the feasibility of deploying methanol production facilities on farms is supported by the adaptation of existing technologies for biomass conversion and methanol synthesis. While these technologies are currently mature, continuous innovations and improvements could further enhance their efficiency and integration into farm operations.

Retrofitting diesel farm equipment to run on methanol requires comprehensive technical modifications that are not considered in this study. Key changes include upgrading the fuel storage and delivery systems with corrosion-resistant materials such as stainless steel or specific polymers, and recalibrating or replacing fuel injectors and pumps to manage methanol's lower energy content and different combustion characteristics. The engine control unit (ECU) must be reprogrammed to adjust fuel injection timing and quantity to optimize methanol's faster burn rate and higher octane. Seals, gaskets, and hoses also need replacing with methanol-resistant materials to prevent leaks and deterioration. Modifications to the exhaust system may be necessary to handle different combustion byproducts, and enhanced safety measures such as improved ventilation, leak detection, and fire suppression systems are essential due to methanol's volatility and toxicity. The feasibility of these adaptations and their costs must be assessed in future studies before methanol can be considered a viable alternative.

In conclusion, the transition to on-farm methanol production is a viable strategy for farms aiming to become more energy self-sufficient and environmentally responsible. This project could set a precedent for rural agricultural energy practices, offering a replicable model for others in the sector. However, careful consideration of economic conditions, technological capabilities, and environmental impacts is essential for each unique implementation. Future research should focus on optimizing plant designs, exploring alternative feedstocks, and assessing long-term operational impacts to fully realize the potential of farm-based methanol production.

6.5 References

(1) Tan, E. C.; Talmadge, M.; Dutta, A.; Hensley, J.; Schaidle, J.; Biddy, M.; Humbird, D.; Snowden-Swan, L. J.; Ross, J.; Sexton, D., et al. *Process design and economics for the conversion of lignocellulosic biomass to hydrocarbons via indirect liquefaction. Thermochemical research pathway to high-octane gasoline blendstock through methanol/dimethyl ether intermediates*; tech. rep.; National Renewable Energy Lab.(NREL), Golden, CO (United States), 2015.

(2) Harris, K.; Nash, C.; Ruddy, D.; Dutta, A.; Dupuis, D.; Christensen, E.; Rein, A.; Tan, E.; Hartley, D.; Cai, H., et al. *High-Octane Gasoline from Lignocellulosic Biomass via Syngas and Methanol/Dimethyl Ether Intermediates (2021 State of Technology)*; tech. rep.; National Renewable Energy Lab.(NREL), Golden, CO (United States), 2022.

(3) Tan, E.; Ruddy, D.; Nash, C.; Dupuis, D.; Harris, K.; Dutta, A.; Hartley, D.; Cai, H. *High-octane gasoline from lignocellulosic biomass via syngas and methanol/dimethyl ether intermediates: 2019 state of technology*; tech. rep.; National Renewable Energy Lab.(NREL), Golden, CO (United States), 2018.

(4) Dutta, A.; Talmadge, M.; Hensley, J.; Worley, M.; Dudgeon, D.; Barton, D.; Groendijk, P.; Ferrari, D.; Stears, B.; Searcy, E. M., et al. *Process design and economics for conversion of lignocellulosic biomass to ethanol: thermochemical pathway by indirect gasification and mixed alcohol synthesis*; tech. rep.; National Renewable Energy Lab.(NREL), Golden, CO (United States), 2011.

(5) Colantoni, A.; Villarini, M.; Monarca, D.; Carlini, M.; Mosconi, E. M.; Bocci, E.; Rajabi Hamedani, S. Economic analysis and risk assessment of biomass gasification CHP systems of different sizes through Monte Carlo simulation. *Energy Reports* **2021**, *7*, 1954–1961.

(6) NREL. NREL Distributed Internal CHP Study, Personal communication, Email to the author, 2023-2024.

(7) Methanex. Methanex posts regional contract methanol prices for Europe, North America, Asia and China. Accessed: April 12th 2024, 2024.

(8) Administration, E. I. Gasoline and Diesel Fuel Update, Accessed: April 15th 2024, 2024.